UNIVERZITET U NOVOM SADU
FAKULTET TEHNIČKIH NAUKA U NOVOM SADU

Sanja Ožvat

MATEMATIČKO MODELIRANJE LINIJSKOG STRUJANJA VODE I TRANSPORTA NANOSA PRIMENOM LATIS BOLCMAN METODE ZA PRIRODNE VODOTOKE

DOKTORSKA DISERTACIJA

Novi Sad, 2018.

UNIVERSITY OF NOVI SAD
FACULTY OF TECHNICAL SCIENCES
NOVI SAD

Sanja Ožvat

ONE-DIMESNIONAL MATHEMATICAL MODELING OF FLOW AND SEDIMENT TRANSPORT IN OPEN CHANNELS USING THE LATTICE BOLTZMANN METHOD

PhD Thesis

Novi Sad, 2018.

УНИВЕРЗИТЕТ У НОВОМ САДУ ● **ФАКУЛТЕТ ТЕХНИЧКИХ НАУКА**
21000 НОВИ САД, Трг Доситеја Обрадовића 6

КЉУЧНА ДОКУМЕНТАЦИЈСКА ИНФОРМАЦИЈА

Редни број, **РБР**:	
Идентификациони број, **ИБР**:	
Тип документације, **ТД**:	Монографска документација
Тип записа, **ТЗ**:	Текстуални штампани материјал
Врста рада, **ВР**:	Докторска дисертација
Аутор, **АУ**:	Сања Ожват
Ментор, **МН**:	др Љубомир Будински, др Бранислава Новаковић
Наслов рада, **НР**:	Математичко моделирање линијског струјања воде и транспорта наноса применом латис Болцман методе за природне водотоке
Језик публикације, **ЈП**:	Енглески
Језик извода, **ЈИ**:	Српски / Енглески
Земља публиковања, **ЗП**:	Република Србија
Уже географско подручје, **УГП**:	Војводина
Година, **ГО**:	2018
Издавач, **ИЗ**:	Ауторски репринт
Место и адреса, **МА**:	Факултет техничких наука, Трг Доситеја Обрадовића 6, 21000 Нови Сад
Физички опис рада, **ФО**: (поглавља/страна/ цитата/табела/слика/графика/прилога)	7 / 97 /78 / 2 / 42 / 0 / 0
Научна област, **НО**:	Машинско инжењерство
Научна дисциплина, **НД**:	Нумеричка хидраулика
Предметна одредница/Кључне речи, **ПО**:	Латис Боцман метода, неустаљено течење, танспорт наноса, природни водотоци
УДК	
Чува се, **ЧУ**:	Библиотека ФТН, Нови Сад
Важна напомена, **ВН**:	
Извод, **ИЗ**:	Развијен је латис Болцман модел линијског струјања воде са транспортом наноса за природне водотоке. Модел неустаљеног течења је заснован на облику Сен-Венанових једначина у ком фигуришу ниво слободне поршине и протицај. За моделирање транспорта наноса коришћен је концепт активног слоја. Једначине су трансформисане из неуниформне физичке мреже у униформну рачунску мрежу. Изведени су нови облици равнотежних дистрибутивних функција и Изведени гранични услови за бифуркације тока. Верификација предложеног модела је добијена тестирањем неустаљеног течења на три примера: устаљено течење у призматичном каналу, неустаљено течење у непризматичном каналу и неустаљено течење у водотоку са природном геометријом на примеру реке Дунав. Модел транспорта наноса је тестиран на два примераадвекција-дифузија у призматичном каналу и неустаљено течење са транспортом наноса у природном водотоку – студија случаја реке Дунав.
Датум прихватања теме, **ДП**:	01. 11. 2018. године
Датум одбране, **ДО**:	
Чланови комисије, **КО**: Председник:	др Ратко Маретић
Члан:	др Марко Иветић
Члан:	др Валентин Главарданов
Члан, ментор:	др Бранислава Новаковић
Члан, ментор:	др Љубомир Будински

Потпис ментора

UNIVERSITY OF NOVI SAD ● **FACULTY OF TECHNICAL SCIENCES**
21000 NOVI SAD, Trg Dositeja Obradovića 6

KEY WORDS DOCUMENTATION

Accession number, **ANO**:	
Identification number, **INO**:	
Document type, **DT**:	Monograph publication
Type of record, **TR**:	Textual printed material
Contents code, **CC**:	PhD thesis
Author, **AU**:	Sanja Ožvat
Mentor, **MN**:	Ljubomir Budinski, PhD, Branislava Novaković, PhD
Title, **TI**:	One-dimensional mathematical modeling of flow and sediment transport in open channels using the lattice Boltzmann method
Language of text, **LT**:	English
Language of abstract, **LA**:	Serbian / English
Country of publication, **CP**:	Republic of Serbia
Locality of publication, **LP**:	Vojvodina
Publication year, **PY**:	2018
Publisher, **PB**:	Author's reprint
Publication place, **PP**:	Faculty of Technical Sciences, Trg Dositeja Obradovića 6, 21000 Novi Sad
Physical description, **PD**: (chapters/pages/ref./tables/pictures/graphs/appendixes)	7 / 97 /78 / 2 / 42 / 0 / 0
Scientific field, **SF**:	Mechanical engineering
Scientific discipline, **SD**:	Numerical Hydraulics
Subject/Key words, **S**/**KW**:	Lattice Boltzmann method, unsteady flow, sediment transport, natural watercourses
UC	
Holding data, **HD**:	Library of Faculty of technical sciences, Novi Sad
Note, **N**:	
Abstract, **AB**:	A one-dimensional unsteady open-channel flow with sediment transport lattice Boltzmann model is developed. The unsteady water flow model is based on the discharge-water level definition of the Saint-Venant equations. For the sediment active-layer concept is used. Geometrical transformations are applied to the governing equations, in order to transform non-uniform physical spatial grid, characteristic for natural geometry, into an uniform computational grid. New form of equilibrium distribution functions is derived. Bifurcation boudary conditions suitable with the lattice Bolcmann method are derived. Verification of the proposed model is obtained by testing unsteady flow model on three cases: steday flow in a prismatic channel, usteady flow in an unprismatic channel and unsteady flow in a natural watercourse – Danube River case study. Sediment transport model is tested on two cases: advection-diffusion in a prismatic channel and unsteady flow with sediment transport in a natural watercouse – Danube River case study.
Accepted by the Scientific Board on, **ASB**:	November 1st, 2018
Defended on, **DE**:	

Defended Board, **DB**:		
	President:	Ratko Maretić, PhD
	Member:	Marko Ivetić, PhD
	Member:	Valentin Glavardanov, PhD
	Member, Mentor:	Branislava Novaković, PhD
	Member, Mentor:	Ljubomir Budinski, PhD

Menthor's sign

Rezime

U okviru teze predstavljen je razvoj, formulacija i verifikacija matematičkog modela jednodimenzionalnog neustaljenog tečenja sa transportom nanosa u prirodnim vodotocima primenom latis Bolcman metode (engl. lattice Boltzmann). Najveći broj istraživača koji se bave modeliranjem jednodimenzionalnog neustaljenog tečenja modele koji se zasnivaju na Prajsmanovoj (engl. Preismann) šemi konačnih razlika i na Holi-Prajsmanovoj (engl. Holly Preismann) šemi. Navedene numeričke šeme su robusne i bezuslovno stabilne. U oblasti modeliranja transporta nanosa ne postoji dominantan pristup. Deljenje nanosa na suspendovani i nanos na i pri dnu omogućava da se kod modeliranja suspendovanog nanosa prihvati pretpostavka da se njegove čestice kreću brzinom koja je približno jednakoj brzini kretanja fluida.

Lattice Bolcmanova (engl. lattice Bolzmann) metoda (LBM) predstavlja hiperstilizovanu verziju Bolcmanovih jednačina, koja je prilagođena rešavanju problema iz oblasti dinamike fluida i šire. Ovaj, relativno novi i obećavajući pristup numeričkog rešavanja nelinearnih parcijalnih diferencijalnih jednačina je efikasan i fleksibilan pri primeni za kompleksnu ili promenljivu geometriju. Srž LBM jednačina je specijalna diskretna forma Boltzmann-ove jednačine, koja opisuje kretanje grupe čestica na jednostavan način, a na makroskopskom nivou daje sliku o kretanju fluida. Prosečne brzine čestica se, u prostoru i vremenu, ponašaju kao fizičke brzine fluida, što daje direktnu vezu između diskretnog mezoskopskog i makroskopskog nivoa. Za razliku od klasične numeričke hidraulike, koja daje direktna rešenja jednačina kretanja fluida, lattice Boltzmann metod je način da se jednačine reše indirektno. Metod podrazumeva jednostavne proračune, paralelne procese programiranja i laku implementaciju graničnih uslova. Preteča latis Bolcmanove metode su latis gas celular automata (lattice gas cellular automata) modeli (LGCA) i Bolcmanova transportna jednačina. U tezi je dat teorijski uvod u latis Bolcman metodu. Opisano je kako je metoda nastala i kako se razvijala i urađen je detaljan prikaz postojećih modela koji će se koristiti kao baza za novi model.

Kako bi se razvio funkcionalan model jednodimenzionalnog neustaljenog tečenja u otvorenim tokovima sa transportom nanosa, neophodno je definisati jednačine koje opisuju navedene fizičke procese. Jednodimenzionalno neustaljeno tečenje u otvorenim tokovima opisano je posebnim oblikom Sen-Venanovih jednačina, gde kao promenljive figurišu kota slobodne površine i proticaj u obliku:

$$\begin{aligned} \frac{\partial A}{\partial t} + \frac{\partial Q}{\partial x} &= q \\ \frac{\partial Q}{\partial t} + \frac{\partial}{\partial x}\left(\omega \frac{Q^2}{A}\right) &= -g_r A \frac{\partial Z}{\partial x} - grAS_f, \end{aligned}$$

gde je $A(x,t)$ površina poprečnog preseka; $Q(x,t)$ je proticaj; $Z(x,t)$ je kota slobodne površine, $q(x,t)$ je lateralni doticaj po jedinici dužine, g_r je gravitaciono ubrzanje; t je vreme, x je prostorna koordinata; a ω je koeficijent neunifornosti brzina. S_f je nagib trenja definisan izrazom:

$$S_f = \frac{n^2 Q^2}{A^2 R^{4/3}}$$

gde je n is Maningov koeficijent trenja a $R = A/O$ je hidraulički radijus, gde je O okvašeni obim. Ovaj oblik jednačina eliminiše član nagiba dna korita, što je prilagođeno modeliranju tokova sa prirodnom geometrijom. Za model transporta nanosa, korišćen je princip aktivnog sloja, tj. suspendovani nanos je odvojen od nanosa na i pri dnu. Mešavina nanosa je predstavljena preko odgovarajućih frakcija $ks = 1, ..., KS$, gde je KS ukupan broj frakcija. Transport frakcije ks suspendovanog nanosa, predstavljen je jednačinom održanja mase suspendovanog nanosa u obliku:

$$\frac{\partial (C_{ks} A)}{\partial t} + \frac{\partial (C_{ks} A u)}{\partial x} = \frac{\partial}{\partial x}\left(\varepsilon_s \frac{\partial (C_{ks})}{\partial x} A\right) + \frac{B}{\rho}\left(E_{ks}^{sed} - D_{ks}^{sed}\right),$$

gde je ρ gustina mešavine vode i nanosa, C_k je koncentracija frakcije ks, ε_s maseni koeficijent difuzije, B je širina slobodnog ogledala, E_{ks}^{sed} je član član erozije, a D_{ks}^{sed} je član deponovanja. Transport nanosa u aktivnom sloju dat je jednačinom održanja mase aktivnog sloja frakcije ks:

$$\rho_s (1 - p_b) \frac{\partial (\beta_{ks} E_m)}{\partial t} + \frac{\partial \phi_{ks}}{\partial x} = D_{ks}^{sed} - E_{ks}^{sed} + (S_f)_{ks},$$

gde je β_{ks} udeo frakcije ks, ϕ_{ks} fluks nanosa na dnu frakcije ks, E_m je debljina aktivnog sloja, p_b je poroznost, ρ_s je gustina sedimenta, a $(S_f)_{ks}$ je član razmene između aktivnog

sloja i aktivnog stratuma frakcije ks. Globalna jednačina održanja mase aktivnog sloja i stratuma je:

$$\rho_s(1-p_b)\frac{\partial(Z_b)}{\partial t}+\frac{\partial}{\partial x}\left(\sum_{ks=1}^{KS}\phi_{ks}\right)=\sum_{ks=1}^{KS}\left(D_{ks}^{sed}-E_{ks}^{sed}\right),$$

gde je Z_b kota dna.

Uniformnost strukture računske mreže je glavno ograničenje latis Bolcman modela, koje značajno smanjuje efikasnost i primenljivost LB modela, naročito kada je u pitanju modeliranje prirodne, nepravilne geometrije. Da bi se ovo ograničenje eliminisalo i istovremeno ispoštovale osnovne karakteristike latis Bolcman modela, uvedena je geometrijska transformacija zasnovana na metričkom mapiranju između fizičkog i računskog domena. Ova tehnika se često koristi u tradicionalnom metodama računske dinamike fluida, a omogućava da se veličine definisane u neekvidistantnom fizičkom prostoru prenesu u ekvidistantan računski okvir. Na taj način prostornu neuniformnost eliminišu transformisane jednačine, umesto samog numeričkog modela.Transformisane jednačine, gde je $Y=\partial x/\partial\xi$ (ξ je nova koordinata), imaju sledeći oblik:

- Transformisane Sen-Venanove jednačine tečenja:

$$\frac{\partial}{\partial t}\left(YA\right)+\frac{\partial Q}{\partial\xi}=qY,$$

$$\frac{\partial Q}{\partial t}+\frac{\partial}{\partial\xi}\left(\omega\frac{Q^2}{YA}\right)=-\frac{g_rA}{Y}\frac{\partial Z}{\partial\xi}-gAS_f+\omega\frac{Q^2}{A}\frac{\partial\left(Y^{-1}\right)}{\partial\xi}.$$

- Transformisane jednačine održanja mase suspendovanog nanosa:

$$\frac{\partial(C_{ks}AY)}{\partial t}+\frac{\partial(C_{ks}Au)}{\partial\xi}=\varepsilon_s\frac{\partial^2(C_{ks}\frac{A}{Y})}{\partial\xi^2}-\varepsilon_s\frac{\partial C_{ks}}{\partial\xi}\frac{\partial(\frac{A}{Y})}{\partial\xi}-\varepsilon_sC_{ks}\frac{\partial^2(\frac{A}{Y})}{\partial\xi^2}+\frac{BY}{\rho}\left(E_{ks}^{sed}-D_{ks}^{sed}\right)$$

- Transformisane jednačine odžanja mase aktivnog sloja:

$$\frac{\partial(\rho_s(1-p_b)\beta_{ks}E_mY)}{\partial t}+\frac{\partial\phi_{ks}}{\partial\xi}=Y\left(D_{ks}^{sed}-E_{ks}^{sed}+\left(S_f\right)_{ks}\right).$$

- Transformisana globalna jednačina održanja mase aktivnog sloja i stratuma:

$$\frac{\partial\left[\rho_s(1-p_b)Z_bY\right]}{\partial t}+\frac{\partial}{\partial\xi}\left(\sum_{ks=1}^{KS}\phi_{ks}\right)=Y\sum_{ks=1}^{KS}\left(D_{ks}^{sed}-E_{ks}^{sed}\right).$$

Na osnovu transformisanih jednačina formirani su adekvatni latis Bolcman modeli. Izabrana je D1Q3 dispozicija mreže, za koju su karakteristične čvorne brzine:

$$e_\alpha = \begin{cases} 0 & ,\alpha = 0, \\ e & ,\alpha = 1, \\ -e & ,\alpha = 2, \end{cases} .$$

Predloženi oblici latis Bolcmanovih jednačina sa odgovarajućim ravnotežnim distributivnim funkcijama su:

- Za jednačine neustaljenog tečenje u otvorenim tokovima:

$$\begin{gathered} f_\alpha(\xi + e_\alpha \Delta t, t + \Delta t) = f_\alpha(\xi, t) - \frac{1}{\tau_f}(f_\alpha - f_\alpha^{eq}) \\ + \frac{\Delta t}{2e^2} e_\alpha (F_\alpha + e_\alpha q Y) \\ - \frac{g\overline{A}}{2\overline{Y}e^2} \left[Z(\xi + e_\alpha \Delta t, t) - Z(\xi, t) \right] \\ + \frac{\omega}{2e^2} \overline{\left(\frac{Q^2}{A} \right)} \left[Y^{-1}(\xi + e_\alpha \Delta t) - Y^{-1}(\xi) \right], \end{gathered}$$

$$F_\alpha = -\frac{g n^2 Q^2}{A R^{4/3}},$$

$$f_\alpha^{eq} = \begin{cases} YA - \frac{1}{e^2}\frac{\omega Q^2}{YA} & ,\alpha = 0 \\ \frac{Q}{2e} + \frac{1}{2e^2}\frac{\omega Q^2}{YA} & ,\alpha = 1 \\ -\frac{Q}{2e} + \frac{1}{2e^2}\frac{\omega Q^2}{YA} & ,\alpha = 2. \end{cases} ;$$

- Za jednačinu održanja mase suspendovanog nanosa frakcije ks:

$$\begin{gathered} g_\alpha(\xi + e_\alpha \Delta t, t + \Delta t) = g_\alpha(\xi, t) - \frac{1}{\tau_g}(g_\alpha - g_\alpha^{eq}) \\ - \frac{\varepsilon_s}{e^2 \Delta t} \overline{C_{ks}} \left[\frac{A}{Y}(\xi + e_\alpha \Delta t, t) - 2\frac{A}{Y}(\xi, t) + \frac{A}{Y}(\xi - e_\alpha \Delta t, t) \right] \\ - \frac{\varepsilon_s}{e^2 \Delta t} \left[C_{ks}(\xi + e_\alpha \Delta t) - C_{ks}(\xi) \right] \left[\frac{A}{Y}(\xi + e_\alpha \Delta t, t) - \frac{A}{Y}(\xi, t) \right] \\ + \Delta t G_\alpha, \end{gathered}$$

$$G_\alpha = \frac{BY}{\rho} \left(E_{ks}^{sed} - D_{ks}^{sed} \right),$$

$$g_\alpha^{eq} = \begin{cases} C_{ks}AY - \lambda C_{ks}A & ,\alpha = 0 \\ \frac{C_{ks}Au}{2e} + \frac{\lambda}{2}C_{ks}A & ,\alpha = 1 \\ -\frac{C_{ks}Au}{2e} + \frac{\lambda}{2}C_{ks}A & ,\alpha = 2. \end{cases},$$

$$\lambda = \frac{\varepsilon_s}{\Delta t Y(\tau_g - 0.5)e^2}.$$

- Za jednačinu održanja mase aktivnog sloja frakcije ks:

$$h_\alpha(\xi + e_\alpha \Delta t, t + \Delta t) = h_\alpha(\xi, t) - \frac{1}{\tau_h}(h_\alpha - h_\alpha^{eq}) + \Delta t H_\alpha,$$

$$H_\alpha = Y\left(D_{ks}^{sed} - E_{ks}^{sed} + (S_f)_{ks}\right),$$

$$h_\alpha^{eq} = \begin{cases} \rho_s(1-p_b)\beta_{ks}E_m Y & ,\alpha = 0 \\ \frac{\phi_{ks}}{2\cdot e^2} & ,\alpha = 1 \\ -\frac{\phi_{ks}}{2\cdot e^2} & ,\alpha = 2 \end{cases};$$

- Za globalnu jednačinu održanja mase aktivnog sloja i stratuma:

$$m_\alpha(\xi + e_\alpha \Delta t, t + \Delta t) = m_\alpha(\xi, t) - \frac{1}{\tau_m}(m_\alpha - m_\alpha^{eq}) + \Delta t M_\alpha.$$

$$M_\alpha = Y\sum_{ks=1}^{KS}\left(D_{ks}^{sed} - E_{ks}^{sed}\right),$$

$$m_\alpha^{eq} = \begin{cases} \rho_s(1-p_b)Z_b Y & ,\alpha = 0 \\ \frac{1}{2e}\sum_{ks=1}^{KS}\phi_{ks} & ,\alpha = 1 \\ -\frac{1}{2e}\sum_{k=1}^{KS}\phi_k & ,\alpha = 2 \end{cases}.$$

Kako bi predloženi model mogao da se primeni na otvorene tokove sa prirodnom geometrijom, izvedeni su granični uslovi za pritoke i grananje toka. Dat je kratak opis kompjuterskog koda sa algoritmom koji će se koristiti za testiranje modela, sa posebno objašnjenim detaljima koji se tiču implementacije prirodne geometrije i optimizacije samog modela.

Predloženi model neustaljenog tečenja je testiran na tri slučaja: ustaljeno tečenje u prizmatičnom kanalu, neustaljeno tečenje u neprizmatičnom kanalu i neustaljeno tečenje u prirodnom vodotoku. Ustaljeno tečenje testirano je na prizmatičnom kanalu pravougaonog

poprečnog preseka dužine $L = 1000\ m$, širine $B = 100\ m$, konstantnog nagiba dna $S_0 = 0.001.$ i Maningovog koeficijenta $n = 0.025\ m^{-1/3}s$. Kota nivoa $Z_d = 1.20\ m$ je postavljena kao nizvodni, a konstantan proticaj $Q_{up} = 100.0\ m^3/s$ kao uzvodni granični uslov. Posmatrane su dve dispozicije računske mreže, ekvidistantna i neekvidistanta.Rezultati latis Bolcmanovog modela su poređeni sa rezultatima odgovarajućeg modela u softverskom paketu HEC-RAS. Dužina simulacije je 50 min, sa vremenskim korakom $\Delta t = 10\ s$ za ekvidistantnu i $\Delta t = 7\ s$ za neekvidistantnu mrežu.Za obe računske mreže su prikazana poređenja nivoa slobodne površine za $t = 50$ min, nivogrami i hidrogrami. Dobijena su odlična poklapanja za obe dispozicije mreže.

Neustaljeno tečenje u neprizmatičnom kanalu je testirano na kanalu dužine $L = 24000\ m$, konstantnog nagiba dna $S_0 = 0.0005$ i Maningovog koeficijenta $n = 0.0667\ m^{-1/3}s$. Širina kanala je određena izrazom $B = 8.0 + 12.0(x/L)$, gde je x odgovarajuća stacionaža poprečnog preseka merena od uzvodne granice modela. Formirane su dve računske mreže, ekvidistantna i neekvidistantna. U slučaju ekvidistantne fizičke mreže rastojanje između 25 računskih tačaka je po $\Delta x = 1000.0\ m$, dok je u slučaju neekvidistantne mreže 25 računskih tačaka formirano tako što su uvedena proizvoljna, nejednaka rastojanja između poprečnih preseka koja se kreću u rasponu od $\Delta x = 500.0\ \div 1700.0\ m$. Rastojanje tačaka u transformisanoj računskoj mreži je $\Delta\xi = 1.0$ za oba slučaja. Uzvodni granični uslov je ulazni hidrogram u obliku poplavnog talasa, dok je nizvodni granični uslov normalna dubina dobijena iz Šezi-Maningove (engl. Chezy-Manning) jednačine. Stabilnost modela je postignuta za $\tau = 0.501$ i $\Delta t = 2.0\ s$ oba slučaja. Ukupno 12600 računskih koraka je izvršeno za simulaciju dugu 420.0 min. Validacija rezultata je izvršena poređenjem sa rezultatima HEC-RAS modela. Upoređeni su nivogrami i hidrogrami za po četiri proizvoljna poprečna preseka za obe računske mreže. Rezultati se jako dobro poklapaju.

Poslednji korak je primena latis Bolcman modela na neustaljeno tečenje u vodotoku sa prirodnom geometrijom. Modelirana je deonica reke Dunav od Smedereva do HE Đerdap I, dužine 145.88 km, koja sadrži četiri pritoke: Velika Morava, Nera, Pek i Porečka i dva rečna ostrva. Za kreiranje modela korišćena su morfološka merenja geometrije reke Dunav (podaci Republičkog Hidrometeorološkog zavoda Srbije). Na datoj deonici, postoje merenja za 160

poprečnih preseka na međusobnom rastojanju u rasponu od $800 \div 1300m$. Kompletna deonica je podeljena na devet sekcija, koje su razdvojene pritokama i račvanjima. Ulazni hidrogram za mesec august 2006 godine na mernoj stanici Smederevo je uzvodni granični uslov, dok je nivogram za isti vremeski period na mernoj stanici HE Đerdap I postavljen kao nizvodni granični uslov (podaci RHMZ). Pritoke Nera, Pek i Porečka nemaju značajan uticaj na tok reke Dunav, zbog malih proticaja, dok je za pritoku Velika Morava proticaj $Q_t = 90\ m^3/s$ uveden kao unutrašnji granični uslov. Maningov koeficijent je $n = 0.0318\ m^{-1/3}s$, transformisano rastojanje $\Delta\xi = 1.0$, a vreme relaksacije $\tau = 0.57$. Stabilnost modela je postignuta za vremenski korak $\Delta t = 10.0\ s$. Pre simulacije neustaljenog tečenja, model je stabilizovan za ustaljeni režim, tako što su nametnuti konstantni granični uslovi $Q = 2570.0\ m^3/s$ i $Z = 69.44\ m$ u trajanju od četiri dana. Iste te vrednosti su korišćene i kao početni uslovi za ceo model. Nakon stabilizacije modela, konstantni granični uslovi su zamenjeni ulaznim hidrogramom i izlaznim nivogramom. Simulacija neustaljenog tečenja u trajanju od 31 dana je postignuta sa 267840 koraka za 12.34 min. Za poređenje rezultata korišćena su časovna merenja nivoa slobodne površine za merne stanice Golubac (rkm 1042.00) i Donji Milanovac (rkm 995.00) i proticaja na mernoj stanici HE Đerdap I tokom augusta 2006. godine. Upoređeni rezultati pokazuju dobra poklapanja. Prosečna odstupanja nivoa slobodne površine su oko 10.0 cm, što je zadovoljavajuće za izrazito neustaljen režim tečenja. Najveće odstupanje je 18 cm u periodu od 16. do 21. augusta na mernom mestu Golubac. Kod poređenja proticaja, prosečna odstupanja su u okviru 200.0 m^3/s, a maksimalno odstupanje od 840.0 m^3/s je primećeno samo jednom, 10. augusta.

U drugoj fazi istraživanja testiran je model transporta nanosa. Prvo je testirana jednačina advekcije i difuzije, a zatim kompletan model neustaljenog tečenja sa transportom suspendovanog nanosa u vodotoku sa prirodnom geometrijom.

Latis Bolcman model advekcije i difuzije je testiran na prizmatičnom kanalu dužine $L = 5000.0\ m$, konstantne površine poprečnog preseka $A = 1.0\ m^2$. Broj frakcija je $KS = 1$. Kao početni granični uslov postavljen je raspored koncentracije duž kanala sa naglim promenama po jednačini:

$$C_{ks}^{init}(x,0) = \frac{C_0}{\sqrt{\varepsilon_s \pi t_0}} e^{\frac{-(x-x_0)^2}{4\varepsilon_s t_0}},$$

gde je $C_0 = 3308.75$, $t_0 = 3484.8\ s$, $x_0 = 1400.00\ m$, $\varepsilon_s = 3.0\ m/s$, a x je prostorna koordinata. Uzvodni granični uslov je određen jednačinom:

$$C_{ks}^{up}(0,t) = \frac{C_0}{\sqrt{\varepsilon_s \pi (t_0 + t)}} e^{\frac{-(-u \cdot t - x_0)^2}{4\varepsilon_s (t + t_0)}},$$

gde je t vreme, a brzina $u = 0.5\ m/s$. Opet su formirane dve računske mreže, ekvidistantna sa rastojanjima $\Delta x = 50.0\ m$i neekvidistantna sa rastojanjima od $40.0 \div 90.0\ m$. Formirana je 101 prostorna tačka. Vreme simulacije je $T = 2520.0\ s$, računsko rastojanje poprečnih preseka $\Delta\xi = 1.0$, vreme relaksacije $\tau = 0.76$, a vremenski korak $\Delta t = 1.0\ s$. Rezultati su upoređeni sa analitičkim rešenjem jednačine u obliku:

$$C_k^{up}(x,t) = \frac{C_0}{\sqrt{\varepsilon_s \pi (t_0 + t)}} e^{\frac{-(x - u \cdot t - x_0)^2}{4\varepsilon_s (t + t_0)}}.$$

Postignuta su odlična poklapanja za obe prostorne mreže.

U poslednjem primeru testiran je latis Bolcman model neustaljenog tečenja sa transportom suspendovanog nanosa u prirodnom vodotoku. Modelirana je deonica Dunava dužine 176.29 km, od merne stanice Bezdan (rkm 1430.44) to merne stanice Novi Sad (rkm 1254.15). Na osnovu dostupnih morfoloških podataka (RHMZ), formirana je prostorna mreža od 73 računske tačke, koje odgovaraju izmerenim poprečnim presecima na međusobnim rastojanjima od. $850.00 \div 5460.00\ m$. Kao uzvodni granični uslovi korišćeni su izmerene prosečne dnevne vrednosti proticaja i koncentracije suspendovanog nanosa na mernoj stanici Bezdan u toku maja 2006. godine. Za nizvodni granični uslov korićena su dnevna merenja nivoa u istom vremenskom periodu na mernoj stanici Novi Sad. U principu, model neustaljenog tečenja radi nezavisno, dok model suspendovanog nanosi koristi vrednosti fizičkih veličina koje su izračunate u prethodnom koraku modela tečenja. Vreme relaksacije za latis Bolcman model neustaljenog tečenja je $\tau_f = 0.58$. Usvojeno vreme relaksacije za model nanosa je $\tau_g = 0.82$, broj frakcija je $KS = 1$, maseni koeficijent difuzije $\varepsilon_s = 20.0\ m/s$. Stabilnost modela je postignuta za vremenski korak $\Delta t = 10.0\ s$. Transformisano rastojanje je $\Delta\xi = 1.0$. Prvo je postignut ustaljen režim tečenja za $Z = 85.77\ m$ i $Q = 4550.0\ m^3/s$. Nakon stabilizacije modela tečenja, zadržavajući isti režim tečenja, model je stabilizovan i za ustaljeno stanje transporta suspendovanog nanosa sa $C_{ks} = 0.0259\ kg/m^3$. Nakon toga je usledila simulacija neustaljenog tečenja sa

transportom nanosa u trajanju od 31 dana. Rezultati su upoređeni sa merenjima RHMZ-a. Poređeni su nivoi slobodne površine za merno mesto Bačka Palanka (rkm 1298.66). Dobijeni rezultati su zadovoljavajući. Srednja odstupanja su oko 10.0 cm, dok je maksimalno odstupanje 25 cm. Merenja suspendovanog nanosa su dostupna samo za mernu stanicu Bezdan i ta merenja su iskorišćena kao uzvodni granični uslov. Kako bi se nadoknadio nedostatak podataka koji bi se mogli koristiti za validaciju modela, formirana je zavisnost između proticaja i koncentacije suspendovanog nanosa na osnovu dostupih podataka. Dobijena zavisnost je aproksimirana jednačinom:

$$C(Q) = 4.0 \cdot 10^{-10} \cdot Q^2 + 5.0 \cdot 10^{-6} Q - 0.0029.$$

Rezultati latis Bolcman modela suspendovanog nanosa upoređeni su sa vrednostima koje su dobijene dobijene zavisnosti na izmerene proticaje na mernom mestu Ledinci (rkm 1260.00) u toku maja 2006. Dobijeni rezulati su zadovoljavajući. Srednja odstupanja su reda veličine 0.002 kg/m^3, a maksimalna su 0.004 kg/m^3. U okviru daljeg istraživanja planirano je da se postojećem modelu Dunava doda model nanosa na i pri dnu i da se dobija celokupna slika neustaljenog tečenja sa transportom nanosa u prirodnim vodotocima.

TABLE OF CONTENTS

LIST OF TABLES . . . . . **xv**

LIST OF FIGURES . . . . . **xvi**

I INTRODUCTION **1**

II LITERATURE OVERVIEW **4**

2.1 One-dimensional flow models 4

2.2 Sediment transport models 6

2.3 Lattice Boltzmann models 7

III THE LATTICE BOLTZMANN METHOD **10**

3.1 The basic lattice Boltzmann method 10

3.1.1 Lattice Gas Cellular Automata (LGCA) 10

3.1.2 From LGCA to the lattice Boltzmann equation 15

3.1.3 From the Boltzmann transport equation to lattice-Boltzmann equation 16

3.2 The equilibrium distribution function 18

3.3 LBM lattice arrangements 19

3.4 The Chapman - Enskog expansion 22

3.5 Improved lattice Boltzmann models 24

3.5.1 LBM Scheme with modified equilibrium distribution function . . . 24

3.5.2 Introduction of the forcing term 25

3.5.3 Enhanced LBMSWE model 28

IV MATHEMATICAL FORMULATION OF THE LBM MODEL **30**

4.1 One-dimensional unsteady open-channel flow lattice Boltzmann model . . 31

4.1.1 Transformation of the SVE using the adaptive grid technique . . . 33

4.1.2 The lattice Boltzmann model for the transformed SVE . . 34

4.1.3 Derivation of the transformed Saint-Venant equations from the lattice Boltzmann equation 35

4.2 One-dimensional open-channel sediment transport LB model 38

4.2.1 Suspended sediment mass-conservation equation 38

4.2.2 Transformation of the suspended-sediment mass-conservation equation using the adaptive grid technique 41

4.2.3 The lattice Boltzmann model for the transformed suspended-sediment mass-conservation equation . . . 42
4.2.4 Derivation of the transformed suspended-sediment mass-conservation equation from the lattice Boltzmann evolution equation . . . 43
4.2.5 Active-layer mass-conservation equations . . . 45
4.2.6 Transformation of the active-layer mass-conservation equations using the adaptive grid technique . . . 47
4.2.7 The lattice Boltzmann model for the transformed active-layer mass-conservation equations . . . 47
4.2.8 Derivation of the transformed active-layer mass-conservation equations from the lattice Boltzmann evolution equation . . . 48
4.2.9 Global active-layer and stratum mass-conservation equation . . . 49
4.2.10 Transformation of the global active-layer and stratum mass-conservation equation using the adaptive grid technique . . . 51
4.2.11 The lattice Boltzmann model for the transformed global active-layer and stratum mass-conservation equation . . . 51
4.2.12 Derivation of the transformed global active-layer and stratum mass-conservation equation from the lattice Boltzmann equation . . . 52
4.3 Boundary conditions . . . 53
4.3.1 Boundary conditions for one-dimensional unsteady flow lattice Boltzmann model . . . 53
4.3.2 Boundary conditions for the sediment transport lattice Boltzmann model . . . 60
V PROGRAMMING CODE . . . 61
VI MODEL TESTING AND VALIDATION . . . 64
6.1 One-dimensional unsteady open-channel flow . . . 64
6.1.1 A steady non-uniform flow in prismatic channel . . . 65
6.1.2 An unsteady flow in non-prismatic channel . . . 70
6.1.3 Unsteady flow in a natural watercourse - Danube River case study 73
6.2 One-dimensional open-channel sediment transport . . . 79
6.2.1 Advection-diffusion in a prismatic channel . . . 79
6.2.2 Unsteady flow with sediment transport in a natural watercourse - Danube River case study . . . 81
VII CONCLUSION . . . 87

VIIIREFERENCES 90

LIST OF TABLES

1 Some lattice arrangements 21

2 Properties of the computational sections 75

LIST OF FIGURES

1 Microscopic, mesoscopic and macrosopis scale. 11

2 Lattice and discrete velocities of the HPP model. 12

3 Lattice and discrete velocities of the FHP model. 13

4 Collision possibilities of the FHP model. 14

5 The influence of the external force. 16

6 1-D lattice arrangements. 19

7 2-D lattice arrangements. 20

8 3-D lattice arrangement. 20

9 The active-layer concept. 38

10 Tributary flow. 55

11 Flow separation. 56

12 Flow merger. 59

13 Code algorithm. 62

14 Comparison of water surface elevation along the channel at t = 50 min - equidistant lattice grid 65

15 Comparison of water surface elevation along the channel at t = 50 min - non-equidistant lattice grid 66

16 Comparison of historical record of water surface elevation in prismatic channel - equidistant lattice grid 67

17 Comparison of historical record of water surface elevation in prismatic channel - non-equidistant lattice grid 67

18 Comparison of historical record of discharge in prismatic channel - equidistant lattice grid 68

19 Comparison of historical record of discharge in prismatic channel - non-equidistant lattice grid 68

20 Geometry of non-prismatic channel. 69

21 Hydrograph - upstream boundary condition. 69

22 Comparison of historical record of water surface elevation in prismatic channel - equidistant grid 71

23 Comparison of historical record of water surface elevation in prismatic channel - non-equidistant grid 71

24 Comparison of historical record of discharge in prismatic channel - equidistant grid . . . 72
25 Comparison of historical record of discharge in prismatic channel - non-equidistant grid . . . 72
26 The Danube River experimental reach . . . 73
27 Shematic model. . . . 74
28 Cross-section of the river bed . . . 74
29 Upstream boundary condition at GS Smederevo. . . . 76
30 Downstream boundary condition at Iron Gate I. . . . 76
31 Comparison of the historical record of water surface elevation at GS Golubac. 77
32 Comparison of the historical record of water surface elevation at GS Donji Milanovac. . . . 78
33 Comparison of the historical record of discharge at GS Iron Gate I. . . . 78
34 Initial suspended-sediment concentration distribution. . . . 80
35 Comparison of suspended-sediment concentation distribution along the prismatic channel for the non-equidistant grid. . . . 81
36 Comparison of suspended-sediment concentation distribution along the prismatic channel for the equidistant grid. . . . 82
37 The location of the experimental reach. . . . 82
38 Upstream boundary condition at GS Bezdan - dicharge. . . . 83
39 Downstream boundary condition at GS Novi Sad - water surface level. . . . 84
40 Upstream boundary condition at GS Bezdan - suspended-sediment concentration. . . . 84
41 Comparison of historical record of water level - GS Bačka Palanka . . . 85
42 Comparison of suspended-sediment concentartions - GS Ledinci . . . 86

CHAPTER I

INTRODUCTION

The main goal of this research is to create a robust mathematical tool that simulates an open channel unsteady flow with sediment transport in complex network of natural watercourses which can efficiently manage variety of hydraulic states using the recently developed lattice Boltzmann method. The accent is given to development of the unsteady flow model that can menage the irregularities as a consequence of natural geometry. Natural watercourses imply complex longitudinal and transverse geometry. Cross-sections are of irregular shape and each differs from another, which means there is no mathematical dependence (or it is very complicated to obtain) between geometrical properties like cross-sectional area, depth, wetted perimeter etc.. This implies a challenging task to create an optimal model, struggling between high accuracy and short computational time. Longitudinal geometry of natural watercourses includes tributary inflows and branching, when a single water flow is separated into two or more separate streams, and then merges back together. This changes amplify unsteadiness of the flow. Natural watercourses go through variety of complex hydraulic states, like shock waves and changes between regimes, which are imposed by the geometry of the watercourse and hydrometeorological conditions. Sediment transport is in a tight correlation with flow regime, the velocity of the water flow moves the sediment particles. Suspended mixture consists of different sediment particle sizes that react to current flow conditions, resulting in local aggradation or degradation of the river bed.

During past years researchers have been using several methods to study unsteady water flow with sediment transport in an open-channel network. These methods include physical model based experimental methods, field measurements and numerical models. It has been shown that the combination of these methods gives the best results. Numerical models are used to solve the governing system of equation that describes the phenomena, field measurements are used to calibrate and verify the results, and the results of laboratory

experiments can be used for further development of individual parts of the model. Numerical models take the lead compared to other methods, by virtue of the ability to anticipate the consequences that some events might have and the fact that one numerical model can be used for a variety of different problems. These advantages are the basic reason of existence of a large number of linear, plane and spatial numerical models. Dimension of the model depends on the problem. Planar and spatial models give a detail image of the observed phenomena in two or three dimensions, respectively, but demand complex data input (in terms of initial and boundary conditions) and a long time is necessary for the computer to perform simulations. Linear models are less demanding in terms of input data and computational time, which is why many researchers choose this kind of model, especially for long-term simulations. Some available unsteady flow models in open-channel network and sediment transport models are given in Chapter II. Along with these models, an overview of the lattice Boltzmann models is presented. Lattice Boltzmann method (LBM) is a recently developed powerful numerical tool, developed with purpose to solve ordinary and partial differential equations. Its strength lies in the ability to easily embody complex physical phenomena, spanning from multiphase flows to interactions between the fluid and it's surroundings. The LBM is an explicit method, where fluid flow is described as particles that stream along the lattice links and collide with its neighbors. The fact that collision and streaming processes are local leads to the possibility of parallel programing, resulting with significantly shorter computational time. Chapter III introduces the basis of the lattice Boltzmann method and the general overview of the method.

In Chapter IV one-dimensional unsteady open-channel flow model and one-dimensional sediment transport model are formulated using the lattice Boltzmann method. One-dimensional unsteady open-channel flow is described by the appropriate form of the Saint-Venant equations (SVE), which eliminates the bed slope term from the system of equations, leading to a more flexible and practical form of the SVE. For the sediment transport the active layer concept is used, where sediment transport domain is divided into three subdomains: suspended-sediment, near-bed sediment (active layer) and bed sediment (stratum). Sediment mixture is modeled as a collection of appropriate sediment-fraction sizes. In order to

overcome one of the major limitations of the LBM, uniformity of the lattice structure, geometric transformation based on metric mapping between the physical and computational domain is introduced. In this way, terms defined in a non-equidistant physical domain can be calculated in a equidistant computational grid. Spatial non-uniformity is managed by the transformed equations rather than with the numerical model itself. Corresponding LBM models are formed based on the transformed equations. A LBM model for the Saint-Venant equations (LABSVE) is autonomous, while the LBM model for sediment transport can be attached to a flow model. Corresponding computer code in the programming language FORTRAN is created with the purpose to solve the governing equations. The implemented algorithm needs to be simple in order to achieve short computational time. Complex geometry is accompanied with great amount of data, therefore, an extra effort has been given to optimize the code, in order to unburden it of any unnecessary calculations. The main features of the algorithm are explained in Chapter V of the thesis.

In order to test and validate the proposed one-dimensional LBM, five case studies have been performed in the Chapter VI. First, water flow model has been tested on three examples: a steady non-uniform flow in a prismatic channel, an unsteady flow in a non-prismatic channel, and an unsteady flow in a natural watercourse - Danube River case study. Verification of the results obtained from the first two LBM models is conducted by comparison with corresponding HEC-RAS models, while in the Danube River case study LBM model results are compared with the measured data obtained by standard geodetic survey by the Republic Hydro-meteorological service of Serbia (RHMZ). Test-example of suspended-sediment advection-diffusion equation lattice Boltzmann model has been performed, and the results are compared with the analytical solution of the governing equation. In order to verify the proposed unsteady open-channel flow with sediment transport on a realistic physical model with natural geometry another Danube River case study is performed,and the results of the LBM model are compared with the available field measurements obtained by the RHMZ. To compensate insufficient suspended-sediment empirical data, additional statistical data processing has been performed, based on the available measured values.

CHAPTER II

LITERATURE OVERVIEW

Open channel hydraulics has been, and still is very popular topic among the researchers. All of them share the tendency to develop more and more powerful mathematical models that solve robust physical domains and make long-term simulations in short computational time. In this Chapter currently available mathematical models from the domain of computational fluid dynamics (CFD) are presented. Furthermore, this Chapter describes the evolution of the lattice Boltzmann method, from basic to the most recent models in the area of river hydraulics..

2.1 One-dimensional flow models

In order to develop mathematical model that simulates the hydrodynamic processes of open channel unsteady flow in natural watercourses, several computational fluid dynamics numerical methods have been used in the past. The majority or authors choose the finite differences method, which is popular due to its simplicity and exact physical meaning of variables in equations. According to this method differential equations are approximated with finite difference equations, in which finite differences approximate the derivatives. Examples of such models are the scheme proposed by Lax and Wendroff (1960) for linear advection, and the scheme that Lax originally proposed for non-linear advection, which can also be applied for linear advection (Lax, 1954). In order to reduce the effect of dispersion on the results, the authors Appadu et al. (2008) combined MacCormack and Lax-Friedrich's two-stage scheme. Authors Ewing and Wang (2001) gave a historical overview of the schematic methods of final differences for advection modeling. From the shown models, the finite difference method was used by Yang and Simoes (2008), Bhallamudi and Chaudhry (1991) used the finite difference method, Bhallamudi and Chaudhry (1991) applied the McCormack scheme with the explanation that the scheme is explicit and easy to use and automatically

eliminates the iterative calculations and the need for inversion of large matrices. Huang et al. (2008) and Kuiry and Bates (2010) used the finite volume method, while Yeh et al. (1995) used the method of characteristics. The four-point implicit finite-difference Preissman scheme (1961) and the method known as Holly-Preissmann method (1977) are the most widely used methods in free-surface one-dimensional subcritical numerical modelling ((Holly and Rahuel (1990a,b), Wu et al., (2004); Fang et al. (2008), Islam et al. (2008), Sart et al. (2010)). In order to find a particular cell face value, Leonard (1979) has introduced Quadratic Upstream Interpolation for Convective Kinematics (QUICK). Furthermore, Abbott (1979) solved characteristic form of the Saint-Venant equations by applying the Method of characteristics (MC) and the Hartree method.

One of the main advantages of one-dimensional models is their ability to simulate long-term events in complex water flow systems. Starting point of a long-term open-channel flow simulation models were quasi-steady models (Yang et. al. (1985), Karim et al., (1987)). Model presented by Karim et al. (1987) was originally proposed to simulate the flow in just one section, but it was later upgraded to also allow tributary flows. Unsteady flow model CHARIMA (Yang, 1986) is used for shorter simulations. This model includes two approaches to solve the given problem. In the case of a steady flow simulation, it uses the energy equation obtained by neglecting the increase of the momentum over time in a momentum conservation equation, while for an unsteady flow simulation, the program uses a complete Saint-Venant equations. Similar to the CHARIMA, the popular commercial HEC-RAS software (Brunner, 2010), also uses the energy equation for steady situations, and Saint-Venant equations the unsteady flow simulations. Today, existing models can simulate unsteady flow in the open-channel network (models allow an arbitrary number of tributaries connected to the main stream), such as Channel Network Model (Husain and Eqnaibli, 1988). Authors Nguyen and Kawano (1995), Fang et al. (2008), Vieira and Wu (2002a), Wu et al. (2004) and DHI (2009) introduced models that simulate flow in the open-channel network, where models Vieira and Wu (2002a) and Wu et al. (2004) also included the possibility to model hydraulic structures. Models that also allow the branching of the network (separating the stream around an island into two or more smaller flows, and

then merging back together) are BRALLUVIAL (Holly and Spasojevic, 1985), CHARIMA (Yang, 1986), CARIMA (Holly and Parrish, 1993), DUFLOW (Clemmens and Holly, 1993), CanalMod by Islam et al. (2008) and MIKE 11 (DHI, 2009). In recent years attempts are made to combine linear and plane models (Chen and Zhu, 2012).

2.2 Sediment transport models

Sediment transport followed with river bed deformations consist of variety of complicated processes, for which there is no generally adopted mathematical formulation. By separating suspended-sediment from the bedload sediment, allows us to assume that the suspended particles move at the approximately same speed as the fluid particle, and that their movement is continuous.

The first difference in modeling approaches refers to the way in which the sediment mixture is described. A large number of existing sediment transport models are based on the assumption that the mixture is uniform, or the mixture is represented with a characteristic particle size (model SUTERNCH-2D by van Rijn et al. (1990) or FAST2D by Rodi (2000)). The first big progress in this area are the models that describe the sediment mixture as a mixture of different size-classes. Model BRALLUVIAL (Holly and Spasojevic (1985)) is based on a quasi-steady model of water flow and sediment transport and uses this approach where a sediment mixture is represented as a mixture of different size-classes. Model SEDICOUP (Holly and Rahuel (1990)) solves the Saint-Venant equations with the suspended-sediment and global active-layer and stratum mass-conservation equations of the mixture.

The formulation of the bedload sediment equations and exchange mechanisms are not uniquely defined. There are three basic ways of modeling the process at bed and near-bed domain. According to the first approach the active-layer is homogeneous (Karim and Kennedy (1982), Karim et al. (1987)). Some models that rely on this concept are BRALLUVIAL model by Holly and Spasojevic (1985), CHARIMA by Holly et al. (1990), models by Armanini and Giampaolo (1988), Rahuel et al. (1989), NMMOC model by Yeh et al. (1995) and many others. In the second approach sediment particle moves as a bedload,

and the thickness of the active-layer is equal to the jump height of these particles. Such models are FAST2D by Bui et al. (1998) or Rodi (2000), FAST3D by Wu et al. (2000), or the later version presented by Bui and Rutschmann (2006,2010). The third approach is the active-layer and active-stratum approach (Spasojevic and Holly (1990)), where it is considered that the active-layer is consisted of sediment grains potentially exposed to movement, as well as grains that are already moving as a bedload sediment. Models that rely on this approach are MOBED2 from the founders of the concept and author Spasojevic and Holly (1990), SEDICOUP by Holly and Rahuel (1990), model CH3D-SED by Gessler et al. (1999), models by Yang and Simoes (2008) and Hung et al. (2009), model 2DVONASK of author Budinski (2011), and others. Continuous interaction of the mixture of water and sediment causes a constant change in the distribution of sediment fractions in space and time, which also determines the availability of a certain fraction to participate in the exchange processes between suspended and bedload sediment. Model by Struksima et al. (1985) does not include suspended-sediment, it exclusively simulates bedload sediment. Model BRALLUVIAL (based on the concept of homogenous layer) determines the change of the bed elevation from the mass-conservation equation of the mass written for each fraction. The thickness of the homogeneous layer changes during every time interval and the thickness of the active-layer is raised or lowered. The CHARIMA model (Holly et al. (1990)) is a linear model that solves the system of the suspended-sediment, active layer and active-stratum mass-conservation equations for an arbitrary number of fractions, where the governing equations are defined for each fraction separately. Similar models are from the authors Holly and Rahuel (1990) and Wu et al. (2004).

2.3 Lattice Boltzmann models

The lattice Boltzmann method (LBM) is relatively new (developed about two decades ago) numerical technique defined in mesoscopic level. It was derived from the lattice gas automata. Statistical noise of the newly introduced model was by eliminated by McNamara and Zanetti (1988) and Shan and Chen (1993). Still, complicated collision operator made the method challenging for wider application. That problem was solved by introduction

of the single relaxation time Bhatnager, Gross, and Krook (LBGK) (1954) scheme (Martys and Chen (1996), Chen and Doolen (1998)). Now it could recover the Navier-Stokes equations. By introducing the two-relaxation time (TRT) and the multiple-relaxation time (MRT) schemes, anisotropy in advection and anisotropic-dispersion equations (AADE) is by solved (Ginzburg (2005) and Yoshida and Nagaoka (2010)). The single-phase transient flow in pipes by using adaptive grid approach is analyzed by Budinski (2016). Furthermore, LBM is an ideal candidate for parallel processing on high performance computers (Shan and Chen (1993); Martys and Chen (1996)). The lattice Boltzmann method is studied by many authors and applied on variety of problems from the domain of the river hydraulics. A multi-component LBM was introduced by Gunstensen and Rotman (1991). Ladd (1994) analyzed particulate suspension using the LBM. Application of the LBM on isotropic groundwater flows was examined by Zhou (2007) and Budinski et al. (2015).

The LBM of depth averaged flow equations (LABSWE) was initially introduced by Salmon (1999). One-dimensional shallow water equations LBM was introduced by Frandsen (2008). Introducing centred scheme for the force term (2004) and deriving a lattice Boltzmann model for the shallow water equations with turbulence modelling (LABSWE^{TM}) (2011) Zhou improved the LABSWE. Zhou (2010) also developed the rectangular lattice Boltzmann model applicable to complex geometry models. Budinski (2014) introduced the MRT-LBM for shallow water equations (SWE) transformed in curvilinear coordinates. The first application of the LBM on open-channel using the simpler form of the Saint-Venant equations has been preformed by van Thang et al. (2010). LBM model of one-dimensional shallow water equations was also done by Frandsen (2010), and Liu et al. (2015) introduced the non-prismatic terms into the model.

Advection–diffusion problems have been an important area of research for many years, and the LBM found its use in modelling such processes. O'Brien et al. (2002) compared experimental data to a 2D lattice Boltzmann method for advection–diffusion model in porous media flow. Furthermore, Ginzburg (2006) utilized a LBM and advection and anisotropic dispersion equations (AADE). Zhou improved the LBM for solute transport (2009) and Li

and Huang (2008) combined a hydrodynamic model with advection and anisotropic dispersion using the LBMSWE. Servan-Camas and Tsai (2009) analyzed the stability constraints for the LBM for the ADE. Peng et al. (2011) showed that for two-dimensional LBM solute transport model in shallow water the MRT terms have better stability than the BGK terms. Ginzburg (2013) showed that numerical diffusion can be eliminated by various anisotropic schemes. Patel et al. (2016) introduced a discontinuous Galerkin lattice Boltzmann scheme, and Markl and Korner (2015) presented a new no-flux free surface boundary condition for the ADE problems.

CHAPTER III

THE LATTICE BOLTZMANN METHOD

Fluid motion can be described on three scale-levels: microscopic, mesoscopic and macroscopic (Fig.1). In the macroscopic approach (the mechanics of continuum) regular or partial differential equations are obtained by applying the conservation laws of mass, momentum and energy on a infinitesimal control volume. These equations are solved using various numerical methods defined in the conventional computational fluid dynamics (CFD). In the microscopic scale, studied by the molecular dynamics (MD), the medium is considered to be made of small particles, atoms or molecules, and these particles collide. Newton's second law equation (the momentum conservation equation) is applied in order to obtain the solution. In between, is an approach at mesoscopic level, the lattice Boltzmann method (LBM) that studies the microdynamics of particles by using simplified kinetic models, representing properties of a collection of particles by a distribution function. LBM combines other two scales, resulting with simple algorithm structure, possibility of parallel programing, easy application for complex domains, possibility to handle multi-phase and multi-scale models, simple implementation of boundary conditions and many more benefits. These appealing features make LBM a powerful numerical tool for simulating complex fluid systems.

3.1 The basic lattice Boltzmann method

The lattice Boltzmann method can be considered to be a special numerical method of solving the Boltzmann equation. Others consider that the lattice Boltzmann equation (LBE) evolved from the lattice gas cellular automata (LGCA).

3.1.1 Lattice Gas Cellular Automata (LGCA)

According to the lattice gas cellular automata the fluid is treated as a set of particles on a regular lattice with certain symmetry properties. Every particle interacts with its neighbor following some described rules, through collision and streaming steps. Every lattice particle

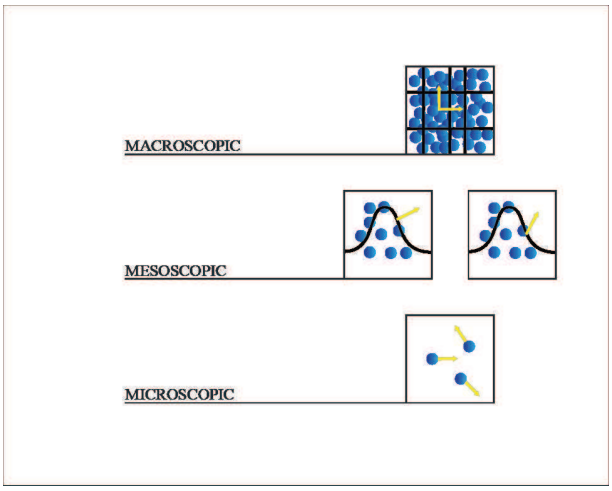


Figure 1: Microscopic, mesoscopic and macrosopis scale.

examines its own state and the states of some of its neighbors at every time step and then resets its own state. The prescribed rules with initial and boundary conditions, determine the evolution of particles in time. The behavior of the fluid at macroscopic scale is obtained as statistical collective result of the micro-dynamics of fluid molecules.

The first LGCA model, the HPP model, was developed by Hardy, Pomeau, and de Pazzis (1976). A two-dimensional square lattice is used, where from any lattice position gas particles can move in the directions of the four nearest neighboring positions along the lattice lines, as shown in Fig.2.The collision of the HPP model follows the head-on rule: when two particles move to the same position with opposite velocities, after the collision their velocities will turn around for 90° after the collision, and in any other case the particle velocities remain unchanged.

The discrete kinetic equation describes the motion of the particles:

$$n_i(\mathbf{x} + \mathbf{c}_i \partial t, t + \partial t) = n_i(\mathbf{x}, t) + C_i\left(n_i(\mathbf{x}, t)\right), \tag{1}$$

where $n_i(\mathbf{x}, t)$ represent the number of particles moving with discrete velocity $\mathbf{c}_i$ at node $\mathbf{x}$ and time t, ∂t is the time step, $C_i\left(n_i(\mathbf{x}, t)\right)$ is the collision operator, that represents the influence of particle collisions. The discrete velocity set is given by

$$\mathbf{c}_i = c\mathbf{e}_i, \tag{2}$$

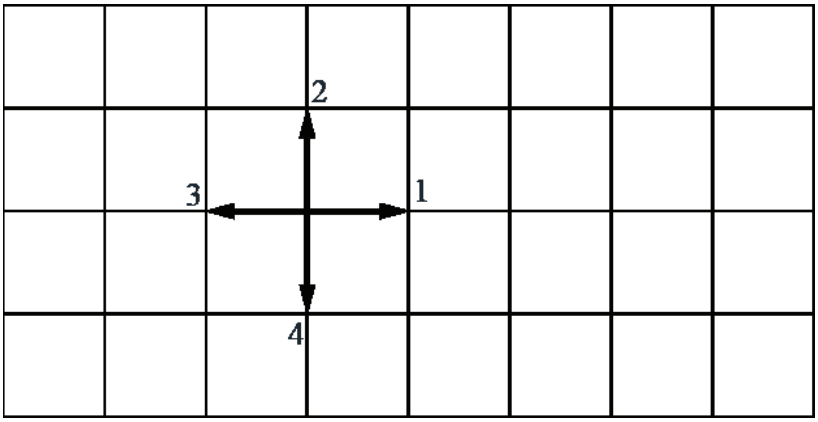


Figure 2: Lattice and discrete velocities of the HPP model.

where $\mathbf{e}_1 = (1,0)$, $\mathbf{e}_2 = (0,1)$, $\mathbf{e}_3 = (-1,0)$, $\mathbf{e}_4 = (0,-1)$. The lattice speed is $c = \delta_x/\delta_t$, where δ_x is the lattice spacing. The collision operator is given by the expression:

$$C_i = n_{i\oplus 1} n_{i\oplus 3}(1-n_i)(1-n_{i\oplus 2}) - (1-n_{i\oplus 1})(1-n_{i\oplus 3}) n_i n_{i\oplus 2}, \tag{3}$$

where "$\oplus$" represents the modulo 4 addition. In this way C_i conserves mass, momentum and energy:

$$\begin{aligned} \sum_i C_i &= 0, \\ \sum_i \mathbf{e}_i C_i &= 0, \\ \sum_i \frac{\mathbf{e}_i^2}{2} C_i &= 0. \end{aligned} \tag{4}$$

The evolution of the can be decomposed into two steps: collision and streaming. The collision step is:

$$n_i'(\mathbf{x},,t) = n_i(\mathbf{x},t) + C_i\left(n_i(\mathbf{x},t)\right), \tag{5}$$

while the streaming step can be expressed as:

$$n_i(\mathbf{x} + \mathbf{c}_i \partial t, t + \partial t) = n_i'(\mathbf{x},t). \tag{6}$$

The macroscopic physical variables are the ensemble average of the distribution function of

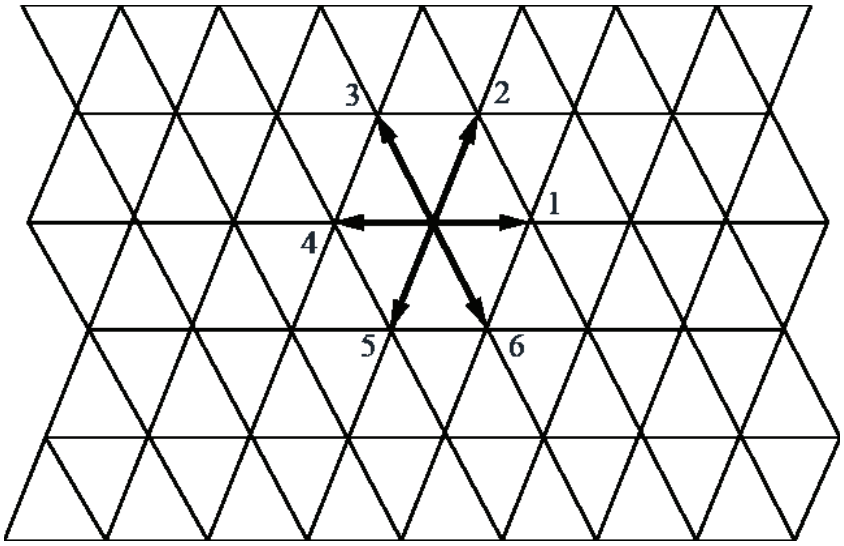


Figure 3: Lattice and discrete velocities of the FHP model.

the Boolean number $f_i \langle n_i \rangle$:

$$\begin{aligned} \sum_i m f_i &= \rho, \\ \sum_i m \mathbf{e}_i f_i &= \rho \mathbf{u}_i, \\ \sum_i m \frac{(\mathbf{c}_i - \mathbf{u}_i)^2}{2} f_i &= \rho e = \rho RT. \end{aligned} \tag{7}$$

where m is the molecular mass of the gas, ρ is velocity and T is temperature. The HPP model satisfies the basic conservation laws, but the macroscopic variables do not satisfy the continuum equations due to the insufficient symmetry of the square lattice.

Frisch, Hasslacher, and Pomeau (1986) proposed their hexagonal LGCA model called the FHP model after the authors. Every node of the lattice, shown in Fig.3, has six nearest neighbors. The discrete velocities are $\mathbf{c}_i = c(\cos\theta_i, \sin\cos\theta_i)$, where $\theta_i = \frac{(i-1)\pi}{3}$, for $i = 1 \div 6$. The state of FHP model can be described by six Boolean numbers n_i that represent the number of particles moving with velocity $\mathbf{c}_i$. Five different collision outcomes are shown in Fig.4. In cases when one input state corresponds to two possible output states

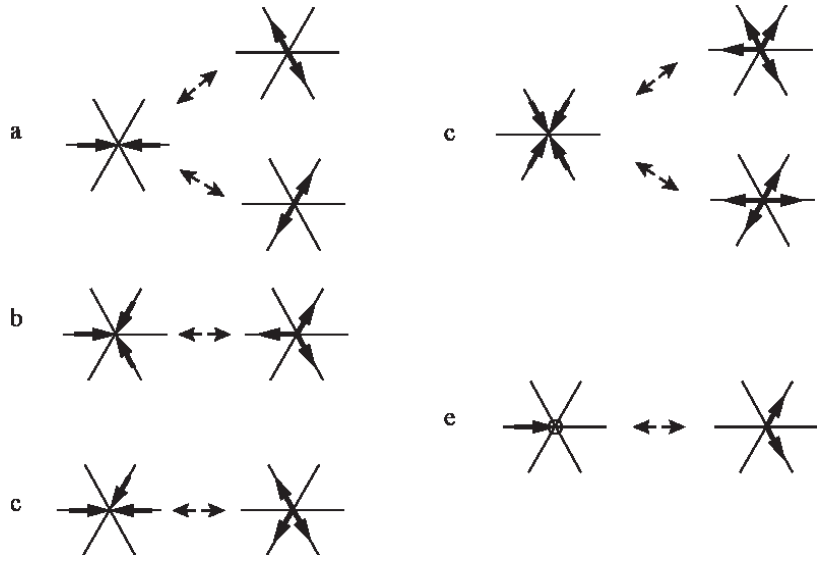


Figure 4: Collision possibilities of the FHP model.

the output is chosen randomly. The collision operator can be expressed as:

$$C_i = n_{i\oplus1}n_{i\oplus3}n_{i\oplus5}\overline{n}_i\overline{n}_{i\oplus2}\overline{n}_{i\oplus4} - \overline{n}_{i\oplus1}\overline{n}_{i\oplus3}\overline{n}_{i\oplus5}n_i n_{i\oplus2}n_{i\oplus4} \tag{8}$$

$$+rn_{i\oplus1}n_{i\oplus4}\overline{n}_i\overline{n}_{i\oplus2}\overline{n}_{i\oplus3}\overline{n}_{i\oplus5} + (1-r)n_{i\oplus2}n_{i\oplus5}\overline{n}_i\overline{n}_{i\oplus1}\overline{n}_{i\oplus3}\overline{n}_{i\oplus4}$$

$$-n_i n_{i\oplus3}\overline{n}_{i\oplus1}\overline{n}_{i\oplus2}\overline{n}_{i\oplus4}\overline{n}_{i\oplus5},$$

where "$\oplus$" represents the modulo 6 addition, and r is the random number chosen from the interval $[0,1]$. At the equilibrium state the collision operator evolves to Fermi-Dirac distribution function:

$$f_i^{eq} = \frac{\rho}{6}\left[1 + \frac{\mathbf{c}_i\cdot\mathbf{u}}{c_s^2} + G(\rho)\frac{\mathbf{Q}_i : \mathrm{u\,u}}{2c_s^4}\right], \tag{9}$$

where $c_s^2 = c^2/2$ is the sound speed, $G(\rho) = (6-2\rho)/(6-\rho)$, and $\mathbf{Q}_i = \mathbf{c}_i\mathbf{c}_i - c_s^2\mathbf{I}$. After some transformations fluid density and velocity satisfy the equations:

$$\nabla\cdot\mathbf{u} = 0, \tag{10}$$

$$\frac{\partial\mathbf{u}}{\partial t} + \mathbf{u}\cdot\nabla\mathbf{u} = -\nabla P + \nu\nabla^2\mathbf{u}. \tag{11}$$

Eqs. (11) and (10) resemble the incompressible Navier-Stokes equations.

With the tendency to develop a 3D LGCA model, the idea was to project the 4D Face-Centered Hyper-Cube (FCHC) lattice (d'Humières et al. (1986)), back onto three-dimensional space. This approach is quite complicated, due to a very large number of

possible states in the collision rule (2^{24}). Regardless, many simulations of the multiphase and complex flows have been made base on this principle.

The main advantages of the LGCA models are easy algorithm implementation, no round-off errors, unconditional stability of the numerical model and algorithm suitable for parallel programing. The main disadvantages of the LGCA models are statistical noise from the Boolean variables, the dependence of velocity of the pressure, and the violation of the Galilean invariance.

3.1.2 From LGCA to the lattice Boltzmann equation

The lattice Boltzmann equation was originally introduced by Frisch et al. (1987), but McNamara and Zanetti first proposed LBE as a computation method (1988). Their idea was to replace the Boolean variable n_i by the real-valued distribution function f_i, while the collision rule for f_i remained is the same as for n_i. The evolution equation of the McNamara and Zanetti method (MZM) yields to:

$$f_i(\mathbf{x} + \mathbf{c}_i \partial t, t + \partial t) - f_i(\mathbf{x}, t) = \Omega_i \left(f(\mathbf{x}, t) \right), \tag{12}$$

where $\Omega_i \left(f(\mathbf{x}, t) \right)$ is the collision operator, that remained rather complicated. Soon after, Higuera and Jimenez proposed an improved version of the model (1989) by assuming that distribution function f_i is close to its equilibrium state f_i^{eq} :

$$f_i = f_i^{eq} + f_i^{neq}, \tag{13}$$

where f_i^{neq} is the non-equilibrium part or the distribution function. This form of the distribution function leads to linearized collision operator:

$$\Omega_i(f) = K_{ij}(f_i - f_i^{eq}), \tag{14}$$

where $K_{ij} = \partial \Omega_i / \partial f_j$ is the collision matrix. Higuera et al. (1989) introduced the HSB model, with collision matrix independent of LGCA. The equilibrium distribution function can be written as:

$$f_i^{eq} = d_0 \left[\frac{\rho}{b d_0} + D \frac{\mathbf{c}_i \cdot \mathbf{u}}{c_i^2} + G(d_0) \mathbf{Q}_i : \mathrm{u\,u} \right], \tag{15}$$

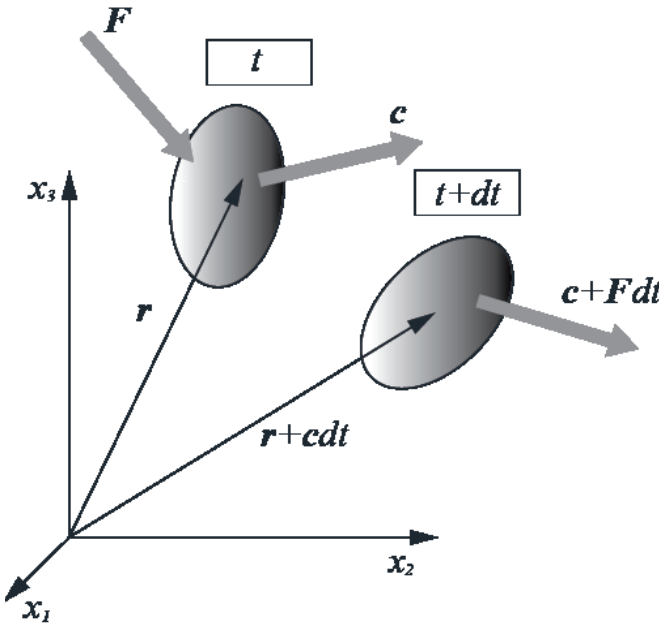


Figure 5: The influence of the external force.

where D is the spatial dimension, b is the number of the discrete velocities, $bd_0 = \rho_0$ is the mean density. Function $G(d_0)$ and tensor $\mathbf{Q}_i$ are:

$$G(d_0) = \frac{D^2(1-2d_0)}{2c_i^4(1-d_0)}, \tag{16}$$

$$\mathbf{Q}_i = \mathbf{c}_i\mathbf{c}_i - \frac{c^2}{D}\mathbf{I}. \tag{17}$$

The collision matrix is further simplified by several groups of authors independently (Chen et al. (1991), Koelman, (1991), Qian et al. (1992)). They introduces the model using the simplified BGK collision operator in form:

$$\Omega_i(f) = -\frac{1}{\tau}(f_i - f_i^{eq}), \tag{18}$$

where τ is the relaxation time. Models that use this form of the collision operator are called LBGK at single-relaxation time (SRT) models, end the evolution LBE is as follows:

$$f_i(\mathbf{x} + \mathbf{c}_i\partial t, t + \partial t) - f_i(\mathbf{x}, t) = -\frac{1}{\tau}(f_i - f_i^{eq}). \tag{19}$$

3.1.3 From the Boltzmann transport equation to lattice-Boltzmann equation

The lattice Boltzmann equation can also be derived from the Boltzmann equation. If the system is described by distribution function $f(\mathbf{r}, \mathbf{c}, t)$,which represents the number of

molecules at time t positioned between $\mathbf{r}$ and $\mathbf{r}+d\mathbf{r}$, that have velocities between $\mathbf{c}$ and $\mathbf{c}+d\mathbf{c}$. Under the influence of an external force $\mathbf{F}$, the gas molecule of unit mass will, in time dt, change its position from $\mathbf{r}$ to $\mathbf{r}+\mathbf{c}dt$, and its velocity from $\mathbf{c}$ to $\mathbf{c}+\mathbf{F}dt$, as shown in Fig.5. If collisions between molecules take place after applying the external force, the difference between the numbers of molecules in the interval $d\mathbf{r}d\mathbf{c}$, will be:

$$f(\mathbf{r}+\mathbf{c}dt, \mathbf{c}+\mathbf{F}dt, t+dt) - f(\mathbf{r}, \mathbf{c}, t) = \mathbf{\Omega}(f)d\mathbf{r}d\mathbf{c}dt. \tag{20}$$

The rate of change between final and initial status of the distribution function is called collision operator Ω. Dividing the above equation by $dtd\mathbf{r}d\mathbf{c}$ and as the limit is set to $dt \to 0$, the above equation yields to:

$$\frac{df}{dt} = \mathbf{\Omega}(f). \tag{21}$$

The LHS of the Eq.(21) can be written as:

$$\frac{df}{dt} = \frac{\partial f}{\partial \mathbf{r}}\mathbf{c} + \frac{\partial f}{\partial \mathbf{c}}\mathbf{a} + \frac{\partial f}{\partial t}, \tag{22}$$

where $a = dc/dt$ is the acceleration, which can be expressed from the Newton's second law as $a = F/m$. Now, the Boltzmann transport equation can be written as:

$$\frac{\partial f}{\partial t} + \frac{\partial f}{\partial r}c + \frac{F}{m}\frac{\partial f}{\partial c} = \mathbf{\Omega}(f). \tag{23}$$

Without an external force, the Boltzmann equation yields to:

$$\frac{\partial f}{\partial t} + \mathbf{c}\cdot\nabla f = \mathbf{\Omega}(f). \tag{24}$$

The relation between the above equation and macroscopic quantities is as follows:

$$\rho(\mathbf{r}, t) = \int m f(\mathbf{r}, \mathbf{c}, t) d\mathbf{c}, \tag{25}$$

$$\rho(\mathbf{r}, t)\mathbf{u}(\mathbf{r}, t) = \int m\mathbf{c} f(\mathbf{r}, \mathbf{c}, t) d\mathbf{c}, \tag{26}$$

$$\rho(\mathbf{r}, t)e(\mathbf{r}, t) = \frac{1}{2}\int m u_a^2 f(\mathbf{r}, \mathbf{c}, t) d\mathbf{c}, \tag{27}$$

where m is the molecular mass, $\rho(\mathbf{r}, t)$ is density, $\mathbf{u}(\mathbf{r}, t)$ is fluid velocity, $e(\mathbf{r}, t)$ is the internal energy, and $u_a = c - u$ is the relative velocity.

The essential problem when solving the Boltzmann equation is complicated nature of the collision term. Bhatnagar, Gross and Krook (1954) introduced a simplified model for collision operator, changing the collision matrix with:

$$\mathbf{\Omega}(f) = \frac{1}{\tau}(f^{eq} - f), \tag{28}$$

where f_i^{eq} is the equilibrium distribution function, parametrized by local conserved quantities, while τ is typical time-scale associated with collisional relaxation to the local equilibrium. After introducing the BGK approximation, the Boltzmann equation (28) yields to:

$$\frac{\partial f}{\partial t} + \mathbf{c} \cdot \nabla f = \frac{1}{\tau}(f^{eq} - f). \tag{29}$$

In the lattice Boltzmann method, Eq. (29) is discredited and valid along the specific direction i:

$$\frac{\partial f_i}{\partial t} + \mathbf{c}_i \cdot \nabla f_i = \frac{1}{\tau}(f_i - f_i^{eq}). \tag{30}$$

After discretization, the above equation yields to the lattice Boltzmann equation:

$$f_i(r + c_i\Delta t, t + \Delta t) = f_i(r, t) + \frac{\Delta t}{\tau}(f_i^{eq}(r, t) - f_i(r, t)). \tag{31}$$

3.2 The equilibrium distribution function

When applying the LBM for different problems, the crucial element is to find the proper equilibrium distribution function (EDF). For particles moving in a medium with macroscopic velocity **u,** the normalized Maxwell distribution function can be written as:

$$f = \frac{\rho}{2\pi/3} e^{-\frac{3}{2}(\mathbf{c}-\mathbf{u})^2}. \tag{32}$$

Which can further be written as:

$$f = \frac{\rho}{2\pi/3} e^{-\frac{3}{2}c^2} e^{3(\mathbf{c}\cdot\mathbf{u}-u^2)/2}. \tag{33}$$

Applying the Taylor series expansion for the exponential term the above equation yields to:

$$f = \frac{\rho}{2\pi/3} e^{-\frac{3}{2}c^2} \left[1 + 3\,(\mathbf{c}\cdot\mathbf{u}) - \frac{3}{2}u^2 + ...\right]. \tag{34}$$



Figure 6: 1-D lattice arrangements.

The general form of the equilibrium function along the link i can be written as:

$$f_i^{eq} = \Phi\omega_i \left[A + Bc_i \cdot u + C\left(c_i \cdot u\right)^2 + D\right], \tag{35}$$

where u is is the macroscopic flow velocity vector; A, B, C, and D are constants, determined from the conservation principle (mass, momentum, and energy), ω_i is weight factor based on the lattice arrangement, where the condition $\sum_i \omega_i = 1$ must be fulfilled. Φ is scalar parameter which needs to be equal to:

$$\Phi = \sum_i f_i^{eq}. \tag{36}$$

Defining Eq. (35) is the key element when defining LBE for a specific model.

3.3 LBM lattice arrangements

The LBGK model is the most widely used LBM model. The common notation of the lattice arrangements, introduced by Qian et al. (1991), is $DnQb$, where n represents the dimension and b is the number of lattice velocities. Lattice velocities of the $DnQb$ models form lattice tensors of certain rank. The n^{th} rank can be defined as:

$$L_{i_1,i_2,\ldots,i_n} = \sum_i c_{i_1} c_{i_2} \ldots c_{in} \tag{37}$$

Some popular lattice arrangements are show: one-dimensional in Fig.6, two dimensional in Fig.7, and three-dimensional in Fig.8. In Table 1 characteristic lattice velocities, belonging weight ω_i and sound speed c_s^2 are given.

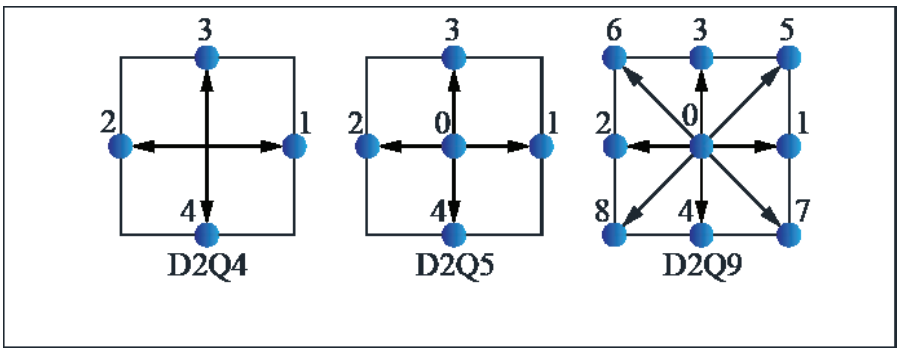


Figure 7: 2-D lattice arrangements.

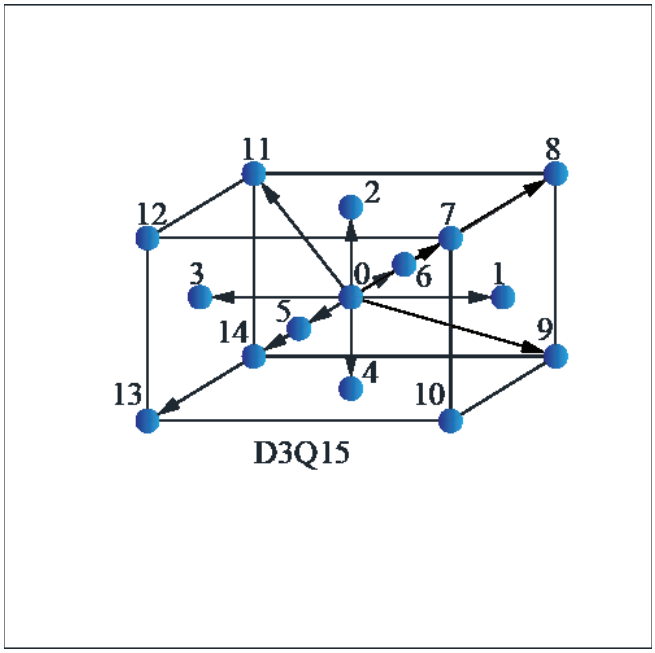


Figure 8: 3-D lattice arrangement.

MODEL	Lattice vector c_i	Weight ω_i	c_s^2
$D1Q3$	0 ± 1	$2/3$ $1/6$	$1/3$
$D1Q5$	0 ± 1 ± 2	$6/12$ $2/12$ $1/12$	1
$D2Q7$	$(0,0)$ $\left(\pm 1/2, \pm\sqrt{3}/2\right)$	$1/2$ $1/12$	$1/4$
$D2Q9$	$(0,0)$ $(\pm 1,0),(0,\pm 1)$ $(\pm 1,\pm 1)$	$4/9$ $1/9$ $1/36$	$1/3$
$D3Q15$	$(0,0,0)$ $(\pm 1,0,0),(0,\pm 1,0),(0,0,\pm 1)$ $(\pm 1,\pm 1,\pm 1)$	$2/9$ $1/9$ $1/72$	$1/3$
$D3Q19$	$(0,0,0)$ $(\pm 1,0,0),(0,\pm 1,0),(0,0,\pm 1)$ $(0,\pm 1,\pm 1),(\pm 1,0,\pm 1),(\pm 1,\pm 1,0)$	$1/3$ $1/18$ $1/36$	$1/3$

Table 1: Some lattice arrangements

A tensor of n^{th} rank is called isotropic if it is invariant with respect to arbitrary orthogonal transformations. (rotations and reflections). Isotropic tensors up to rank 4 are defined as follows:

- 1^{st} rank: There are no isotropic tensors;
- 2^{nd} rank: Isotropic tensors are proportional to the second Kronecker's delta tensor $\delta_{\alpha\beta}$:

$$[\delta_{\alpha\beta}] = \begin{bmatrix} 1 & 0 & 0 \\ 0 & 1 & 0 \\ 0 & 0 & 1 \end{bmatrix} \tag{38}$$

- 3^{rd} rank: Isotropic tensors are proportional to the permutational symbol tensor $\varepsilon_{i\beta\gamma}$ according to the following rules:

$$\varepsilon_{\alpha\beta\gamma} = \begin{cases} 1 & \text{, when } \alpha,\ \beta \text{ and } \gamma \text{ form an even permutation of 1, 2 and 3} \\ -1 & \text{, when } \alpha,\ \beta \text{ and } \gamma \text{ form an odd permutation of 1, 2 and 3} \\ 0 & \text{, when } \alpha,\ \beta \text{ and } \gamma \text{ form do not form an permutation of 1, 2 and 3} \end{cases} \tag{39}$$

- 4^{th} rank: There are three linearly independent isotropic tensors. The general form can be written as:

$$L_{\alpha\beta\gamma\eta} = a\delta_{\alpha\beta}\delta_{\gamma\eta} + b\delta_{\alpha\gamma}\delta_{\beta\eta} + c\delta_{\alpha\eta}\delta_{\beta\gamma}, \tag{40}$$

  where a, b and c are arbitrary constants.

It is easy to find several statical moments of the discrete EDF:

$$\sum_i f_i^{eq} = \rho, \sum_i \mathbf{c}_i f_i^{eq} = \rho\mathbf{u}, \sum_i \mathbf{c}_i\mathbf{c}_i f_i^{eq} = \rho\mathbf{uu}+p\mathbf{I}, \tag{41}$$

$$\sum_i c_{i\alpha}c_{i\beta}c_{i\gamma}f_i^{eq} = c_s^2\rho\left(u_\alpha\delta_{\beta\gamma} + u_\beta\delta_{\alpha\gamma} + u_\gamma\delta_{\alpha\beta}\right). \tag{42}$$

3.4 The Chapman - Enskog expansion

The Navier-Stokes equations (NSE) describe behavior of the fluid particles in the system. The Chapman-Enskog expansion is a multi-scale analysis developed by authors Chapman and Enskog in order to derive the macroscopic NSE from the LBE. As an example, an analysis of D2Q9 model have been performed, with the LBGK evolution equation, derived earlier:

$$f_i(\mathbf{x} + \mathbf{c}_i\partial t, t + \partial t) - f_i(\mathbf{x}, t) = -\frac{1}{\tau}(f_i - f_i^{eq}). \tag{43}$$

and using Eq. (25):

$$\rho = \sum_i f_i, \rho\mathbf{u} = \sum_i \mathbf{c}_i f_i, \rho\mathbf{uu}+p\mathbf{I} = \sum_i \mathbf{c}_i\mathbf{c}_i f_i. \tag{44}$$

First, multiscale expansions are introduced:

$$f_i = f_i^{(0)} + \varepsilon f_i^{(1)} + \varepsilon^2 f_i^{(2)} + O(\varepsilon^3), \tag{45}$$

$$\partial_t = \varepsilon\partial_{t_0} + \varepsilon^2\partial_{t_1},\ \partial_\alpha = \varepsilon\partial_{0\alpha} \tag{46}$$

where ε is a small number proportional to the Knudsen number K_n, ∂_t and ∂_α are short notations for $\partial/\partial t$ and $\partial/\partial x_\alpha$, respectively, t_0 is the fast convective scale, and t_1 is the slow diffusive scale. Applying the second order Taylor series expansion to the LBGK Eq. (43) yields:

$$D_i f_i + \frac{\delta_t}{2}D_i^2 f_i = -\frac{1}{\tau\delta_t}(f_i - f_i^{eq}) + O(\partial_t^2), \tag{47}$$

where $D_i = \partial_t + c_{i\alpha}\partial_\alpha$, according to the Einstein summation rule. Substituting Eq. (46) into Eq. (47), and collecting the elements of each order of ε, yields:

Order ε^0 :

$$f_i^{(0)} = f_i^{eq}; \tag{48}$$

Order ε^1 :

$$D_i^{(0)} f_i^{(0)} = -\frac{1}{\tau\delta_t} f_i^{(1)}; \tag{49}$$

Order ε^2 :

$$\partial_{t_1} f_i^{(0)} + \left(1 - \frac{1}{2\tau}\right) D_i^{(0)} f_i^{(1)} = -\frac{1}{\tau\delta_t} f_i^{(2)} \tag{50}$$

From Eq.(48), using Eqs.(44) and (41) it follows:

$$\sum_i f_i^{(k)} = 0; \ \sum_i \mathbf{c}_i f_i^{(k)} = \mathbf{0} \text{ for } k > 0. \tag{51}$$

Minding Eq. (44), and taking summation over i, Eq. (49) yields to mass conservation equation of order ε :

$$\partial_{t_0}\rho + \nabla_0(\rho\mathbf{u}) = 0. \tag{52}$$

Multiplying Eq. (49) with c_i, and taking summation over i, Eq. (49), momentum conservation equation of order ε is obtained:

$$\partial_{t_0}(\rho\mathbf{u}) + \nabla_0\boldsymbol{\pi}^{(0)} = 0, \tag{53}$$

where $\boldsymbol{\pi}^{(0)} = \rho u_\alpha u_\beta + p\boldsymbol{\delta}_{\alpha\beta}$, where $p = c_s^2\rho$.The following properties of $D2Q9$ model have been used:

$$\sum_i \omega_i c_{i\alpha} = \sum_i \omega_i c_{i\alpha} c_{i\beta} c_{i\gamma} = 0, \tag{54}$$

$$\sum_i \omega_i c_{i\alpha} c_{i\beta} = c_s^2 \boldsymbol{\delta}_{\alpha\beta}, \tag{55}$$

$$\sum_i \omega_i c_{i\alpha} c_{i\beta} c_{i\gamma} c_{i\eta} = c_s^4 \Delta_{\alpha\beta\gamma\eta}, \tag{56}$$

where $\Delta_{\alpha\beta\gamma\eta} = \delta_{\alpha\beta}\delta_{\gamma\eta} + \delta_{\alpha\gamma}\delta_{\beta\eta} + \delta_{\alpha\eta}\delta_{\beta\gamma}$. In the similar way, zeroth and first statical moment leads to equations of the order ε^2 :

$$\partial_{t_1}\rho = 0, \tag{57}$$

$$\partial_{t_1}(\rho\mathbf{u}) + \left(1 - \frac{1}{2\tau}\right)\nabla_0\boldsymbol{\pi}^{(1)} = 0, \tag{58}$$

where the term $\boldsymbol{\pi}^{(1)}_{\alpha\beta} = \sum_i c_{i\alpha}c_{i\beta}f_i^{(1)}$ needs to be evaluated. Multiplying Eq. (49) by $c_{i\alpha}c_{i\beta}$ and taking the sum over i yields to:

$$-\frac{1}{\tau\delta_t}c_{i\alpha}c_{i\beta}f_i^{(1)} = c_s^2\rho\left[\partial_{0\alpha}u_\beta + \partial_{0\beta}u_\alpha\right] + O(M^3), \tag{59}$$

where M is the Mash number. From Eq. (59) yields $\boldsymbol{\pi}^{(1)}_{\alpha\beta} = \tau p\delta_t\left[\partial_{0\alpha}u_\beta + \partial_{0\beta}u_\alpha\right]$, after neglecting terms of $O(M^3)$. Combining the mass and momentum conservation equations for both scales the NS equations are obtained:

$$\partial_t\rho + \nabla\cdot(\rho\mathbf{u}) = 0, \tag{60}$$

$$\frac{\partial(\rho\mathbf{u})}{\partial t} + \nabla(\rho\mathbf{u}\mathbf{u}) = -\nabla p + \nabla\cdot\left[\rho\nu(\nabla\mathbf{u}+\nabla\mathbf{u}^T)\right], \tag{61}$$

where kinematic viscosity is $\nu = c_s^2\left(1-\frac{\tau}{2}\right)\delta_t$. For the small Mach number, the density variations are negligible, and incompressible NSE are obtained:

$$\nabla\cdot\mathbf{u} = 0, \tag{62}$$

$$\frac{\partial\mathbf{u}}{\partial t} + \mathbf{u}\cdot\nabla\mathbf{u} = -\frac{1}{\rho}\nabla p + \nu\nabla^2\mathbf{u}. \tag{63}$$

3.5 Improved lattice Boltzmann models

Generally, fluid flows are under the influence of internal and external forces, such as gravity or intermolecular interactions. Such forces need to be implemented into the basic LBE defined by Eq. (19). Numerous methods have been proposed depending on the physics of the model, and selected few will be introduced.

3.5.1 LBM Scheme with modified equilibrium distribution function

Force term can be included into LBE by modifying the EDF. Convenient form of the EDF as function of density and fluid velocity will be used:

$$f_i^{eq} = \omega_i u\left[1 + \frac{\mathbf{c}_i\cdot\mathbf{u}}{c_s^2} + \frac{(\mathbf{c}_i\cdot\mathbf{u})^2}{2c_s^4} - \frac{\mathbf{u}^2}{2c_s^2}\right]. \tag{64}$$

In the case when the force is induced by a potential Φ and the density variation is small, Buick and Greated (2000) proposed the following EDF:

$$\overline{f}_0^{eq} = \rho\left[1-(1-\omega_0)\frac{p(\Phi)}{c_s^2\rho}-\omega_0\frac{u^2}{2c_s^2}\right], \tag{65}$$

$$\overline{f}_i^{eq} = \omega_i\rho\left[\frac{p(\Phi)}{c_s^2\rho}+\frac{c_i\cdot u}{c_s^2}+\frac{(c_i\cdot u)^2}{2c_s^4}-\frac{u^2}{2c_s^2}\right], i\neq 0, \tag{66}$$

where $p(\Phi)=(c_s^2+\Phi)\rho$, and $\rho u=\sum_i c_i f_i$.For the EDF in this form, zeroth, first and third statical moment are the same as those for the standard $DnQb$ models (Eq. (41)). The second statical moment yields to:

$$\sum_i c_{i\alpha}c_{i\beta}\overline{f}_i^{eq} = p(\Phi)\delta_{\alpha\beta}+\rho u_\alpha u_\beta. \tag{67}$$

Now, the momentum flux at the order ε in the Chapman-Enskog expansion is:

$$\boldsymbol{\pi}_{\alpha\beta}^{(1)} = -\tau\delta_t\left[c_s^2\rho(\partial_{0\alpha}u_\beta+\partial_{0\beta}u_\alpha)+\partial_{t_0}\partial_{0\alpha}(\rho\Phi)-\partial_\beta(u_\alpha\partial_{0\beta}(\rho\Phi)+u_\beta\partial_{0\alpha}(\rho\Phi))\right], \tag{68}$$

and momentum equation yields to:

$$\frac{\partial(\rho\mathbf{u})}{\partial t}+\nabla(\rho\mathbf{uu}) = -\nabla(c_s^2\rho)+\nabla\cdot\left[\rho\nu(\nabla\mathbf{u}+\nabla\mathbf{u}^T)\right]+\mathbf{F}+R, \tag{69}$$

where the residual term is:

$$R = \tau\delta_t\left[-\partial_t F_\alpha+\partial_\beta(u_\alpha F_\beta+u_\beta F_\alpha)\right]. \tag{70}$$

In general, this term does not vanish and bring additional error, but most often the error is negligible.

3.5.2 Introduction of the forcing term

Another popular way to imply the body force is to add a forcing term to the LBE as follows:

$$f_i(\mathbf{x}+\mathbf{c}_i\partial t, t+\partial t)-f_i(\mathbf{x},t) = -\frac{1}{\tau}(f_i-f_i^{eq})+\delta_t\mathbf{F}_i. \tag{71}$$

where the forcing term $\mathbf{F}_i$ depends on the body force $\mathbf{F}$. A variety of expressions for $\mathbf{F}_i$ have been proposed. In nature of this research, a centered-scheme forcing term proposed by Zhou (2004), proposed in order do derive the lattice Boltzmann model for the shallow water equations (LBMSWE), will be presented.

The force term is evaluated at the mid-point between the lattice point and its neighboring lattice point as:

$$F_i = F_i\left(\mathbf{x} + \frac{1}{2}\mathbf{c}_\alpha \Delta t, t + \frac{1}{2}\Delta t\right). \tag{72}$$

A Chapman-Enskog expansion will be applied on D2Q9 LBGK model with LBE in form:

$$f_\alpha(x + e_\alpha \Delta t, t + \Delta t) = f_\alpha(x,t) - \frac{1}{\tau}(f_\alpha - f_\alpha^{eq}) + \frac{\Delta t}{6e^2} e_{\alpha i} F_i \tag{73}$$

,where following notation is used: α denotes the lattice link, Δt is time step, e_α is lattice velocity along the link α defines as

$$e_\alpha = \begin{cases} (0,0) & ,\alpha = 0 \\ e\left[\cos\frac{(\alpha-1)\pi}{4}, \sin\frac{(\alpha-1)\pi}{4}\right] & ,\alpha = 1,3,5,7 \\ \sqrt{2}e\left[\cos\frac{(\alpha-1)\pi}{4}, \sin\frac{(\alpha-1)\pi}{4}\right] & ,\alpha = 2,4,6,9 \end{cases}. \tag{74}$$

The EDF is defined as:

$$f_\alpha^{eq} = \begin{cases} h - \frac{5g_r h^2}{6e^2} - \frac{2h}{3e^2}u_i u_i & ,\alpha = 0 \\ \frac{g_r h^2}{6e^2} + \frac{h}{3e^2}e_{\alpha i}u_i + \frac{h}{2e^4}e_{\alpha i}u_i e_{\alpha j}u_j - \frac{h}{6e^2}u_i u_i & ,\alpha = 1,3,5,7 \\ \frac{g_r h^2}{24e^2} + \frac{h}{12e^2}e_{\alpha i}u_i + \frac{h}{8e^4}e_{\alpha i}u_i e_{\alpha j}u_j - \frac{h}{24e^2}u_i u_i & ,\alpha = 2,4,6,9 \end{cases}. \tag{75}$$

Taylor series expansion of the LHS of Eq. (71) yields:

$$f_\alpha(x + e_\alpha \Delta t, t + \Delta t) - f_\alpha(x,t) = \varepsilon\left(\frac{\partial}{\partial t} + e_\alpha \frac{\partial}{\partial x}\right) f_\alpha + \frac{1}{2}\varepsilon^2\left(\frac{\partial}{\partial t} + e_\alpha \frac{\partial}{\partial x}\right)^2 f_\alpha + O(\varepsilon^3). \tag{76}$$

The distribution function f_α is expanded as

$$f_\alpha = f_\alpha^{(0)} + \varepsilon f_\alpha^{(1)} + \varepsilon^2 f_\alpha^{(2)} + O(\varepsilon^3), \tag{77}$$

while the centered-scheme force term is expressed as

$$F_i\left(x + \frac{1}{2}e_\alpha \Delta t, t + \frac{1}{2}\Delta t\right) = F_i(x,t) + \frac{1}{2}\varepsilon\left(\frac{\partial}{\partial t} + e_{\alpha j}\frac{\partial}{\partial x_j}\right) F_{\alpha i} + O(\varepsilon^2). \tag{78}$$

Substituting Eqs. (76), (77), (78) into Eq. (73) the evaluating to order ε^0 yields

$$f_\alpha^{(0)} = f_\alpha^{eq}, \tag{79}$$

to order ε is obtained:

$$\left(\frac{\partial}{\partial t}+e_{\alpha j}\frac{\partial}{\partial x_j}\right)f_\alpha^{(0)}=-\frac{1}{\tau}f_\alpha^{(1)}+\frac{e_{\alpha i}}{6e^2}F_i, \tag{80}$$

and to the order ε^2 yields to:

$$\left(\frac{\partial}{\partial t}+e_{\alpha j}\frac{\partial}{\partial x_j}\right)f_\alpha^{(1)}+\frac{1}{2}\left(\frac{\partial}{\partial t}+e_{\alpha j}\frac{\partial}{\partial x_j}\right)^2 f_\alpha^{(0)}=-\frac{1}{\tau}f_\alpha^{(2)}+\frac{1}{12e^2}\left(\frac{\partial}{\partial t}+e_{\alpha j}\frac{\partial}{\partial x_j}\right)e_{\alpha i}F_i, \tag{81}$$

Substituting Eq. (80) into Eq. (81) leads to

$$\left(1-\frac{1}{2\tau}\right)\left(\frac{\partial}{\partial t}+e_{\alpha j}\frac{\partial}{\partial x_j}\right)f_\alpha^{(1)}=-\frac{1}{\tau}f_\alpha^{(2)}. \tag{82}$$

Taking $\sum_\alpha\left[(80)+\varepsilon(82)\right]$, and enforcing conditions $\sum_\alpha f_\alpha^{(n)}=0$, and $\sum_\alpha e_\alpha f_\alpha^{(n)}=0$, for $n\geq 1$ gives

$$\frac{\partial}{\partial t}\left(\sum_\alpha f_\alpha^{(0)}\right)+\frac{\partial}{\partial x_j}\left(\sum_\alpha e_{\alpha j}f_\alpha^{(0)}\right)=0. \tag{83}$$

Evaluation of the terms in the above equation results in the second-order accurate continuity equation. Now, taking $\sum_\alpha e_\alpha\left[(80)+\varepsilon(82)\right]$ provides

$$\frac{\partial}{\partial t}\left(\sum_\alpha e_{\alpha i}f_\alpha^{(0)}\right)+\frac{\partial}{\partial x_j}\left(\sum_\alpha e_{\alpha i}e_{\alpha j}f_\alpha^{(0)}\right)+\varepsilon\left(1-\frac{1}{2\tau}\right)\frac{\partial}{\partial x_j}\left(\sum_\alpha e_{\alpha i}e_{\alpha j}f_\alpha^{(1)}\right)=F_i. \tag{84}$$

Using

$$\sum_\alpha f_\alpha^{(0)}=h, \tag{85}$$

$$\sum_\alpha e_{\alpha i}f_\alpha^{(0)}=hu_i, \tag{86}$$

$$\sum_\alpha e_{\alpha i}e_{\alpha j}f_\alpha^{(0)}=\frac{g_r h^2}{2}\delta_{ij}+hu_iuj, \tag{87}$$

where h is the averaged depth, Eqs. (83) and (84) yield to:

$$\frac{\partial h}{\partial t}+\frac{\partial}{\partial x_j}\left(hu_j\right)=0, \tag{88}$$

$$\frac{\partial}{\partial t}\left(hu_i\right)+\frac{\partial}{\partial x_j}\left(hu_iuj\right)=-g_r\frac{\partial}{\partial x_i}\left(\frac{h^2}{2}\right)-\frac{\partial}{\partial x_j}\Lambda_{ij}+F_i. \tag{89}$$

where

$$\Lambda_{ij}=\varepsilon\left(1-\frac{1}{2\tau}\right)\sum_\alpha e_{\alpha i}e_{\alpha j}f_\alpha^{(1)}. \tag{90}$$

Using Eqs. (74), (75) and (80), following expression is obtained:

$$\Lambda_{ij} \approx -\nu \left(\frac{\partial}{\partial x_j} (hu_i) + \frac{\partial}{\partial x_i} (hu_j) \right). \tag{91}$$

Substituting Eq. (91) into (89) yields to:

$$\frac{\partial}{\partial t} (hu_i) + \frac{\partial}{\partial x_j} (hu_i uj) = -g_r \frac{\partial}{\partial x_i} \left(\frac{h^2}{2} \right) + \nu \frac{\partial^2 (hu_i)}{\partial x_j \partial x_j} + F_{i.} \tag{92}$$

The forcing term is defined as:

$$F_i = -g_r h \frac{\partial Z_b}{\partial xi} - \frac{\tau_{wi}}{\rho} - \frac{\tau_{bi}}{\rho} + E_i, \tag{93}$$

where τ_{wi} and $\tau_{bi,}$ are wind shear stress and bed shear stress, respectively, Z_b is the bed elevation, and E_i is the Coriolis term. Eq. (92) yields:

$$\begin{aligned} \frac{\partial}{\partial t} (hu_i) + \frac{\partial}{\partial x_j} (hu_i uj) = -g_r \frac{\partial}{\partial x_i} \left(\frac{h^2}{2} \right) + \nu \frac{\partial^2 (hu_i)}{\partial x_j \partial x_j} \\ -gh \frac{\partial Z_b}{\partial xi} - \frac{\tau_{wi}}{\rho} - \frac{\tau_{bi}}{\rho} + E_i. \end{aligned} \tag{94}$$

Eq. (88) into (94) are the shallow water equations.

3.5.3 Enhanced LBMSWE model

In the LABSWE, the centred scheme force term includes the evaluation of the first derivative a bed slope, term which is inconsistent with the spirit of the lattice Boltzmann hydrodynamics. Therefore, Zhou (2011) proposed a novel incorporation of that term into the lattice Boltzmann equation, and eliminated the calculation of the derivative. The proposed D2Q9 lattice Boltzmann equation, with lattice velocities defined with Eq. (74), is:

$$\begin{aligned} f_\alpha(x + e_\alpha \Delta t, t + \Delta t) = f_\alpha(x,t) - \frac{1}{\tau}(f_\alpha - f_\alpha^{eq}) \\ -\frac{g_r h}{6e^2} \left[Z_b(x + e_\alpha \Delta t, t) - Z_b(x,t) \right] + \frac{\Delta t}{6e^2} e_{\alpha i} F_i. \end{aligned} \tag{95}$$

The EDF is given by Eqs. (75) and the force term is:

$$F_i = -\frac{\tau_{wi}}{\rho} - \frac{\tau_{bi}}{\rho} + E_i. \tag{96}$$

The second term from the RHS of Eq. (95) is new in comparison with the LBMSWE (Eq. (73)). The CE expansion will be conducted. Taking the Taylor expansion of the second

term of the RHS of Eq. (95) leads to:

$$-\frac{g_r}{6e^2}\left[h+\frac{\varepsilon}{2}\left(\frac{\partial}{\partial t}+e_{\alpha j}\frac{\partial}{\partial x_j}\right)h\right]\left(\varepsilon e_{\alpha j}\frac{\partial Z_b}{\partial x_j}+\frac{\varepsilon^2}{2}e_{\alpha i}e_{\alpha j}\frac{\partial^2 Z_b}{\partial x_i \partial x_j}Z_b\right)+O(\varepsilon^3). \tag{97}$$

The term of order ε is:

$$-\frac{g_r}{6e^2}he_{\alpha j}\frac{\partial Z_b}{\partial x_j}, \tag{98}$$

and terms of order ε^2 are:

$$-\frac{g_r h}{12e^2}e_{\alpha i}e_{\alpha j}\frac{\partial^2 Z_b}{\partial x_i \partial x_j}-\frac{g_r e_{\alpha j}}{12}\left(\frac{\partial h}{\partial t}+e_{\alpha j}\frac{\partial h}{\partial x_j}\right)\frac{\partial Z_b}{\partial x_j}. \tag{99}$$

Adding this terms to Eqs. (80) and (81) leads to:

$$\left(\frac{\partial}{\partial t}+e_{\alpha j}\frac{\partial}{\partial x_j}\right)f_\alpha^{(0)}=-\frac{1}{\tau}f_\alpha^{(1)}-\frac{g_r}{6e^2}he_{\alpha j}\frac{\partial Z_b}{\partial x_j}+\frac{e_{\alpha i}}{6e^2}F_i, \tag{100}$$

$$\left(\frac{\partial}{\partial t}+e_{\alpha j}\frac{\partial}{\partial x_j}\right)f_\alpha^{(1)}+\frac{1}{2}\left(\frac{\partial}{\partial t}+e_{\alpha j}\frac{\partial}{\partial x_j}\right)^2 f_\alpha^{(0)}=-\frac{1}{\tau}f_\alpha^{(2)}-\frac{g_r h}{12e^2}e_{\alpha i}e_{\alpha j}\frac{\partial^2 Z_b}{\partial x_i \partial x_j} \tag{101}$$

$$-\frac{g_r e_{\alpha j}}{12}\left(\frac{\partial h}{\partial t}+e_{\alpha j}\frac{\partial h}{\partial x_j}\right)\frac{\partial Z_b}{\partial x_j}+\frac{1}{12e^2}\left(\frac{\partial}{\partial t}+e_{\alpha j}\frac{\partial}{\partial x_j}\right)e_{\alpha i}F_i. \tag{102}$$

Substituting Eq. (100) into Eq. (101) leads to the unchanged Eq. (82).Taking $\sum_\alpha[(100)+\varepsilon(82)]$, and enforcing conditions $\sum_\alpha f_\alpha^{(n)}=0$, and $\sum_\alpha e_\alpha f_\alpha^{(n)}=0$, for $n\geq 1$ gives

$$\frac{\partial}{\partial t}\left(\sum_\alpha f_\alpha^{(0)}\right)+\frac{\partial}{\partial x_j}\left(\sum_\alpha e_{\alpha j}f_\alpha^{(0)}\right)=0. \tag{103}$$

Evaluation of the terms in the above equation gives the continuity equation, which is second-order accurate. Now, taking $\sum_\alpha e_\alpha[(80)+\varepsilon(82)]$ provides

$$\frac{\partial}{\partial t}\left(\sum_\alpha e_{\alpha i}f_\alpha^{(0)}\right)+\frac{\partial}{\partial x_j}\left(\sum_\alpha e_{\alpha i}e_{\alpha j}f_\alpha^{(0)}\right)+\varepsilon\left(1-\frac{1}{2\tau}\right)\frac{\partial}{\partial x_j}\left(\sum_\alpha e_{\alpha i}e_{\alpha j}f_\alpha^{(1)}\right) \tag{104}$$

$$=-g_r h\frac{\partial Z_b}{\partial x_i}+F_{i.} \tag{105}$$

After the terms are evaluated and some algebra, the above equation becomes the second-order accurate momentum conservation equation.

CHAPTER IV

MATHEMATICAL FORMULATION OF THE LBM MODEL

In this chapter, the goal is to develop a functional lattice Boltzmann model for one-dimensional unsteady open-channel flow with sediment transport for natural watercourses. One-dimensional unsteady flow is described by the shallow water equations, also known as the Saint-Venant equations. For the sediment transport model, suspended-sediment is detached from the bed and near-bed sediment. Sediment mixture is represented as a collection of a suitable number of sediment size-classes. Mass-conservation equations are defined for suspended-sediment and the active-layer for each sediment size-class separately, followed with the global active-layer and stratum mass-conservation equation. Governing equations include the exchange mechanisms between the sub-domains.

Uniformity of the lattice structure results with a decrease of the efficiency and the applicability of the lattice models when especially when natural, arbitrary geometry are modelled. In order to eliminate this restriction and maintain the basic features of the lattice Boltzmann model, geometric transformation between the physical and computational domain is introduced, and in this way the limitations of the LBM are spanned. This technique is often used in traditional CFD for managing complex geometries – it enables calculation of terms defined in the non-equidistant physical space in the equidistant grid computational frame. In this way utilization of the standard uniform lattice based models is not restricted on the physical domains with uniform computational grid.

Corresponding LBM models are developed, deriving new forms of the equilibrium distribution functions based on the transformed unsteady flow and sediment equations. A LBM model for unsteady flow is autonomous, while the LBM model for sediment transport can be attached to a flow model. A LBGK model Eq. (19) is used with the centered-sheme forcing term Eq.72. Some additional terms are added to the LBM model, based on the

enhanced LBMSWE proposed by Zhou, in order to obtain governing equations after the CE expansion.

To derive a fully operational mathematical model which can be applied on natural watercourses characterized by arbitrary cross-section geometry and variable longitudinal profile (river bifurcation, meandering, contraction and expansion), set of appropriate inner and outer boundary conditions are defined.

4.1 One-dimensional unsteady open-channel flow lattice Boltzmann model

The motion of incompressible Newtonian viscous fluid is described by the well known Navier-Stokes equations (NSE), written herein in tensor notation (Lai, (1991)). The first equation is the continuity equation:

$$\frac{\partial u_j}{\partial x_j} = \mathbf{0}, \tag{106}$$

and the following equation are the equations of motion

$$\rho\left(\frac{\partial u_i}{\partial t} + u_j\frac{u_i}{\partial x_j}\right) = \rho B_i - \frac{\partial p}{\partial x_i} + \mu\frac{\partial^2 u_i}{\partial x_j \partial x_j}, \tag{107}$$

where ρ is mass density, u_i is i-direction component of flow velocity, x_i is i-coordinate direction, B_i is body force for unit mass, and p is hydrostatic pressure.

The one-dimensional Saint-Venant equations (SVE) are a set of partial differential equations that describe the incompressible flow below the pressure surface in a open channel flow of an arbitrary cross section. The SVE are derived from the NSE under following assumptions:

- Flow is one-dimensional. The horizontal length scale is much greater then the vertical length scale;
- The river bed is gradually sloped;
- The pressure inside the water flow obeys the hydrostatic law;
- The cross section of the water surface is horizontal;

- The flow is smoothly varying;
- The water discharge $Q(x,t)$ and the free surface elevation $Z(x,t)$ are averaged over the cross section.

There are four basic formulations of the SVE depending on the dependent variables involved. Which form is used is determined by practical limitations like geometry or complexity of the examined flow cases. When flow systems with simple cross sectional geometry and straightforward presentation of bed slope are considered, discharge-sectional area form of the SVE is used. However, when natural watercourses with complex cross sectional and longitudinal geometry are modelled, like in this thesis, this form becomes inadequate. Hence, the hybrid discharge-water surface elevation form of the SVE is adopted, as follows

$$\frac{\partial A}{\partial t} + \frac{\partial Q}{\partial x} = q \tag{108}$$

$$\frac{\partial Q}{\partial t} + \frac{\partial}{\partial x}\left(\omega \frac{Q^2}{A}\right) = -g_r A \frac{\partial Z}{\partial x} - grAS_f, \tag{109}$$

where $A(x,t)$ is cross-sectional area; $Q(x,t)$ is discharge; $Z(x,t)$ is free surface elevation, $q(x,t)$ is lateral inflow per unit length, g_r is the gravitational acceleration; t is time; x is the Cartesian coordinate; and and ω is the coefficient of velocity non-uniformity. S_f represents the friction slope defined as

$$S_f = \frac{n^2 Q^2}{A^2 R^{4/3}} \tag{110}$$

where n is Manning's roughness coefficient and R is hydraulic radius formulated as $R = A/O$, where O is wetted perimeter. The first equation, Eq. (108) is the continuity equation (CE), derived from the mass conservation law, while the second equation Eq. (109) is the momentum equation (ME), derived from the conservation of linear momentum law. The main reason this form of SVE is chosen is completely eliminated bed slope term from the system of equations, leading to a more flexible and practical form of the SVE, and therefore this form is suitable when applied to natural watercourses with complex and non-uniform geometry.

4.1.1 Transformation of the SVE using the adaptive grid technique

By applying the basic rules of coordinate transformation between two systems (Simmonds (1994)), Eqs. (108) and (109) will be transformed to the alternative coordinate system. The goal is to eliminate the $\frac{\partial}{\partial x}$ term, and transform it into $\frac{\partial}{\partial \xi}$, where ξ represents the new coordinate, which forms the equidistant grid, without changing the other dependant variables. We apply the transformation on the one-dimensional CE, Eq. (108), in form:

$$\frac{\partial A}{\partial t} + \frac{\partial Q}{\partial \xi}\frac{\partial \xi}{\partial x} = q, \tag{111}$$

then we multiply it with transformation term $Y = \partial x/\partial \xi$, so the Eq. (111) becomes

$$\frac{\partial}{\partial t}(YA) + \frac{\partial Q}{\partial \xi} = qY, \tag{112}$$

which is the desired form. We apply the same transformation on the ME, Eq. (109):

$$\frac{\partial Q}{\partial t} + \frac{\partial}{\partial \xi}\left(\omega\frac{Q^2}{A}\right)\frac{\partial \xi}{\partial x} = -gA\frac{\partial Z}{\partial \xi}\frac{\partial \xi}{\partial x} - g_r A S_f, \tag{113}$$

then, again we introduce the replacement $Y = \partial x/\partial \xi$ in the equation above, and apply the derivative of product rule:

$$\frac{\partial}{\partial \xi}\left(\omega\frac{Q^2}{YA}\right) = \frac{\partial}{\partial \xi}\left(\omega\frac{Q^2}{A}\right)Y^{-1} + \omega\frac{Q^2}{A}\frac{\partial\left(Y^{-1}\right)}{\partial \xi}, \tag{114}$$

so the ME equation finally becomes

$$\frac{\partial Q}{\partial t} + \frac{\partial}{\partial \xi}\left(\omega\frac{Q^2}{YA}\right) = -\frac{g_r A}{Y}\frac{\partial Z}{\partial \xi} - gAS_f + \omega\frac{Q^2}{A}\frac{\partial\left(Y^{-1}\right)}{\partial \xi}. \tag{115}$$

To summaries, the final, transformed form of the SVE, which will be used in the LB model is the following set of equations:

$$\frac{\partial}{\partial t}(YA) + \frac{\partial Q}{\partial \xi} = qY, \tag{116}$$

$$\frac{\partial Q}{\partial t} + \frac{\partial}{\partial \xi}\left(\omega\frac{Q^2}{YA}\right) = -\frac{g_r A}{Y}\frac{\partial Z}{\partial \xi} - gAS_f + \omega\frac{Q^2}{A}\frac{\partial\left(Y^{-1}\right)}{\partial \xi}. \tag{117}$$

4.1.2 The lattice Boltzmann model for the transformed SVE

In this thesis a D1Q3 lattice LBGK model is used, as shown in Fig. (6). The evolution equation is defined as:

$$\begin{aligned} f_\alpha(\xi + e_\alpha \Delta t, t + \Delta t) = f_\alpha(\xi, t) - \frac{1}{\tau_f}(f_\alpha - f_\alpha^{eq}) \\ + \frac{\Delta t}{2e^2} e_\alpha (F_\alpha + e_\alpha q Y) \\ - \frac{g\overline{A}}{2\overline{Y}e^2} \left[Z(\xi + e_\alpha \Delta t, t) - Z(\xi, t) \right] \\ + \frac{\omega}{2e^2} \overline{\left(\frac{Q^2}{A} \right)} \left[Y^{-1}(\xi + e_\alpha \Delta t) - Y^{-1}(\xi) \right], \end{aligned} \tag{118}$$

where f_α is the particle distribution function (DF) along the α link, f_α^{eq} is the local equilibrium distribution function; ξ is the position vector in the 1D domain; Δt is time step; F_α is the force term; τ_f is relaxation time; e_α is the particle velocity vector along the α link; $e = \Delta\xi/\Delta t$ and $\Delta\xi$ are the lattice sizes. To make the model fully consistent with the nature of the LBM, procedure proposed by Zhou (2011) is adopted for the first and third term on the RHS of Eq. (118). Terms noted $\overline{*}$ are evaluated using the centered-sheme as follows:

$$\begin{aligned} \overline{A} &= A\left(\xi + \frac{1}{2} e_\alpha \Delta t, t + \frac{1}{2}\Delta t \right) \\ \overline{Y} &= Y\left(\xi + \frac{1}{2} e_\alpha \Delta t, t + \frac{1}{2}\Delta t \right) \\ \overline{\left(\frac{Q^2}{A} \right)} &= \left(\frac{Q^2}{A} \right) \left(\xi + \frac{1}{2} e_\alpha \Delta t, t + \frac{1}{2}\Delta t \right) \end{aligned} \tag{119}$$

It should be noted that Eq. (118) is defined using the new ξ-domain, therefore the required symmetry for the discrete particle velocities e_α is ensured. For the three-velocity lattice particle velocities are defined as

$$e_\alpha = \begin{cases} 0 & , \alpha = 0, \\ e & , \alpha = 1, \\ -e & , \alpha = 2, \end{cases} \tag{120}$$

The equilibrium distribution function (EDF) must satisfy following relations :

$$\begin{aligned} \sum_{\alpha} f_{\alpha}^{eq} &= AY \\ \sum_{\alpha} e_{\alpha} f_{\alpha}^{(eq)} &= Q \\ \sum_{\alpha} e_{\alpha} e_{\alpha} f_{\alpha}^{(eq)} &= \omega \frac{Q^2}{YA}, \end{aligned} \tag{121}$$

so, the proposed equilibrium distribution function is

$$f_{\alpha}^{eq} = \begin{cases} YA - \frac{1}{e^2}\frac{\omega Q^2}{YA} & , \alpha = 0 \\ \frac{Q}{2e} + \frac{1}{2e^2}\frac{\omega Q^2}{YA} & , \alpha = 1 \\ -\frac{Q}{2e} + \frac{1}{2e^2}\frac{\omega Q^2}{YA} & , \alpha = 2. \end{cases} \tag{122}$$

The force term is simulated as

$$F_{\alpha} = -\frac{g n^2 Q^2}{A R^{4/3}} \tag{123}$$

to ensure second-order accuracy to the method, the force term is evaluated using the centered-sheme. Its values are calculated halfway between the lattice points and its neighboring lattice points as

$$F_{\alpha} = F_{\alpha}\left(\xi + \frac{1}{2} e_{\alpha} \Delta t, t + \frac{1}{2}\Delta t\right). \tag{124}$$

The physical variables of cross-section area A and discharge Q can be calculated as the zeroth and first statical moment as follows

$$A(\xi, t) = \frac{1}{Y}\sum_{\alpha} f_{\alpha}(\xi, t) \tag{125}$$

$$Q(\xi, t) = \sum_{\alpha} e_{\alpha} f_{\alpha}(\xi, t). \tag{126}$$

4.1.3 Derivation of the transformed Saint-Venant equations from the lattice Boltzmann equation

The goal is to develop Eqs. (116) and (117) from the lattice Boltzmann equation (118), and the relations (120)-(125). The Chapman-Enskog analysis will be applied. The first step is applying Taylors expansion to the each term of the Eq. (118) in time and space. The first

term on the LHS of the Eq. (118), assuming $\Delta t = \varepsilon$, becomes

$$f_\alpha(\xi + e_\alpha \Delta t, t + \Delta t) - f_\alpha(\xi, t) = \varepsilon \left(\frac{\partial}{\partial t} + e_\alpha \frac{\partial}{\partial \xi} \right) f_\alpha + \frac{1}{2}\varepsilon^2 \left(\frac{\partial}{\partial t} + e_\alpha \frac{\partial}{\partial \xi} \right)^2 f_\alpha + O(\varepsilon^3). \tag{127}$$

The distribution function f_α is expanded as

$$f_\alpha = f_\alpha^{(0)} + \varepsilon f_\alpha^{(1)} + \varepsilon^2 f_\alpha^{(2)} + O(\varepsilon^3), \tag{128}$$

while the centered-sheme force term is expressed as

$$F_\alpha \left(\xi + \frac{1}{2} e_\alpha \Delta t, t + \frac{1}{2}\Delta t \right) = F_\alpha + \frac{1}{2}\varepsilon \left(\frac{\partial}{\partial t} + e_\alpha \frac{\partial}{\partial \xi} \right) F_\alpha + O(\varepsilon^2). \tag{129}$$

Taylor series expansion can also be applied to the last two terms on the RHS of Eq. (118), resulting

$$\frac{g\overline{A}}{2\overline{G}e^2} \left[Z(\xi + e_\alpha \Delta t, t) - Z(\xi, t) \right] = \frac{g}{2e^2} \left[\frac{A}{Y} + \frac{\varepsilon}{2} \left(\frac{\partial}{\partial t} + e_\alpha \frac{\partial}{\partial \xi} \right) \frac{A}{Y} \right] \left[\varepsilon \left(\frac{\partial}{\partial t} + e_\alpha \frac{\partial}{\partial \xi} \right) Z + \frac{\varepsilon^2}{2} \left(\frac{\partial}{\partial t} + e_\alpha \frac{\partial}{\partial \xi} \right)^2 Z \right] + O(\varepsilon^3), \tag{130}$$

$$\frac{\omega}{2e^2} \overline{\left(\frac{Q^2}{A} \right)} \left[Y^{-1}(\xi + e_\alpha \Delta t) - Y^{-1}(\xi) \right] = \frac{1}{2e^2} \left[\omega \frac{Q^2}{A} + \frac{\varepsilon}{2} \left(\frac{\partial}{\partial t} + e_\alpha \frac{\partial}{\partial \xi} \right) \omega \frac{Q^2}{A} \right] \left[\varepsilon \left(\frac{\partial}{\partial t} + e_\alpha \frac{\partial}{\partial \xi} \right) Y^{-1} + \frac{\varepsilon^2}{2} \left(\frac{\partial}{\partial t} + e_\alpha \frac{\partial}{\partial \xi} \right)^2 Y^{-1} \right] + O(\varepsilon^3). \tag{131}$$

Substituting Eqs. (127), (128), (129), (130) and (131) into Eq. (118) the evaluation to order ε^0 is

$$f_\alpha^{(0)} = f_\alpha^{eq}, \tag{132}$$

to order ε it is

$$\left(\frac{\partial}{\partial t} + e_\alpha \frac{\partial}{\partial \xi} \right) f_\alpha^{(0)} = -\frac{1}{\tau_f} f_\alpha^{(1)} + \frac{e_\alpha}{2e^2} \left(F_\alpha + e_\alpha q Y \right) - \frac{gA}{2Ye^2} \left(\frac{\partial}{\partial t} + e_\alpha \frac{\partial}{\partial \xi} \right) Z + \frac{\omega Q^2}{2Ae^2} \left(\frac{\partial}{\partial t} + e_\alpha \frac{\partial}{\partial \xi} \right) Y^{-1}, \tag{133}$$

and to the order ε^2 it is

$$\left(\frac{\partial}{\partial t}+e_\alpha\frac{\partial}{\partial \xi}\right)f_\alpha^{(1)}+\frac{1}{2}\left(\frac{\partial}{\partial t}+e_\alpha\frac{\partial}{\partial \xi}\right)^2 f_\alpha^{(0)}=-\frac{1}{\tau_f}f_\alpha^{(2)}+\frac{e_\alpha}{4e^2}\left(\frac{\partial}{\partial t}+e_\alpha\frac{\partial}{\partial \xi}\right)F_\alpha \tag{134}$$
$$-\frac{gA}{4Ye^2}\left(\frac{\partial}{\partial t}+e_\alpha\frac{\partial}{\partial \xi}\right)^2 Z-\frac{g_r}{4e^2}\left(\frac{\partial}{\partial t}+e_\alpha\frac{\partial}{\partial \xi}\right)\frac{A}{Y}\left(\frac{\partial}{\partial t}+e_\alpha\frac{\partial}{\partial \xi}\right)Z$$
$$+\frac{\omega Q^2}{4Ae^2}\left(\frac{\partial}{\partial t}+e_\alpha\frac{\partial}{\partial \xi}\right)^2 Y^{-1}+\frac{1}{4e^2}\left(\frac{\partial}{\partial t}+e_\alpha\frac{\partial}{\partial \xi}\right)\omega\frac{Q^2}{A}\left(\frac{\partial}{\partial t}+e_\alpha\frac{\partial}{\partial \xi}\right)Y^{-1}.$$

Substituting Eq. (133) into Eq. (134) leads to

$$\left(1-\frac{1}{2\tau_f}\right)\left(\frac{\partial}{\partial t}+e_\alpha\frac{\partial}{\partial \xi}\right)f_\alpha^{(1)}=-\frac{1}{\tau}f_\alpha^{(2)}. \tag{135}$$

Taking $\sum_\alpha[(133)+\varepsilon(135)]$, and enforcing conditions $\sum_\alpha f_\alpha^{(n)}=0$, and $\sum_\alpha e_\alpha f_\alpha^{(n)}=0$, for $n\geq 1$ gives

$$\frac{\partial}{\partial t}\sum_\alpha f_\alpha^{(0)}+\frac{\partial}{\partial \xi}\sum_\alpha e_\alpha f_\alpha^{(0)}=qY. \tag{136}$$

Evaluating of terms in the Eq. (136) using Eqs. (122), (125) and (132), neglecting the term $\frac{gA}{2Ye^2}\frac{\partial Z}{\partial t}$, due to a small time scale imposed by the LBM, the continuity equation of second-order accuracy Eq. (108) is obtained:

$$\frac{\partial}{\partial t}(YA)+\frac{\partial Q}{\partial \xi}=qY. \tag{137}$$

Now, taking $\sum_\alpha e_\alpha[(133)+\varepsilon(135)]$ provides

$$\frac{\partial}{\partial t}\sum_\alpha e_\alpha f_\alpha^{(0)}+\frac{\partial}{\partial \xi}\sum_\alpha e_\alpha e_\alpha f_\alpha^{(0)}+\varepsilon\left(1-\frac{1}{2\tau_f}\right)\frac{\partial}{\partial \xi}\left(\sum_\alpha e_\alpha e_\alpha f_\alpha^{(1)}\right) \tag{138}$$
$$=F-\frac{gA}{Y}\frac{\partial Z}{\partial \xi}+\omega\frac{Q^2}{A}\frac{\partial\left(Y^{-1}\right)}{\partial \xi}.$$

Following the terms evaluated with Eqs. (121), (123) and (132), using $\tau=0.5$, the above equation becomes the momentum conservation equation:

$$\frac{\partial Q}{\partial t}+\frac{\partial}{\partial \xi}\left(\omega\frac{Q^2}{YA}\right)=-\frac{gA}{Y}\frac{\partial Z}{\partial \xi}-gAS_f+\omega\frac{Q^2}{A}\frac{\partial\left(Y^{-1}\right)}{\partial \xi}. \tag{139}$$

It should be noted that the fourth term on the RHS actually denotes the second-order velocity derivative (diffusion), therefore τ_f parameter acts like an artificial viscosity parameter which can be used for dispersion (oscillations) control in the vicinity of the shocks.

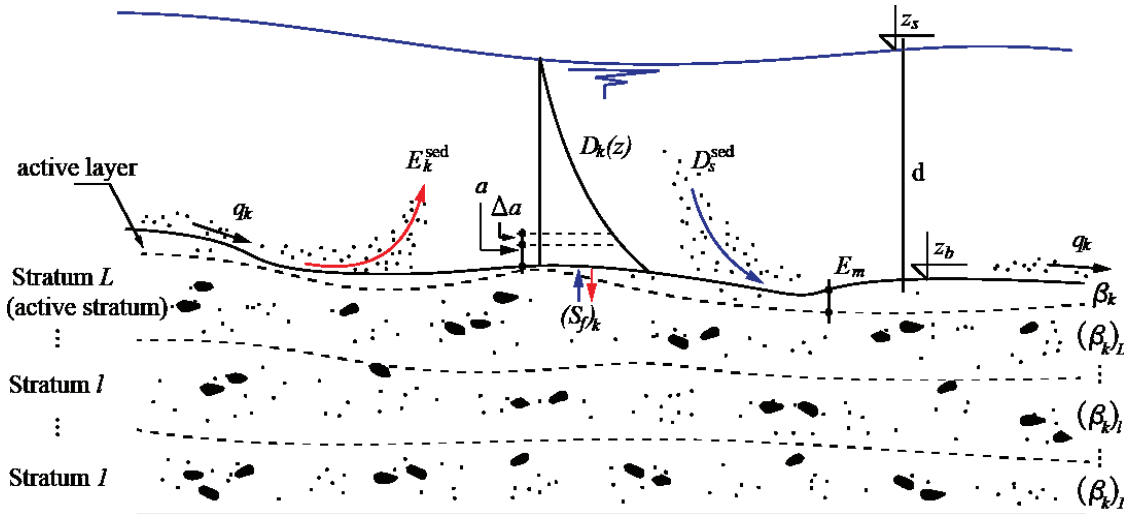


Figure 9: The active-layer concept.

4.2 One-dimensional open-channel sediment transport LB model

The concept of the active layer is considered, which accounts for sediment-flow interaction in natural watercourses, such as: suspended-sediment transport, bedload transport, bed deformations and interaction between the flow and sediment mixture. Traditionally single domain of sediment-processes is divided into three subdomains: suspended-sediment, active-layer and stratum (Fig.9). Sediment mixture is represented through a suitable number of sediment size-classes $ks = 1, ..., KS$, where KS represents the total number of size-classes. The governing equations are defined for each subdomain, including exchange mechanisms between them, and solved simultaneously, so the behavior of a non-uniform sediment is described. The governing equations will be defined in this section.

4.2.1 Suspended sediment mass-conservation equation

Assuming that the suspended-sediment particles are advected by the local flow velocity, except for the downward gravitational settling, the mass-conservation equation for a size-class ks of suspended-sediment domain in the elemental volume in Cartesian coordinates is

$$\frac{\partial(C_{ks}A)}{\partial t} + \frac{\partial(C_{ks}Au)}{\partial x} = \frac{\partial}{\partial x}\left(\varepsilon_s \frac{\partial(C_{ks})}{\partial x} A\right) + \frac{B}{\rho}\left(E_{ks}^{sed} - D_{ks}^{sed}\right), \tag{140}$$

where ρ is density of mixture of water and suspended sediment (including the whole

mixture, all size-classes), C_k is dimensionless concentration of the size-class ks particles, ε_s is sediment mass-diffusivity coefficient, B is water surface width, E_{ks}^{sed} is the bed-material erosion into suspension, and D_{ks}^{sed} is suspended-sediment deposition onto the bed. There will be KS equations, one for each sediment size-class.

4.2.1.1 Suspended-sediment source terms

Suspended-sediment source terms represent interaction between suspended-sediment and bedload sediment, i.e. erosion and deposition. The upward active-layer sediment entrainment flux E_{ks}^{sed} and the downward suspended-sediment deposition flux $D_{ks}^{sed}$of the size-class ks, are modeled as a near-bed upward turbulent mass-diffusion flux, and a near-bed downward fall-velocity flux (Spasojević and Holly, 1993) as

$$E_{ks}^{sed} = \beta_{ks} \cdot \varepsilon_s^v \cdot \frac{(C_{ks})_{a+\Delta a} - (C_{ks})_a}{\Delta a} \tag{141}$$

$$D_{ks}^{sed} = \rho_s \cdot w_{f_{ks}} \cdot (C_{ks})^d, \tag{142}$$

One-dimensional models give the averaged concentration values, which can be used for calculation of the suspended-sediment deposition flux $(C_{ks})^d = C_{ks}$,therefore, it follows:

$$D_{ks}^{sed} = \rho_s \cdot w_{f_{ks}} \cdot C_{ks} \tag{143}$$

In the Eqs. (141) and (143) $[(C_{ks})_{a+\Delta a} - (C_{ks})_a] / \Delta a$ is near-bed non-equilibrium concentration gradient, subscript a denotes that the mass-diffusion flux is evaluated at some distance a above the bed, and it is a calibration parameter. $(C_{ks})_a$ is near-bed active-layer sediment concentration, $(C_{ks})_{a+\Delta a}$ is near-bed non-equilibrium concentration at distance $a + \Delta a$ above the bed-surface, extrapolated from the suspended-sediment calculations and $w_{f_{ks}}$ is particle fall velocity for the size-class ks.

The near-bed active-layer concentration $(C_{ks})_a$ is empirical value, and can be calculated by the equation proposed by van Rijn (van Rijn, 1984):

$$(C_{ks})_a = \beta_{ks} 0.015 \frac{D_{ks}}{a} \frac{T_{ks}^{1.5}}{(D_*)_{ks}^{0.3}}, \tag{144}$$

where, D_{ks} is is the representative particle diameter, T_{ks} is transport stage parameter, $(D_*)_{ks}$ is dimensionless particle parameter, β_{ks} is active-layer fraction of the size-class ks,

and a is near-bed distance. The dimensionless particle parameter $(D_*)_{ks}$ is given by the expression:

$$(D_*)_{ks} = D_{ks}\left(\frac{(\rho_s/\rho - 1)\, g_r}{\nu^2}\right)^{1/3}. \tag{145}$$

In the Eq.(145) ρ_s is sediment density, ρ is water-sediment mixture density, g_r is gravitational acceleration, and ν denotes kinematic viscosity coefficient.

The transport stage parameter T_{ks} in Eq. (144) is evaluated by the expression:

$$T_{ks} = \frac{u_*^2 - (u_*^{cr})^2}{(u_*^{cr})^2}, \tag{146}$$

where u_* denotes the bed-shear velocity, while u_*^{cr} stands for the critical bed-shear velocity, given by the following relation:

$$u_* = u\frac{\sqrt{g_r}}{C_{ch}}, \tag{147}$$

where

$$C_{ch} = 18 \cdot \log\left(\frac{12 \cdot R}{3 \cdot D_{90}}\right) \tag{148}$$

is the Chezy coefficient, where R is hydraulic radius, and D_{90} is particle diameter representing the 90% cumulative percentile value. The critical bed-shear velocity is given by Shields:

$$(u_*^{cr})_{ks} = \sqrt{(\Theta_c)_{ck} \cdot g_r \cdot (\rho_s/\rho - 1) \cdot D_{ks}} \tag{149}$$

$$\Theta_c = \begin{cases} 0.24 \cdot D_*^{-1} & , 1 < D_* \leq 4 \\ 0.14 \cdot D_*^{-0.64} & , 4 < D_* \leq 10 \\ 0.04 \cdot D_*^{-0.1} & , 10 < D_* \leq 20 \\ 0.013 \cdot D_*^{0.29} & , 20 < D_* \leq 150 \\ 0.056 & , D_* > 150 \end{cases}. \tag{150}$$

The near-bed non-equilibrium concentration at distance $a + \Delta a$ above the bed-surface can be calculated by the expression given by Rouse:

$$(C_{ks})_{a+\Delta a} = C_k \frac{(h - a - \Delta a)\left(\frac{h-a-\Delta a}{a+\Delta a}\right)^{z_{ks}^*}}{\int\limits_{a+\Delta a}^{h} \left(\frac{h}{z} - 1\right)^{z_{ks}^*} dz}, \tag{151}$$

where h is the averaged depth, z is the vertical coordinate, and z^*_{ks} is the Rouse number. It is a ratio between the sediment fall velocity $w_{f_{ks}}$ and the upwards velocity on the grain, as a product of the von Kármán constant κ and the shear velocity u_*, defined in Eq. (147):

$$z^*_{ks} = \frac{w_{f_{ks}}}{\kappa \cdot u_*}. \tag{152}$$

The particle fall velocity for the size-class ks, $w_{f_{ks}}$ is given by expression given by van Rijn::

$$w_{f_{ks}} = \begin{cases} \frac{1}{18} \cdot \frac{(\rho_s/\rho - 1) \cdot g_r \cdot D^2_{ks}}{\nu} & , D_{ks} < 1 \cdot 10^{-4} m \\ 10 \cdot \frac{\nu}{D_{ks}} \cdot \left[\left(1 + \frac{0.01 \cdot (\rho_s/\rho - 1) \cdot g_r \cdot D^3_{ks}}{\nu^2} \right)^{0.5} - 1 \right] & , 1 \cdot 10^{-4} m \leq D_{ks} < 1 \cdot 10^{-3} m \\ 1.1 \cdot \left[(\rho_s/\rho - 1) \cdot g_r \cdot D^2_{ks} \right]^{0.5} & , D_{ks} \geq 1 \cdot 10^{-3} m \end{cases} . \tag{153}$$

4.2.2 Transformation of the suspended-sediment mass-conservation equation using the adaptive grid technique

Like in the section before, when the SVE were transformed, the suspended-sediment mass-conservation equation needs to be transformed in respect to the new basis. The transformation is applied on the Eq. (140):

$$\frac{\partial (C_{ks} A)}{\partial t} + \frac{\partial (C_{ks} A u)}{\partial \xi} \frac{\partial \xi}{\partial x} = \frac{\partial}{\partial \xi} \left(\varepsilon_s \frac{\partial (C_{ks})}{\partial \xi} \frac{\partial \xi}{\partial x} A \right) \frac{\partial \xi}{\partial x} + \frac{B}{\rho} \left(E^{sed}_{ks} - D^{sed}_{ks} \right). \tag{154}$$

The next step is to multiply the above equation with $Y = \partial x / \partial \xi$, so the Eq. (154) becomes

$$\frac{\partial (C_{ks} A Y)}{\partial t} + \frac{\partial (C_{ks} A u)}{\partial \xi} = \frac{\partial}{\partial \xi} \left(\varepsilon_s \frac{\partial (C_{ks})}{\partial \xi} \frac{A}{Y} \right) + \frac{BY}{\rho} \left(E^{sed}_{ks} - D^{sed}_{ks} \right), \tag{155}$$

or, when the derivative of product rule is applied

$$\frac{\partial (C_{ks} A Y)}{\partial t} + \frac{\partial (C_{ks} A u)}{\partial \xi} = \frac{\partial}{\partial \xi} \left[\varepsilon_s \left(\frac{\partial (C_{ks} \frac{A}{Y})}{\partial \xi} - C_{ks} \frac{\partial (\frac{A}{Y})}{\partial \xi} \right) \right] + \frac{BY}{\rho} \left(E^{sed}_{ks} - D^{sed}_{ks} \right). \tag{156}$$

Further, applying the derivative of summation rule, and the derivative of product rule again, it follows

$$\begin{aligned} \frac{\partial (C_{ks} A Y)}{\partial t} + \frac{\partial (C_{ks} A u)}{\partial \xi} = \varepsilon_s \frac{\partial^2 (C_{ks} \frac{A}{Y})}{\partial \xi^2} - \varepsilon_s \frac{\partial C_{ks}}{\partial \xi} \frac{\partial (\frac{A}{Y})}{\partial \xi} \\ - \varepsilon_s C_{ks} \frac{\partial^2 (\frac{A}{Y})}{\partial \xi^2} + \frac{BY}{\rho} \left(E^{sed}_{ks} - D^{sed}_{ks} \right) \end{aligned} \tag{157}$$

which is the final form of the transformed Eq. (140).

4.2.3 The lattice Boltzmann model for the transformed suspended-sediment mass-conservation equation

Again, a D1Q3 lattice Boltzmann LBGK model is used. The evolution equation corresponding to Eq. (157) of a size-class ks is defined as:

$$\begin{aligned} g_\alpha(\xi + e_\alpha \Delta t, t + \Delta t) = g_\alpha(\xi, t) - \frac{1}{\tau_g}(g_\alpha - g_\alpha^{eq}) \\ -\frac{\varepsilon_s}{e^2 \Delta t}\overline{C_{ks}}\left[\frac{A}{Y}(\xi + e_\alpha \Delta t, t) - 2\frac{A}{Y}(\xi, t) + \frac{A}{Y}(\xi - e_\alpha \Delta t, t)\right] \\ -\frac{\varepsilon_s}{e^2 \Delta t}\left[C_{ks}(\xi + e_\alpha \Delta t) - C_{ks}(\xi)\right]\left[\frac{A}{Y}(\xi + e_\alpha \Delta t, t) - \frac{A}{Y}(\xi, t)\right] \\ +\Delta t G_\alpha. \end{aligned} \tag{158}$$

where g_α is the particle distribution function along the α link, g_α^{eq} is the local equilibrium distribution function; ξ is the position vector in the 1D domain; Δt is time step; G_α is the force term; τ_g is relaxation time; e_α is the particle velocity vector along the α link; $e = \Delta\xi/\Delta t$ and $\Delta\xi$ are the lattice sizes. The finite difference procedure is proposed for the second and third term on RHS of Eq. (157).Term noted $\overline{C_{ks}}$ is evaluated using the centered-sheme as follows:

$$\overline{C_{ks}} = C_{ks}\left(\xi + \frac{1}{2}e_\alpha \Delta t, t + \frac{1}{2}\Delta t\right). \tag{159}$$

Three-velocity lattice particle velocities are defined in the same way as for the water flow model, therefore Eq. (120) will be used.

The equilibrium distribution function in this case must satisfy following relations :

$$\begin{aligned} \sum_\alpha g_\alpha^{eq} &= C_{ks} A Y, \\ \sum_\alpha e_\alpha g_\alpha^{eq} &= C_{ks} A u, \\ \sum_\alpha e_\alpha e_\alpha g_\alpha^{eq} &= \lambda C_{ks} A, \end{aligned} \tag{160}$$

where

$$\lambda = \frac{\varepsilon_s}{\Delta t Y(\tau_g - 0.5)e^2}. \tag{161}$$

The proposed equilibrium distribution function is

$$g_\alpha^{eq} = \begin{cases} C_{ks}AY - \lambda C_{ks}A & ,\alpha = 0 \\ \frac{C_{ks}Au}{2e} + \frac{\lambda}{2}C_{ks}A & ,\alpha = 1 \\ -\frac{C_{ks}Au}{2e} + \frac{\lambda}{2}C_{ks}A & ,\alpha = 2. \end{cases} \tag{162}$$

The force term is simulated as

$$G_\alpha = \frac{BY}{\rho}\left(E_{ks}^{sed} - D_{ks}^{sed}\right), \tag{163}$$

where E_{ks}^{sed} and D_{ks}^{sed} are defined by Eqs. (141) and (143). To ensure second-order accuracy to the method, the force term is evaluated using the centered-sheme:

$$G_\alpha = G_\alpha\left(\xi + \frac{1}{2}e_\alpha\Delta t, t + \frac{1}{2}\Delta t\right). \tag{164}$$

The physical variables of concentration C_{ks} can be calculated as the zeroth statical moment as follows

$$C_{ks}(\xi, t) = \frac{1}{AY}\sum_\alpha g_\alpha(\xi, t) \tag{165}$$

4.2.4 Derivation of the transformed suspended-sediment mass-conservation equation from the lattice Boltzmann evolution equation

The goal is to develop Eq. (157) from the lattice Boltzmann equation (158), and the relations (159)-(165). The Chapman-Enskog analysis will be applied again. The first step is applying Taylors expansion to the each term of the Eq. (158) in time and space. The first term on the LHS of the Eq. (158), assuming $\Delta t = \varepsilon$, becomes

$$\begin{aligned} g_\alpha(\xi + e_\alpha\Delta t, t + \Delta t) - g_\alpha(\xi, t) = \varepsilon\left(\frac{\partial}{\partial t} + e_\alpha\frac{\partial}{\partial \xi}\right)g_\alpha \\ + \frac{1}{2}\varepsilon^2\left(\frac{\partial}{\partial t} + e_\alpha\frac{\partial}{\partial \xi}\right)^2 g_\alpha + O(\varepsilon^3). \end{aligned} \tag{166}$$

The distribution function g_α is expanded as

$$g_\alpha = g_\alpha^{(0)} + \varepsilon g_\alpha^{(1)} + \varepsilon^2 g_\alpha^{(2)} + O(\varepsilon^3), \tag{167}$$

while the centered-sheme force term is expressed as

$$G_\alpha\left(\xi + \frac{1}{2}e_\alpha\Delta t, t + \frac{1}{2}\Delta t\right) = G_\alpha + \frac{1}{2}\varepsilon\left(\frac{\partial}{\partial t} + e_\alpha\frac{\partial}{\partial \xi}\right)G_\alpha + O(\varepsilon^2). \tag{168}$$

Taylor series expansion can also be applied to the second and third term on the RHS of Eq. (158), resulting

$$\frac{\varepsilon_s}{e^2\Delta t}\overline{C_{ks}}\left[\frac{A}{Y}(\xi+e_\alpha\Delta t,t)-2\frac{A}{Y}(\xi,t)+\frac{A}{Y}(\xi-e_\alpha\Delta t,t)\right]= \tag{169}$$
$$\frac{\varepsilon_s}{e^2\varepsilon}\left[C_{ks}+\frac{\varepsilon}{2}\left(\frac{\partial}{\partial t}+e_\alpha\frac{\partial}{\partial\xi}\right)C_{ks}\right]\left[\varepsilon^2\left(\frac{\partial}{\partial t}+e_\alpha\frac{\partial}{\partial\xi}\right)^2\frac{A}{Y}\right]+O(\varepsilon^3),$$

$$\frac{\varepsilon_s}{e^2\Delta t}\left[C_{ks}(\xi+e_\alpha\Delta t)-C_{ks}(\xi)\right]\left[\frac{A}{Y}(\xi+e_\alpha\Delta t,t)-\frac{A}{Y}(\xi,t)\right]= \tag{170}$$
$$\frac{\varepsilon_s}{e^2\varepsilon}\left[\varepsilon\left(\frac{\partial}{\partial t}+e_\alpha\frac{\partial}{\partial\xi}\right)C_{ks}+\frac{\varepsilon^2}{2}\left(\frac{\partial}{\partial t}+e_\alpha\frac{\partial}{\partial\xi}\right)^2C_{ks}\right]$$
$$\left[\varepsilon\left(\frac{\partial}{\partial t}+e_\alpha\frac{\partial}{\partial\xi}\right)\frac{A}{Y}+\frac{\varepsilon^2}{2}\left(\frac{\partial}{\partial t}+e_\alpha\frac{\partial}{\partial\xi}\right)^2\frac{A}{Y}\right]+O(\varepsilon^3).$$

Substituting Eqs. (167) - (170) into Eq. (166) the evaluation to order ε^0 is

$$g_\alpha^{(0)}=g_\alpha^{eq}, \tag{171}$$

to order ε it is

$$\left(\frac{\partial}{\partial t}+e_\alpha\frac{\partial}{\partial\xi}\right)g_\alpha^{(0)}=-\frac{1}{\tau_g}g_\alpha^{(1)}+G_\alpha-\frac{\varepsilon_s}{e^2}\left(\frac{\partial}{\partial t}+e_\alpha\frac{\partial}{\partial\xi}\right)C_k\left(\frac{\partial}{\partial t}+e_\alpha\frac{\partial}{\partial\xi}\right)\frac{A}{Y} \tag{172}$$
$$-\frac{\varepsilon_s}{e^2}C_k\left(\frac{\partial}{\partial t}+e_\alpha\frac{\partial}{\partial\xi}\right)^2\frac{A}{Y},$$

and to the order ε^2 it is

$$\left(\frac{\partial}{\partial t}+e_\alpha\frac{\partial}{\partial\xi}\right)g_\alpha^{(1)}+\frac{1}{2}\left(\frac{\partial}{\partial t}+e_\alpha\frac{\partial}{\partial\xi}\right)^2g_\alpha^{(0)}=-\frac{1}{\tau_g}g_\alpha^{(2)}-\frac{1}{2}\left(\frac{\partial}{\partial t}+e_\alpha\frac{\partial}{\partial\xi}\right)G_\alpha \tag{173}$$
$$-\frac{\varepsilon_s}{2e^2}\left(\frac{\partial}{\partial t}+e_\alpha\frac{\partial}{\partial\xi}\right)C_{ks}\left(\frac{\partial}{\partial t}+e_\alpha\frac{\partial}{\partial\xi}\right)^2\frac{A}{Y}$$
$$-\frac{\varepsilon_s}{e^2}\left(\frac{\partial}{\partial t}+e_\alpha\frac{\partial}{\partial\xi}\right)^2C_{ks}\left(\frac{\partial}{\partial t}+e_\alpha\frac{\partial}{\partial\xi}\right)\frac{A}{Y}.$$

Substituting Eq. (172) into Eq. (173) leads to

$$\left(1-\frac{1}{2\tau_g}\right)\left(\frac{\partial}{\partial t}+e_\alpha\frac{\partial}{\partial\xi}\right)g_\alpha^{(1)}=-\frac{1}{\tau_g}g_\alpha^{(2)}-\frac{\varepsilon_s}{2e^2}C_{ks}\left(\frac{\partial}{\partial t}+e_\alpha\frac{\partial}{\partial\xi}\right)^3\frac{A}{Y}, \tag{174}$$

where the last term in the above equation will be neglected due to an effect of the third derivative is not significant in comparison to the other terms, therefore, we obtain

$$\left(1-\frac{1}{2\tau_g}\right)\left(\frac{\partial}{\partial t}+e_\alpha\frac{\partial}{\partial\xi}\right)g_\alpha^{(1)}=-\frac{1}{\tau_g}g_\alpha^{(2)} \tag{175}$$

Adding Eq. (172) into (175)

$$\left(\frac{\partial}{\partial t}+e_\alpha\frac{\partial}{\partial \xi}\right)g_\alpha^{(0)}+\varepsilon\left(1-\frac{1}{2\tau_g}\right)\left(\frac{\partial}{\partial t}+e_\alpha\frac{\partial}{\partial \xi}\right)g_\alpha^{(1)}=-\frac{1}{\tau_g}\left(g_\alpha^{(1)}+\varepsilon g_\alpha^{(2)}\right)+G_\alpha \quad (176)$$
$$-\frac{\varepsilon_s}{e^2}\left(\frac{\partial}{\partial t}+e_\alpha\frac{\partial}{\partial \xi}\right)C_{ks}\left(\frac{\partial}{\partial t}+e_\alpha\frac{\partial}{\partial \xi}\right)\frac{A}{Y}-\frac{\varepsilon_s}{e^2}C_{ks}\left(\frac{\partial}{\partial t}+e_\alpha\frac{\partial}{\partial \xi}\right)^2\frac{A}{Y},$$

Substituting Eq. (172) in the above expression and then taking the sum, Eq. (176) takes the form:

$$\frac{\partial}{\partial t}\sum_\alpha g_\alpha^{(0)}+\frac{\partial}{\partial \xi}\sum_\alpha e_\alpha g_\alpha^{(0)}=\varepsilon\left(\tau_g-\frac{1}{2}\right)\frac{\partial^2}{\partial \xi^2}\sum_\alpha\left(e_\alpha e_\alpha g_\alpha^{(0)}\right) \quad (177)$$
$$+G_\alpha-\frac{\varepsilon_s}{e^2}\left(\frac{\partial}{\partial t}+e_\alpha\frac{\partial}{\partial \xi}\right)C_{ks}\left(\frac{\partial}{\partial t}+e_\alpha\frac{\partial}{\partial \xi}\right)\frac{A}{Y}-\frac{\varepsilon_s}{e^2}C_{ks}\left(\frac{\partial}{\partial t}+e_\alpha\frac{\partial}{\partial \xi}\right)^2\frac{A}{Y}$$
$$-\frac{\varepsilon_s}{e^2}\varepsilon\left(2\tau_g-1\right)\frac{\partial}{\partial \xi}\left(\sum_\alpha e_\alpha e_\alpha\frac{\partial C_{ks}}{\partial t}\frac{\partial\frac{A}{Y}}{\partial \xi}+C_{ks}\frac{\partial^2}{\partial \xi^2}\sum_\alpha e_\alpha e_\alpha\frac{A}{Y}\right)$$
$$+\varepsilon\left(\tau_g-\frac{1}{2}\right)\frac{\partial}{\partial t}\frac{\partial}{\partial \xi}\sum_\alpha e_\alpha g_\alpha^{(0)},$$

Evaluating Eq. (177) using Eq. (171), (160) and (163), and neglecting the last two terms on the RHS in the equation above, the transformed sediment continuity equation is obtained as follows:

$$\frac{\partial(C_kAY)}{\partial t}+\frac{\partial(C_kAu)}{\partial \xi}=\varepsilon_s\frac{\partial^2(C_k\frac{A}{Y})}{\partial \xi^2}-\varepsilon_s\frac{\partial C_k}{\partial \xi}\frac{\partial(\frac{A}{Y})}{\partial \xi} \quad (178)$$
$$-\varepsilon_sC_k\frac{\partial^2(\frac{A}{Y})}{\partial \xi^2}+\frac{BY}{\rho}\left(E_k^{sed}-D_k^{sed}\right).$$

4.2.5 Active-layer mass-conservation equations

The active-layer is assumed to be composed of sediment moving as bedload, and as bed-surface and immediate subsurface sediment, that is already agitated and ready to be set into motion. Since it is difficult to account for the exact position and size of each sediment particle being entrained from the bed or ending its trajectory at a certain spot on the bed surface, a the active-layer is assumed to have a uniform size-class distribution over its thickness E_m. Furthermore, it is assumed that the sediment particles of the same size-class are equally exposed to the flow, wherever to the position in the layer. Therefore, the bedload flux represents bedload exchange between two neighboring elemental areas. The

mass-conservation equation for size-class ks of sediment in active-layer control volume ΔV is:

$$\rho_s(1-p_b)\frac{\partial(\beta_{ks}E_m)}{\partial t}+\frac{\partial\phi_{ks}}{\partial x}=D_{ks}^{sed}-E_{ks}^{sed}+(S_f)_{ks}\,, \tag{179}$$

where β_{ks} is active-layer fraction of the size-class ks , ϕ_{ks} is bedload flux component of size-class ks, E_m is active-layer thickness, p_b is bed-material porosity, ρ_s is sediment density, E_{ks}^{sed} and D_{ks}^{sed} are erosion and deposition source terms, defined by Eqs. (141) and (143), and $(S_f)_{ks}$ is the active-layer floor source for the class-size ks.

As a result of dominant erosion, some particles move upwards from the active-layer into the suspension, bringing the floor of the active-layer floor to descend, and enter the active stratum, and the active layer thickness is given by equation (Spasojević,1990., Budinski, 2011):

$$E_m=\frac{D_A}{1-p_b}-C_{Ea}\left(Z_b^{n+1}-Z_b^n\right), \tag{180}$$

where D_A presents the diameter of the smallest non-mobile sediment size-class, and C_{Ea} is a calibration parameter. The bed-load flux ϕ_{ks} is calculated using the empirical equation proposed by van Rijn:

$$\phi_{ks}=(1-\gamma_{ks})\zeta_{ks}\beta_{ks}\rho_s\sqrt{\left(\frac{\rho_s}{\rho}-1\right)g_rD_{ks}}D_{ks}0.053T_{ks}^{2.1}\left(D_*\right)_{ks}^{-0.3}, \tag{181}$$

where γ_{ks} is the allocation parameter, reflecting the fact that some fraction of the particular size-class is expected to be transported only as suspended load, ζ_{ks} is hiding factor accounting for the reduction or increase in a particular size-class transport rate when it is part of a mixture.

The active-layer floor source $(S_f)_{ks}$ for the class-size ks represents the exchange of sediment particles between the active-layer and the active-stratum control volumes from active-layer floor movement. The active-layer wall is at the same time the active-stratum ceiling, and it descends or rises whenever the bed elevation changes, because of erosion or deposition occurring in the active-layer control volume. The active-layer floor source (Spasojević and Holly, 1990), when the active-layer floor descends is:

$$(S_f)_{ks}=-\rho_s(1-p_b)\frac{\partial}{\partial t}\left[\beta_{ks,l}(Z_b-E_m)\right], \tag{182}$$

where $\beta_{ks,l}$ is the active-stratum class-size fraction, and when the active-layer floor rises:

$$(S_f)_{ks} = -\rho_s(1-p_b)\frac{\partial}{\partial t}\left[\beta_{ks}(Z_b - E_m)\right], \tag{183}$$

here β_{ks} is the active-stratum class-size fraction.

4.2.6 Transformation of the active-layer mass-conservation equations using the adaptive grid technique

The transformation is applied on Eq. (179) in form

$$\rho_s(1-p_b)\frac{\partial(\beta_{ks}E_m)}{\partial t} + \frac{\partial\phi_{ks}}{\partial\xi}\frac{\partial\xi}{\partial x} = D_{ks}^{sed} - E_{ks}^{sed} + (S_f)_{ks}, \tag{184}$$

and then multiplied with $Y = \partial x/\partial\xi$, which yields to transformed active-layer sediment equations

$$\frac{\partial(\rho_s(1-p_b)\beta_{ks}E_mY)}{\partial t} + \frac{\partial\phi_{ks}}{\partial\xi} = Y\left(D_{ks}^{sed} - E_{ks}^{sed} + (S_f)_{ks}\right). \tag{185}$$

The governing equation will be used to form a LB model.

4.2.7 The lattice Boltzmann model for the transformed active-layer mass-conservation equations

For every sediment size-class ks a LB model will be formed separately. There will be KS of the these equations. The evolution equation in D1Q3 LBGK model corresponding to Eq. (185) of class ks is defined as

$$h_\alpha(\xi + e_\alpha\Delta t, t+\Delta t) = h_\alpha(\xi,t) - \frac{1}{\tau_h}(h_\alpha - h_\alpha^{eq}) + \Delta t H_\alpha, \tag{186}$$

where h_α is the particle distribution function (DF) along the α link, h_α^{eq} is the local equilibrium distribution function; ξ is the position vector in the 1D domain; Δt is time step; H_α is the force term; τ_h is relaxation time; e_α is the particle velocity vector along the α link; $e = \Delta\xi/\Delta t$ and $\Delta\xi$ are the lattice sizes. Three-velocity lattice particle velocities are defined in Eq. (120) .The equilibrium distribution function (EDF) in this case must satisfy following relations :

$$\sum_\alpha h_\alpha^{eq} = \rho_s(1-p_b)\beta_{ks}E_mY, \tag{187}$$

$$\sum_\alpha e_\alpha h_\alpha^{eq} = \phi_{ks}.$$

The proposed equilibrium distribution function is

$$h_\alpha^{eq} = \begin{cases} \rho_s(1-p_b)\beta_{ks}E_m Y & ,\alpha = 0 \\ \frac{\phi_{ks}}{2\cdot e^2} & ,\alpha = 1 \\ -\frac{\phi_{ks}}{2\cdot e^2} & ,\alpha = 2 \end{cases} . \tag{188}$$

The force term is simulated as

$$H_\alpha = Y\left(D_{ks}^{sed} - E_{ks}^{sed} + (S_f)_{ks}\right), \tag{189}$$

where $D_{ks}^{sed}, E_{ks}^{sed}$ and $(S_f)_{ks}$ are defined in Eqs. (143) - (141) and (182). To ensure second-order accuracy to the method, the force term is evaluated using the centered-sheme:

$$H_\alpha = H_\alpha\left(\xi + \frac{1}{2}e_\alpha\Delta t, t + \frac{1}{2}\Delta t\right). \tag{190}$$

The physical variables the active-layer depth can be calculated as the zeroth statical moment as follows

$$\beta_{ks}(\xi,t) = \frac{1}{\rho_s(1-p_b)YE_m}\sum_\alpha h_\alpha(\xi,t), \tag{191}$$

where active-layer thickness is defined in Eq. (180).

4.2.8 Derivation of the transformed active-layer mass-conservation equations from the lattice Boltzmann evolution equation

To develop Eq. (185) from the lattice Boltzmann equation (186), and the relations (187)-(191) the Chapman-Enskog analysis will be used. Applying Taylors expansion to the each term of the Eq. (186) in time and space, the first term on the LHS, assuming $\Delta t = \varepsilon$, becomes

$$h_\alpha(\xi + e_\alpha\Delta t, t + \Delta t) - h_\alpha(\xi,t) = \varepsilon\left(\frac{\partial}{\partial t} + e_\alpha\frac{\partial}{\partial\xi}\right)h_\alpha \tag{192}$$

$$+\frac{1}{2}\varepsilon^2\left(\frac{\partial}{\partial t} + e_\alpha\frac{\partial}{\partial\xi}\right)^2 h_\alpha + O(\varepsilon^3). \tag{193}$$

The distribution function h_α is expanded as usual

$$h_\alpha = h_\alpha^{(0)} + \varepsilon h_\alpha^{(1)} + \varepsilon^2 h_\alpha^{(2)} + O(\varepsilon^3), \tag{194}$$

and the centered-sheme force term is expressed as

$$H_\alpha\left(\xi + \frac{1}{2}e_\alpha\Delta t, t + \frac{1}{2}\Delta t\right) = H_\alpha + \frac{1}{2}\varepsilon\left(\frac{\partial}{\partial t} + e_\alpha\frac{\partial}{\partial\xi}\right)H_\alpha + O(\varepsilon^2). \tag{195}$$

Substituting Eqs. (192) - (195) into Eq. (166) the evaluating to order ε^0 is

$$h_\alpha^{(0)} = h_\alpha^{eq}, \tag{196}$$

to order ε it is

$$\left(\frac{\partial}{\partial t} + e_\alpha \frac{\partial}{\partial \xi}\right) h_\alpha^{(0)} = -\frac{1}{\tau_h} h_\alpha^{(1)} + H_\alpha \tag{197}$$

and to the order ε^2 it is

$$\left(\frac{\partial}{\partial t} + e_\alpha \frac{\partial}{\partial \xi}\right) h_\alpha^{(1)} + \frac{1}{2}\left(\frac{\partial}{\partial t} + e_\alpha \frac{\partial}{\partial \xi}\right)^2 h_\alpha^{(0)} = -\frac{1}{\tau_h} h_\alpha^{(2)} - \frac{1}{2}\left(\frac{\partial}{\partial t} + e_\alpha \frac{\partial}{\partial \xi}\right) H_\alpha \tag{198}$$

Substituting Eq. (197) into Eq. (198) leads to

$$\left(1 - \frac{1}{2\tau_h}\right)\left(\frac{\partial}{\partial t} + e_\alpha \frac{\partial}{\partial \xi}\right) h_\alpha^{(1)} = -\frac{1}{\tau_h} h_\alpha^{(2)} \tag{199}$$

Taking $\sum_\alpha [(197) + \varepsilon(199)]$, and enforcing conditions $\sum_\alpha f_\alpha^{(n)} = 0$, and $\sum_\alpha e_\alpha f_\alpha^{(n)} = 0$, for $n \geq 1$ gives

$$\frac{\partial}{\partial t} \sum_\alpha h_\alpha^{(0)} + \frac{\partial}{\partial \xi} \sum_\alpha e_\alpha h_\alpha^{(0)} = H_\alpha. \tag{200}$$

In this way the active-layer sediment equation for the sediment class ks is obtained, minding Eq. (189):

$$\frac{\partial(\rho_s(1-p_b)\beta_{ks} E_m Y)}{\partial t} + \frac{\partial \phi_{ks}}{\partial \xi} = Y\left(D_{ks}^{sed} - E_{ks}^{sed} + (S_f)_{ks}\right). \tag{201}$$

4.2.9 Global active-layer and stratum mass-conservation equation

Taking the sum of the active-layer mass-conservation equations Eq. (179) for every sediment size-class ks it follows

$$\rho_s(1-p_b)\frac{\partial}{\partial t}\left(E_m \sum_{ks=1}^{KS} \beta_{ks}\right) + \frac{\partial}{\partial x}\left(\sum_{ks=1}^{KS} \phi_{ks}\right) = \sum_{ks=1}^{KS}\left(D_{ks}^{sed} - E_{ks}^{sed} + (S_f)_{ks}\right). \tag{202}$$

The sum of the size-class fractions over the whole mixture is, by definition:

$$\sum_{ks=1}^{KS} \beta_{ks} = 1. \tag{203}$$

Inserting Eq. (203) into Eq. (202), the global active-layer mass-conservation equation is obtained:

$$\rho_s(1-p_b)\frac{\partial E_m}{\partial t} + \frac{\partial}{\partial x}\left(\sum_{ks=1}^{KS} \phi_{ks}\right) = \sum_{ks=1}^{KS}\left(D_{ks}^{sed} - E_{ks}^{sed} + (S_f)_{ks}\right). \tag{204}$$

The active-layer thickness is defined as the difference between the bed elevation $Z_b$and the active-layer floor elevation $E_m = Z_b - Z_{bf}$.The change of the active-layer thickness will occur due to the particle exchange between the active-layer and suspended-sediment mixture by erosion and deposition, and due to the active-layer and active-stratum particle exchange. The active-stratum l mass-conservation equation of the particle class-size ks is:

$$\rho_s(1-p_b)\frac{\partial}{\partial t}\left(E_{s,l}\beta_{ks,l}\right) = -\left(S_f\right)_{ks,l}, \tag{205}$$

minding that the active-stratum has no contact with the sediment-suspension, therefore there will be no erosion and deposition source terms. Also, in this layer there is no bedload flux, since there is no bedload movement. The only source term is due to particle exchange between the active-layer and the active-stratum. Taking the sum over all class-sizes ks, and applying that $\sum_{k=1}^{KS}\beta_{ks,l} = 1$, the global active-stratum equation is:

$$\rho_s(1-p_b)\frac{\partial E_{s,l}}{\partial t} = \sum_{ks=1}^{KS}\left(S_f\right)_{ks}. \tag{206}$$

Going further down, for every stratum there will no longer be particle exchange between the given stratum and the active-layer, therefore the mass-conservation equation for the stratum k, where $k = 1, 2, ..., l-1$,is

$$\rho_s(1-p_b)\frac{\partial}{\partial t}\left(E_{s,k}\beta_{ks,k}\right) = 0. \tag{207}$$

Applying that $\sum_{ks=1}^{KS}\beta_{ks,k} = 1$, the global stratum k mass-conservation equation is

$$\rho_s(1-p_b)\frac{\partial E_{s,k}}{\partial t} = 0. \tag{208}$$

Adding the given global active-layer mass-conservation equations for active-layer (204), active-stratum (206), and all other stratums from 1 to $l-1$ (208), if the stratum 1 has floor elevation $Z_{bf} = 0$, the global active-layer and stratum mass-conservation equation is obtained:

$$\rho_s(1-p_b)\frac{\partial(Z_b)}{\partial t} + \frac{\partial}{\partial x}\left(\sum_{ks=1}^{KS}\phi_{ks}\right) = \sum_{ks=1}^{KS}\left(D_{ks}^{sed} - E_{ks}^{sed}\right). \tag{209}$$

4.2.10 Transformation of the global active-layer and stratum mass-conservation equation using the adaptive grid technique

The transformation is applied on Eq. (209) in form

$$\rho_s(1-p_b)\frac{\partial(Z_b)}{\partial t}+\frac{\partial}{\partial \xi}\left(\sum_{ks=1}^{KS}\phi_{ks}\right)\frac{\partial \xi}{\partial x}=\sum_{ks=1}^{KS}\left(D_{ks}^{sed}-E_{ks}^{sed}\right), \tag{210}$$

and then multiplied with $Y=\partial x/\partial \xi$, which yields to transformed global active-layer and stratum mass-conservation:

$$\frac{\partial\left[\rho_s(1-p_b)Z_bY\right]}{\partial t}+\frac{\partial}{\partial \xi}\left(\sum_{ks=1}^{KS}\phi_{ks}\right)=Y\sum_{ks=1}^{KS}\left(D_{ks}^{sed}-E_{ks}^{sed}\right). \tag{211}$$

4.2.11 The lattice Boltzmann model for the transformed global active-layer and stratum mass-conservation equation

The evolution equation corresponding to Eq. (211) is defined as:

$$m_\alpha(\xi+e_\alpha\Delta t,t+\Delta t)=m_\alpha(\xi,t)-\frac{1}{\tau_m}(m_\alpha-m_\alpha^{eq})+\Delta t M_\alpha. \tag{212}$$

where m_α is the particle distribution function (DF) along the α link, m_α^{eq} is the local equilibrium distribution function; ξ is the position vector in the 1D domain; Δt is time step; M_α is the force term; τ_m is relaxation time; e_α is the particle velocity vector along the α link; $e=\partial\xi/\partial t$ and $\partial\xi$ are the lattice sizes. Three-velocity lattice particle velocities are defined in Eq. (120) .The equilibrium distribution function (EDF) in this case must satisfy following relations:

$$\sum_\alpha m_\alpha^{eq}=\rho_s(1-p_b)Z_bY \tag{213}$$

$$\sum_\alpha e_\alpha m_\alpha^{eq}=\sum_{ks=1}^{KS}\phi_{ks}$$

The proposed equilibrium distribution function is

$$m_\alpha^{eq}=\begin{cases}\rho_s(1-p_b)Z_bY & ,\alpha=0\\ \frac{1}{2e}\sum\limits_{ks=1}^{KS}\phi_{ks} & ,\alpha=1\\ -\frac{1}{2e}\sum\limits_{k=1}^{KS}\phi_k & ,\alpha=2\end{cases}. \tag{214}$$

The force term is evaluated as

$$M_\alpha = Y \sum_{ks=1}^{KS} \left(D_{ks}^{sed} - E_{ks}^{sed} \right), \tag{215}$$

to ensure second-order accuracy to the method, the force term is evaluated using the centered-sheme:

$$M_\alpha = M_\alpha \left(\xi + \frac{1}{2} e_\alpha \Delta t, t + \frac{1}{2} \Delta t \right). \tag{216}$$

The bed-load elevation can be calculated as the zeroth statical moment as follows

$$Z_b(\xi, t) = \frac{1}{\rho_s (1 - p_b) Y} \sum_\alpha m_\alpha(\xi, t). \tag{217}$$

4.2.12 Derivation of the transformed global active-layer and stratum mass-conservation equation from the lattice Boltzmann equation

The goal is to develop Eq. (211) from the lattice Boltzmann equation (212), and the relations (213)-(217) using the Chapman-Enskog analysis. Applying Taylors expansion to the each term of the Eq. (212) in time and space, the first term on the LHS, assuming $\Delta t = \varepsilon$, becomes

$$\begin{aligned} m_\alpha(\xi + e_\alpha \Delta t, t + \Delta t) - m_\alpha(\xi, t) = \varepsilon \left(\frac{\partial}{\partial t} + e_\alpha \frac{\partial}{\partial \xi} \right) m_\alpha \\ + \frac{1}{2} \varepsilon^2 \left(\frac{\partial}{\partial t} + e_\alpha \frac{\partial}{\partial \xi} \right)^2 m_\alpha + O(\varepsilon^3). \end{aligned} \tag{218}$$

The distribution function m_α is expanded as:

$$m_\alpha = m_\alpha^{(0)} + \varepsilon m_\alpha^{(1)} + \varepsilon^2 m_\alpha^{(2)} + O(\varepsilon^3), \tag{219}$$

and the centered-sheme force term is expressed as

$$M_\alpha \left(\xi + \frac{1}{2} e_\alpha \Delta t, t + \frac{1}{2} \Delta t \right) = M_\alpha + \frac{1}{2} \varepsilon \left(\frac{\partial}{\partial t} + e_\alpha \frac{\partial}{\partial \xi} \right) M_\alpha + O(\varepsilon^2). \tag{220}$$

Substituting Eqs. (218) - (220) into Eq. (212) the evaluating to order ε^0 is

$$m_\alpha^{(0)} = m_\alpha^{eq}. \tag{221}$$

Collecting the terms of order ε it is

$$\left(\frac{\partial}{\partial t} + e_\alpha \frac{\partial}{\partial \xi} \right) m_\alpha^{(0)} = -\frac{1}{\tau_m} m_\alpha^{(1)} + M_\alpha \tag{222}$$

and to the order ε^2 it is

$$\left(\frac{\partial}{\partial t}+e_\alpha\frac{\partial}{\partial \xi}\right)m_\alpha^{(1)}+\frac{1}{2}\left(\frac{\partial}{\partial t}+e_\alpha\frac{\partial}{\partial \xi}\right)^2 m_\alpha^{(0)}=-\frac{1}{\tau_m}m_\alpha^{(2)} \\ -\frac{1}{2}\left(\frac{\partial}{\partial t}+e_\alpha\frac{\partial}{\partial \xi}\right)M_\alpha \tag{223}$$

Substituting Eq. (222) into Eq. (223) leads to

$$\left(1-\frac{1}{2\tau_m}\right)\left(\frac{\partial}{\partial t}+e_\alpha\frac{\partial}{\partial \xi}\right)m_\alpha^{(1)}=-\frac{1}{\tau_m}m_\alpha^{(2)} \tag{224}$$

Taking $\sum_\alpha[(222)+\varepsilon(224)]$, and enforcing conditions $\sum_\alpha m_\alpha^{(n)}=0$, and $\sum_\alpha e_\alpha m_\alpha^{(n)}=0$, for $n\geq 1$ gives

$$\frac{\partial}{\partial t}\sum_\alpha m_\alpha^{(0)}+\frac{\partial}{\partial \xi}\sum_\alpha e_\alpha m_\alpha^{(0)}=M_\alpha. \tag{225}$$

Using relations (213) and (215), the transformed global active-layer and stratum equation is obtained:

$$\frac{\partial\left[\rho_s(1-p_b)Z_bY\right]}{\partial t}+\frac{\partial}{\partial \xi}\left(\sum_{ks=1}^{KS}\phi_{ks}\right)=Y\sum_{ks=1}^{KS}\left(D_{ks}^{sed}-E_{ks}^{sed}\right). \tag{226}$$

4.3 Boundary conditions

In order to develop a fully operational one-dimensional flow-sediment mathematical model, set of outer and inner boundary conditions must be defined. The flow-sediment model consists of four sets of LB equations, defined in the previous section, therefore, appropriate boundary conditions must be defined for every set.

4.3.1 Boundary conditions for one-dimensional unsteady flow lattice Boltzmann model

4.3.1.1 Outer boundary conditions

Unsteady flow model demands upstream and downstream boundary conditions. For the upstream boundary condition discharge, represented by hydrograph, is prescribed, and the downstream boundary condition is water level, represented by stage hydrograph. This is a common practice in river modeling when specification of outer boundary conditions is considered. This conditions need to be customized for the LB unsteady flow model presented by Eq. (118).

The macroscopic variable upstream discharge Q_{up} is related to the distribution function at upstream boundary as (minding Eqs. (126) and (120)) :

$$Q_{up} = e_1 \cdot f^*_{1(i=1,j)} + e_2 \cdot f_{2(i=1,j)}, \tag{227}$$

where index $i = 1, 2, ..., N$ denotes computational node (cross-section) along the section $j = 1, 2, ..., M$.For the standard LB D1Q3 lattice arrangement, using that $e_1 = -e_2 = e$ the unknown distribution function is:

$$f^*_{1(i=1,j)} = f_{2(i=1,j)} + \frac{Q_{up}}{e}. \tag{228}$$

The downstream boundary condition is, from Eq. (125):

$$A_{down} Y_{(i=N,j)} = f_{0(i=N,j)} + f_{1(i=N,j)} + f^*_{2(i=N,j)}, \tag{229}$$

where downstream cross-sectional area A_{down} is obtained from the water level - cross-section area curve for a specific downstream water level value. The unknown distribution function is:

$$f^*_{2(i=N,j)} = A_{down} Y_{(i=N,j)} - f_{0(i=N,j)} - f_{1(i=N,j)}. \tag{230}$$

Another commonly used boundary condition for unsteady flow, which will be used in one of the unsteady flow in a non-prismatic channel, is normal depth boudary condition according to the Chezy-Manning equation:

$$Q = \frac{1}{n} A R^{2/3} \sqrt{S_0}. \tag{231}$$

In this model, cross-section is rectangular, therefore $A = Bh$ can be applied, and from the zeroth and first statical moment defined in Eqs. (125) and (126), Eq. (231) yields to:

$$e_1 \cdot f_1 + e_2 \cdot f^*_2 = \frac{1}{n} \left(f_0 + f_1 + f^*_2\right) \left(\frac{f_0 + f_1 + f^*_2}{2 \cdot \frac{f_0 + f_1 + f^*_2}{B} + B} \right)^{2/3} \sqrt{S_0}. \tag{232}$$

As one can see, Eq. (232) has an implicit form, and it is solved by iterative method where the value of the unknown distribution function f^*_2 is first speculated, and then corrected until LHS and RHS of the Eq. (232) are equal.

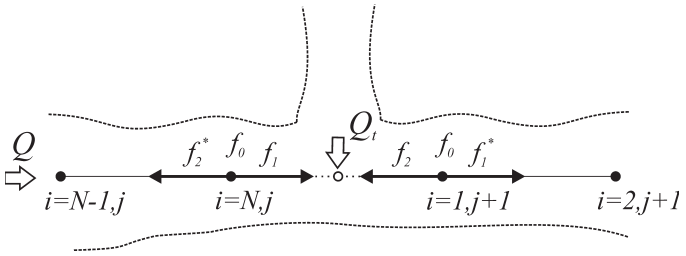


Figure 10: Tributary flow.

4.3.1.2 Inner boundary conditions

Natural watercourses are characterized by complex geometry, and represent a challenge in numerical modeling. Besides arbitrary cross-sections, there is variable longitudinal geometry which needs to be modeled as inner boudary conditions. In this section, solutions for tributary flow and bifurcations will be presented.

Tributary flow Formulation of the inner boundary condition, which incorporates tributary flow into one-dimensional LB model, is based on the lattice disposition shown in Fig.10. The unknown distribution functions $f^*_{2(i=N,j)}$ and $f^*_{1(i=1,j+1)}$ corresponding to the end and the beginning of the sections j and $j+1$, respectively, are derived using the continuity equation and water level equality between cross sections:

$$Q_{(i=1,j+1)} = Q_{(i=N,j)} + Q_{t,} \tag{233}$$

$$Z_{(_{(i=1,j+1)})=}Z_{(i=N,j)}, \tag{234}$$

where Q_t stands for tributary flow. For simplicity, cross-sections $(i=1, j+1)$ and $(i=N, j)$ are chosen to be the same, since the distance between the two is small, and tributary flow is modeled as nodal inflow, resulting that the water level equality can be replaced with the cross-section area equality, which is more suitable with the used one-dimensional LB unsteady flow model. Now, Eq. (234) can be written as:

$$A_{(i=1,j+1)=}A_{(i=N,j),} \tag{235}$$

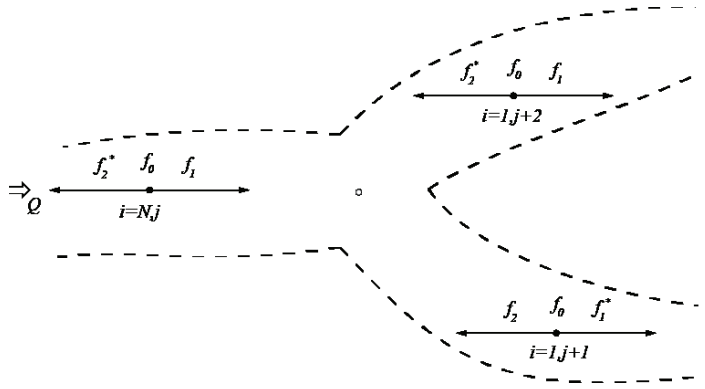


Figure 11: Flow separation.

and with Eq. (233) represent two necessary equations for solving two unknown distribution functions using the zeroth and first statical moment, defined in Eq. (125):

$$f^*_{1(i=1,j+1)} \cdot e_1 + f_{2(i=1,j+1)} \cdot e_2 = f_{1(i=N,j)} \cdot e_1 + f^*_{2(i=N,j)} \cdot e_2 + Q_t, \tag{236}$$

$$\frac{f_{0(i=1,j+1)} + f^*_{1(i=1,j+1)} + f_{2(i=1,j+1)}}{Y_{(i=1,j+1)}} = \frac{f_{0(i=N,j)} + f_{1(i=N,j)} + f^*_{2(i=N,j)}}{Y_{(i=N,j)}} \tag{237}$$

After some elementary algebra, Eqs. (236) and (237) yield to:

$$f^*_{2(i=N,j)} = \left(\frac{Y_{(i=N,j)}}{Y_{(i=1,j+1)}} + 1 \right)^{-1} \tag{238}$$

$$\left[\left(f_{0(i=1,j+1)} + 2 \cdot f_{2(i=1,j+1)} + f_{1(i=N,j)} + \frac{Q_t}{e} \right) \frac{Y_{(i=N,j)}}{Y_{(i=1,j+1)}} - f_{0(i=N,j)} - f_{1(i=N,j)} \right] \tag{239}$$

$$f^*_{1(i=1,j+1)} = f_{1(i=N,j)} - f^*_{2(i=N,j)} + f_{2(i=1,j+1)} + \frac{Q_t}{e} \tag{240}$$

which determines the unknown functions $f^*_{1(i=1,j+1)}$ and $f^*_{2(i=N,j)}$.

Bifurcation

Flow separation River bifurcation occurs when one stream separates into two or more streams. If they merge downstream, one or more river islands are created, and the closed system consisting of two or more river branches is created in hydraulic sense, requiring additional inner boundary conditions in the separation and merging locations. To derive three unknown distribution functions at the separation locations, using the disposition

shown in Fig.11, three equations are necessary: the continuity equation and two water level equalities:

$$Q_{(i=N,j)} = Q_{(i=1,j+1)} + Q_{(i=1,j+2),} \tag{241}$$

$$Z_{(i=N,j)} = Z_{(i=1,j+1)} = Z_{(i=1,j+2)}. \tag{242}$$

Using the first statical moment, Eq. (241) yields to:

$$f^*_{2(i=N,j)} + f^*_{1(i=1,j+1)} + f^*_{1(i=1,j+2)} = f_{1(i=N,j)} + f_{2(i=1,j+1)} + f_{2(i=1,j+2).} \tag{243a}$$

Equality equation $Z_{(i=N,j)} = Z_{(i=1,j+1)}$ is expressed using the linear interpolation of $Z - A$ curve in form

$$Z = WL^{(m)} + S^{(m)} \cdot (A - AR^{(m)}), \tag{244}$$

where $WL^{(m)}$ and $AR^{(m)}$, are water level and area at point m, respectively, and $S^{(m)}$ denotes the slope between two points m and $m+1$ of the $Z - A$ curve:

$$S^{(m)} = \frac{WL^{(m+1)} - WL^{(m)}}{AR^{(m+1)} - AR^{(m)}}. \tag{245}$$

Now, using the given correspondence equality equation can be written as :

$$WL^{(m)}_{(i=N,j)} + S^{(m)}_{(i=N,j)} \cdot (A_{(i=N,j)} - AR^{(m)}_{(i=N,j)}) \tag{246a}$$
$$= WL^{(m)}_{(i=1,j+1)} + S^{(m)}_{(i=1,j+1)} \cdot (A_{(i=1,j+1)} - AR^{(m)}_{(i=1,j+1)}).$$

Applying the zeroth statical moment, Eq. (246a) yields to

$$WL^{(m)}_{(i=N,j)} + S^{(m)}_{(i=N,j)} \cdot \left(\frac{f_{0(i=N,j)} + f_{1(i=N,j)} + f^*_{2(i=N,j)}}{Y_{(i=N,j)}} - AR^{(m)}_{(i=N,j)} \right) \tag{247}$$
$$= WL^{(m)}_{(i=1,j+1)} + S^{(m)}_{(i=1,j+1)} \cdot \left(\frac{f_{0(i=1,j+1)} + f^*_{1(i=1,j+1)} + f_{2(i=1,j+1)}}{Y_{(i=1,j+1)}} - AR^{(m)}_{(i=1,j+1)} \right).$$

Similarly, the second equality equation $Z_{(i=N,j)} = Z_{(i=1,j+2)}$ is obtained in form:

$$WL^{(m)}_{(i=N,j)} + S^{(m)}_{(i=N,j)} \cdot \left(\frac{f_{0(i=N,j)} + f_{1(i=N,j)} + f^*_{2(i=N,j)}}{Y_{(i=N,j)}} - AR^{(m)}_{(i=N,j)} \right) \tag{248}$$
$$= WL^{(m)}_{(i=1,j+2)} + S^{(m)}_{(i=1,j+2)} \cdot \left(\frac{f_{0(i=1,j+2)} + f^*_{1(i=1,j+2)} + f_{2(i=1,j+2)}}{Y_{(i=1,j+2)}} - AR^{(m)}_{(i=1,j+2)} \right). \tag{249}$$

Finally, if matrix notation is used in form $\mathbf{AX} = \mathbf{B}$, where, from Eqs. (243a), (247) and (248):

$$\mathbf{A} = \begin{bmatrix} 1 & 1 & 1 \\ \frac{S^{(m)}_{(i=N,j)}}{Y_{(i=N,j)}} & -\frac{S^{(m)}_{(i=1,j+1)}}{Y_{(i=1,j+1)}} & 0 \\ \frac{S^{(m)}_{(i=N,j)}}{Y_{(i=N,j)}} & 0 & -\frac{S^{(m)}_{(i=1,j+2)}}{Y_{(i=1,j+2)}} \end{bmatrix}, \tag{250}$$

$$\mathbf{X} = \begin{bmatrix} f^*_{2(i=N,j)} \\ f^*_{1(i=1,j+1)} \\ f^*_{1(i=1,j+2)} \end{bmatrix}, \tag{251}$$

and

$$\mathbf{B} = \begin{bmatrix} f_{1(i=N,j)} + f_{2(i=1,j+1)} + f_{2(i=1,j+2).} \\ S^{(m)}_{(i=1,j+1)} B_{(i=N,j)} - S^{(m)}_{(i=N,j)} B_{(i=1,j+1)} \\ S^{(m)}_{(i=1,j+2)} B_{(i=1,j+2)} - S^{(m)}_{(i=N,j)} B_{(i=N,j)} \end{bmatrix}, \tag{252}$$

where

$$B_{(i=N,j)} = \frac{f_{0(i=N,j)} + f_{1(i=N,j)}}{Y_{(i=N,j)}} - AR^{(m)}_{(i=N,j)}, \tag{253}$$

$$B_{(i=1,j+1)} = \frac{f_{0(i=1,j+1)} + f_{2(i=1,j+1)}}{Y_{(i=1,j+1)}} - AR^{(m)}_{(i=1,j+1)}, \tag{254}$$

$$B_{(i=1,j+2)} = \frac{f_{0(i=1,j+2)} + f_{2(i=1,j+2)}}{Y_{(i=1,j+2)}} - AR^{(m)}_{(i=1,j+2)}. \tag{255}$$

Solution can be obtained by solving the matrix equation in form:

$$\mathbf{X} = \mathbf{A}^{-1}\mathbf{B}. \tag{256a}$$

Flow merger Similarly, for the flow merger inner boundary conditions, three equations are needed to solve three unknown distribution functions, $f^*_{1(i=1,j+2)}$, $f^*_{2(i=N,j)}$ and $f^*_{2(i=N,j+1)}$ shown if Fig.12, the continuity equation, and two water level equality equations:

$$Q_{(i=1,j+2)} = Q_{(i=N,j)} + Q_{(i=N,j+1),} \tag{257}$$

$$Z_{(i=1,j+2)} = Z_{(i=N,j)} = Z_{(i=N,j+1)}. \tag{258}$$

Using the same procedure as for the flow separation boundary condition, the matrix equation can be formed as $\mathbf{CY} = \mathbf{D}$, where

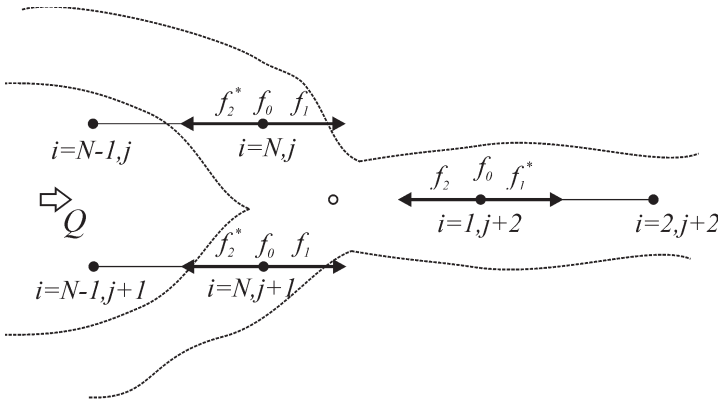


Figure 12: Flow merger.

$$\mathbf{C} = \begin{bmatrix} 1 & 1 & 1 \\ \frac{S^{(m)}_{(i=N,j)}}{Y_{(i=N,j)}} & -\frac{S^{(m)}_{(i=1,j+1)}}{Y_{(i=1,j+1)}} & 0 \\ \frac{S^{(m)}_{(i=N,j)}}{Y_{(i=N,j)}} & 0 & -\frac{S^{(m)}_{(i=1,j+2)}}{Y_{(i=1,j+2)}} \end{bmatrix}, \tag{259}$$

$$\mathbf{Y} = \begin{bmatrix} f^*_{1(i=1,j+2)} \\ f^*_{2(i=N,j)} \\ f^*_{2(i=N,j+1)} \end{bmatrix}, \tag{260}$$

and

$$\mathbf{D} = \begin{bmatrix} f_{1(i=N,j)} + f_{1(i=N,j+1)} + f_{2(i=1,j+2).} \\ S^{(m)}_{(i=N,j)} D_{(i=N,j)} - S^{(m)}_{(i=1,j+2)} D_{(i=1,j+2)} \\ S^{(m)}_{(i=N,j+1)} D_{(i=1,j+1)} - S^{(m)}_{(i=1,j+2)} D_{(i=1,j+2)} \end{bmatrix}, \tag{261}$$

where

$$D_{(i=N,j)} = \frac{f_{0(i=N,j)} + f_{2(i=N,j)}}{Y_{(i=N,j)}} - AR^{(m)}_{(i=N,j)}, \tag{262}$$

$$D_{(i=1,j+1)} = \frac{f_{0(i=1,j+1)} + f_{2(i=1,j+1)}}{Y_{(i=1,j+1)}} - AR^{(m)}_{(i=1,j+1)}, \tag{263}$$

$$D_{(i=1,j+2)} = \frac{f_{0(i=1,j+2)} + f_{1(i=1,j+2)}}{Y_{(i=1,j+2)}} - AR^{(m)}_{(i=1,j+2)}. \tag{264}$$

Solution can be obtained, again, by solving the matrix equation in form

$$\mathbf{Y} = \mathbf{C}^{-1}\mathbf{D}. \tag{265}$$

4.3.2 Boundary conditions for the sediment transport lattice Boltzmann model

The suspended-sediment transport LB model demands upstream and downstream boundary condition. For the upstream boundary, D_{up}, the non-dimensional concentration for the size-class ks is used. Using the zeroth statical moment given in Eq. (165), it follows:

$$C_{up}A_{(i=1,j)}Y_{(i=1,j)} = g_{0(i=1,j)} + g^{*}_{1(i=1,j)} + g_{2(i=1,j)}. \tag{266}$$

Now, the unknown distribution function is

$$g^{*}_{1(i=1,j)} = C_{up}A_{(i=1,j)}Y_{(i=1,j)} - g_{0(i=1,j)} - g_{2(i=1,j)}. \tag{267}$$

For the downstream boudary, the conventional bounce-back boundary scheme is used, which reads that an incoming particle is bounced back into fluid. For the proposed D1Q3 lattice arrangement the unknown distribution function, after bouncing back from the wall after streaming can be calculated as:

$$g^{*}_{2(i=N,j)} = g_{2(i=N-1,j)}. \tag{268}$$

CHAPTER V

PROGRAMMING CODE

In the previous chapter the lattice-Boltzmann models are formed, which evolve the one-dimensional transformed Saint-Venant equations and transformed suspended-sediment mass conservation equations after the Chapman-Enskog expansion. Also, the corresponding boundary conditions have been defined, suitable with longitudinal changes at the watercourse, and derived in the way to satisfy the requirements of the LBM. Corresponding programming code in the programming language FORTRAN has been written, with the purpose to solve the governing equations. Natural watercourses are characterized with complex geometry accompanied with great amount of data. Therefore, an extra effort has been given to the optimization of the code, in order to unburden the of any unnecessary calculations. In the Fig.13 the schematic representation of the used algorithm is given, and in further text, every part of the algorithm is explained.

With purpose to unburden the code with unnecessary operations, which implies repetitive execution of numerous operations in order to calculate the geometrical characteristics of cross-sections (cross-section area, water surface level, wetted perimeter, and water surface width) depending on water surface level, a separate program **CURVES** is written. Every cross-section is divided into equal, smaller, intervals over depth, and for every predetermined depth-step geometrical characteristics are calculated and written in external files. The depth-step is chosen to be $\Delta z = 30\ cm$, as optimal value between the accuracy and the tendency to form the dependence curves with the minimal amount of data. Resulting curves are later used in the main program. If the water surface level is between the assigned depth-steps, linear interpolation between those values is used to trace the desired value.

Program **WS-LBM** is the main program that solves lattice Boltzmann model for the transformed Saint-Venant equations and for the suspended-sediment mass-conservation equation, simultaneously. It consists of 10 chronologically placed subroutines, that form

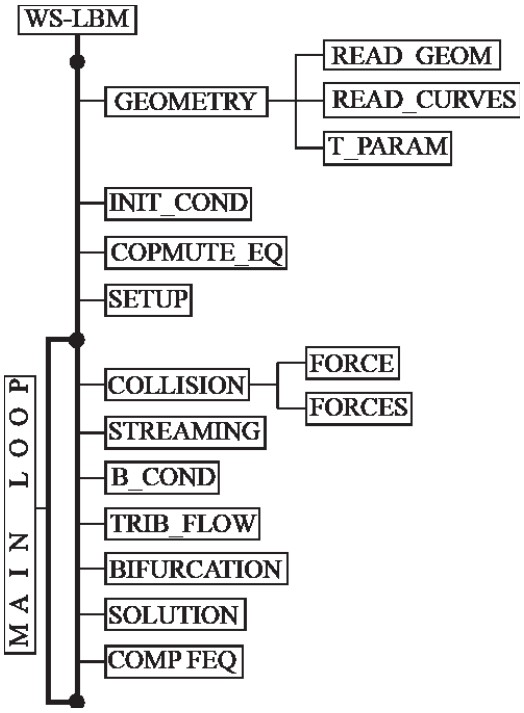


Figure 13: Code algorithm.

the algorithm. After loading the general parameters (number of sections, number of lattice nodes for each section, time step, relaxation times, iteration number, etc.), from assigned external files, first subroutine **GEOMETRY** is summoned, that consists of three sub-subroutines, which are executed one after another:

- **READ_GEOM** - reads the cross-section characteristics: stationery and cross-section geometry;
- **READ_CURVES** - reads the cross-section area-water surface level curve, wetted perimeter - water surface level curve and water surface width - water surface level for each cross-section, previously calculated using the program **CURVES;**
- **T_PARAM** - calculates the transformation parameter for every computational point (cross-section), using the discrete form of the first derivative:

$$Y(j,i) = \frac{x_{(j,i+1)} - x_{(j,i-1)}}{2 \cdot \Delta\xi}, \tag{269}$$

where x is the cross-section stationary, $\Delta\xi$ is the lattice size, $j = 1, ..., N$ is the section

number, and $i = 1, ..., M(j)$ is the computational point number.

Within the subroutine **INIT_COND**, the initial conditions are assigned. Subroutine **COMPUTE_EQ** is summoned, to calculate the initial equilibrium distribution functions values. Within the subroutine **SETUP**, all distribution functions values take over the values of the initial equilibrium distribution function. Prior entering the main loop, variable *time* is set to zero, to indicate initial state. Within the main loop, at each iteration, the value of *time* is increased by 1. The main loop consists of six subroutines:

- **COLLISION** - calculates the values of the distribution functions after the collision step. The force terms are calculated within the separate sub-subroutines **FORCE** (for the water) and **FORCE_S** (for the sediment transport);
- **STREAMING** - calculates the values of the distribution functions after the streaming step;
- **B_COND** - calculates the unknown boudary distribution functions at the model boundaries;
- **TRIB_FLOW** - calculates the unknown distribution functions at the boundary points between the sections where tributary flow is foreseen;
- **BIFURCATION** - calculates the unknown distribution functions at the boudary points between the sections where flow merges or separates;
- **SOLUTION** - calculates new physical variables (discharge, water surface level, cross-section area, depth, velocity, water surface width, concentration);
- **COMPUTE _EQ** - calculates new equilibrium distribution functions.

After every iteration, results are written in external files, within

CHAPTER VI

MODEL TESTING AND VALIDATION

Model testing and validations has two phases. First, the unsteady open-channel flow lattice Boltzmann model has been tested in three steps, each imposing more complex conditions. Within the second phase, sediment transport is attached on the fully functional water flow model, in order to develop a multiphase water - sediment unsteady open-channel flow LBM model.

6.1 One-dimensional unsteady open-channel flow

In order to test and validate the proposed one-dimensional lattice Boltzmann model for the transformed Saint-Venant equations, three case are studied: a steady flow in a prismatic channel with rectangular cross-section, an unsteady flow in a non-prismatic channel and unsteady flow in a natural watercourse. Steady non-uniform flow in a prismatic channel is modeled for two lattice grid dispositions, uniform and non-uniform. For the same physical model, equidistant and non-equidistant grid is formed, and the results are compared with the corresponding model obtained by commercial HEC-RAS software. Within the second test model, unsteadiness is introduced by applying a shock wave as upstream boundary condition and using a non-prismatic channel. Again, physical model is tested for both equidistant and non-equidistant lattice grid. Validation is obtained by the corresponding HEC-RAS models. In the last step, unsteady flow in natural conditions is tested, in order to prove that the developed LBM model is comparable to the standard modelling software. A 31 day long unsteady flow simulation on a chosen section of the Danube River is performed. Besides arbitrary cross-sectional geometry, the chosen section contains four tributaries and two river islands. The verification of the LBM model is obtained by comparison with the measured flow and water level data obtained by standard geodetic survey by the Republic Hydrometeorological service of Serbia (RHMZ).

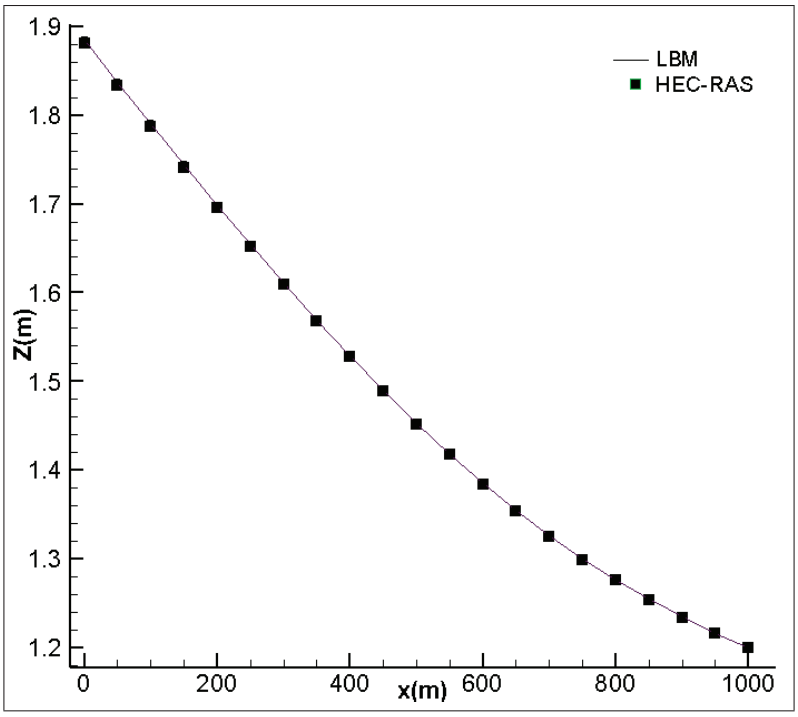


Figure 14: Comparison of water surface elevation along the channel at t = 50 min - equidistant lattice grid

6.1.1 A steady non-uniform flow in prismatic channel

Previously derived D1Q3 LBM for the transformed Saint-Venant equations, defined by Eq. (118), using the relations (120), (122), (123), (125) and (126), is first tested on a prismatic channel of rectangular cross-section having total length $L = 1000\ m$, width $B = 100\ m$, and constant slope $S_0 = 0.001$ is selected. Manning's roughness coefficient is $n = 0.025\ m^{-1/3}s$. Water surface elevation $Z_d = 1.20\ m$ is set as downstream, and discharge $Q_{up} = 100.0\ m^3/s$ as upstream boundary condition, where the unknown distribution functions at the model boundaries are determined using the Eqs. (228) and (230). Initial conditions are set to $Q_{init} = 100.0\ m^3/s$ and $h_{init} = 1.20\ m$ for the entire model. Two cases are observed, one with uniform spatial grid, and one with non-uniform grid, under the same physical conditions. For the uniform grid case, computational lattice size $\Delta\xi = 1.0$ and physical distance between cross sections $\Delta x = 50.0\ m$ is used. For the non-equidistant physical grid, the minimal cross-section distance is $\Delta x_{\min} = 20.0\ m$ and the maximal distance is $\Delta x_{\max} = 81.72\ m$. The computational lattice size is left to be $\Delta\xi = 1.0$. In both cases grid

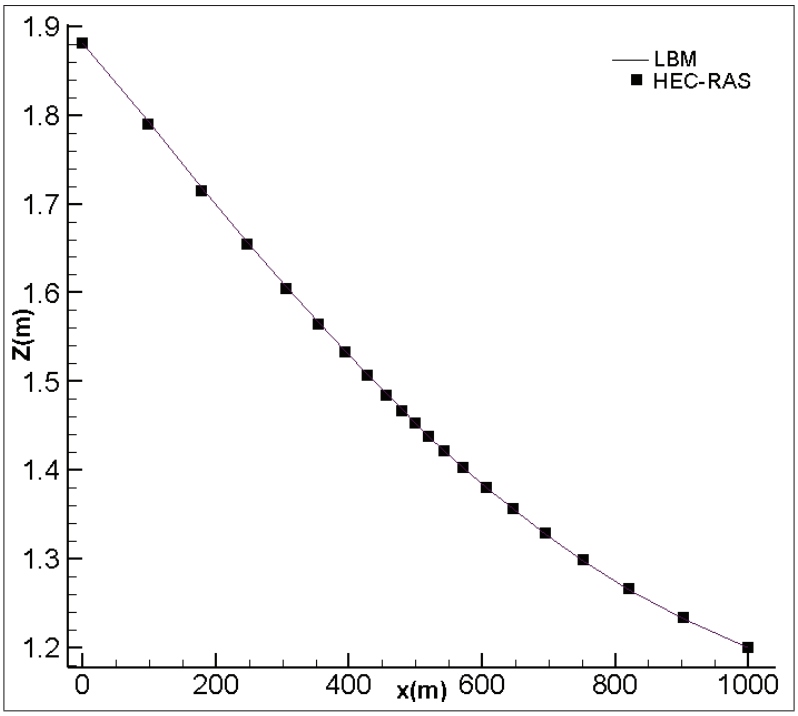


Figure 15: Comparison of water surface elevation along the channel at t = 50 min - non-equidistant lattice grid

has total of 21 computational points, and relaxation time is set to $\tau = 0.505$. The stability for the equidistant grid model is obtained for $\Delta t = 1.0\ s$, while for the non-equidistant grid lower value of $\Delta t = 0.7\ s$ was necessary. Comparison of the water surface elevation for $t = 50$ min with corresponding HEC-RAS model is shown in Fig.(14) and Fig.(15), for the equidistant and non-equidistant model, respectively. Comparison of historical record of water surface elevation for equidistant and non-equidistant lattice grid is shown in Fig.16 and Fig.17, respectively. Comparison of historical record of discharge is shown in Fig.18 and Fig.19, for uniform and non-uniform grid, respectively. Three arbitrary cross-sections are chosen to manifest the results, where cross-section stations shown are measured from the upstream boundary. As one can see from the shown comparisons, very good agreement is achieved for both equidistant and non-equidistant physical grid models.

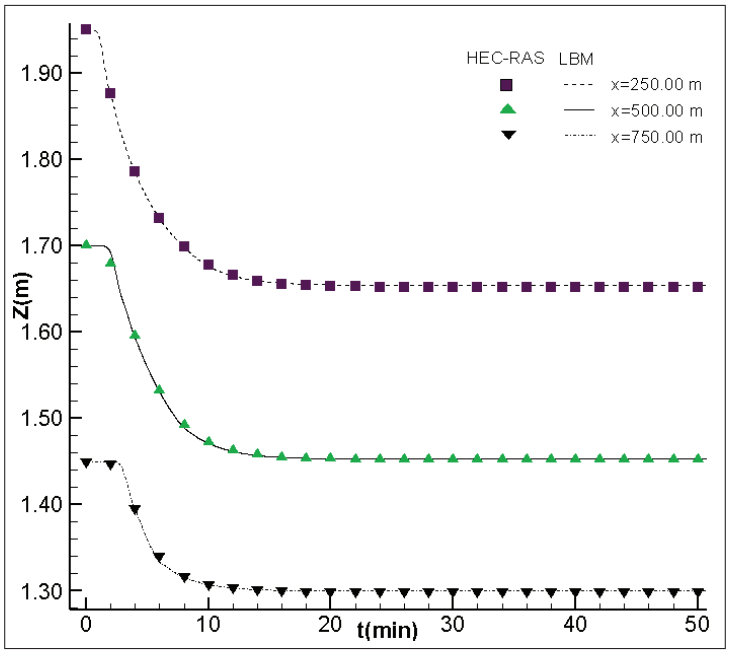


Figure 16: Comparison of historical record of water surface elevation in prismatic channel - equidistant lattice grid

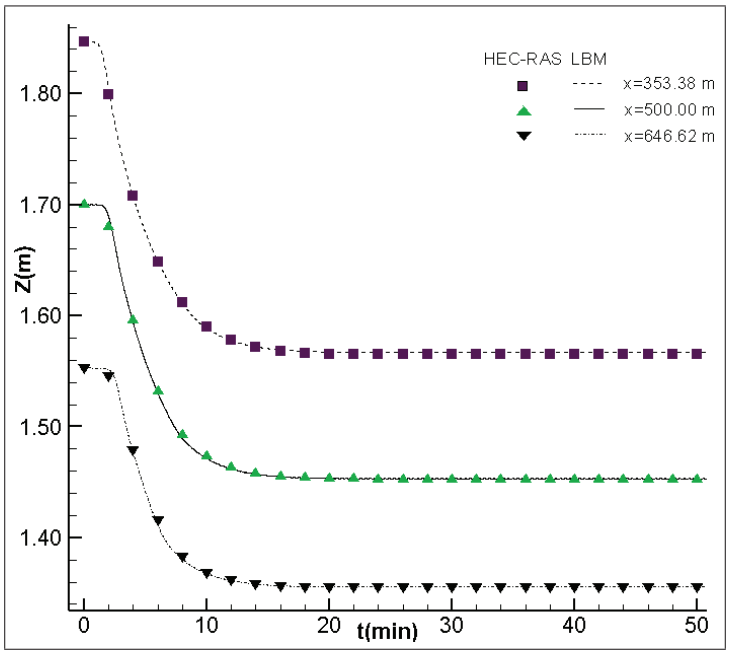


Figure 17: Comparison of historical record of water surface elevation in prismatic channel - non-equidistant lattice grid

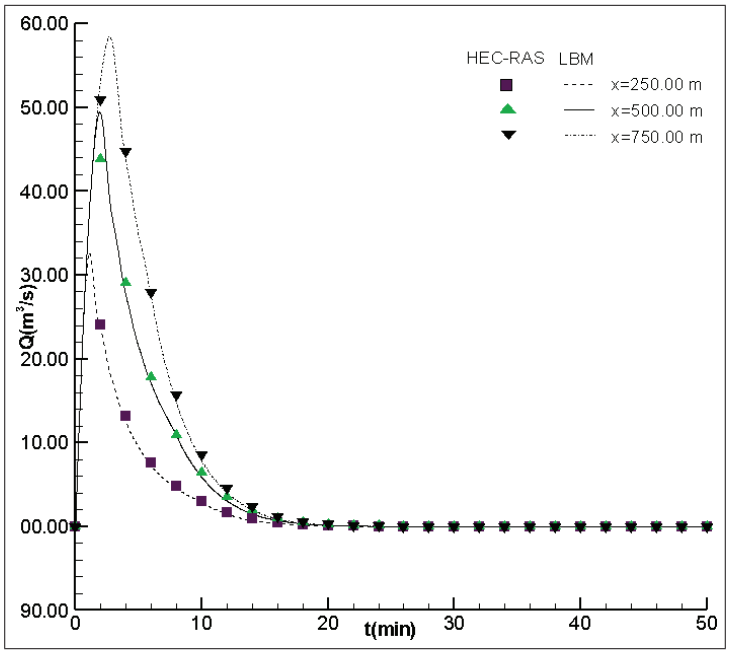


Figure 18: Comparison of historical record of discharge in prismatic channel - equidistant lattice grid

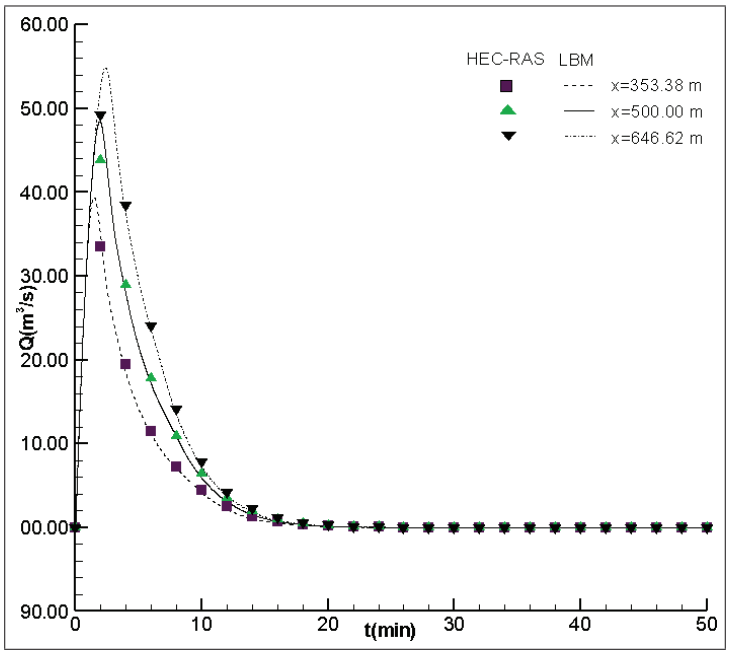


Figure 19: Comparison of historical record of discharge in prismatic channel - non-equidistant lattice grid

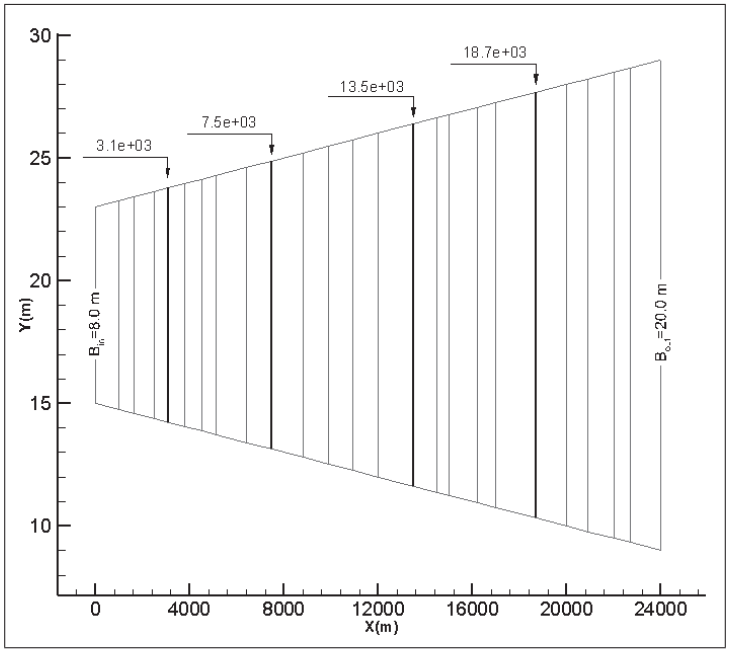


Figure 20: Geometry of non-prismatic channel.

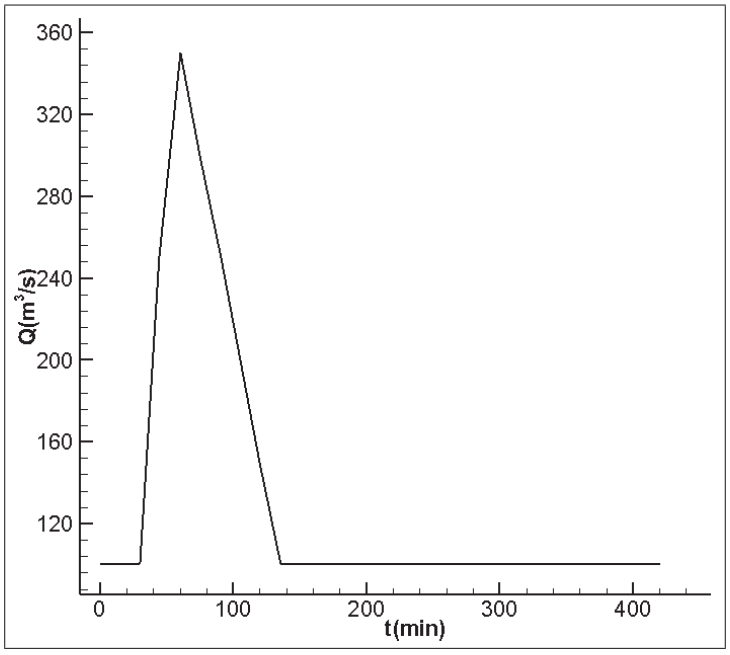


Figure 21: Hydrograph - upstream boundary condition.

6.1.2 An unsteady flow in non-prismatic channel

The same LBM as used in the previous example is now tested for unsteady conditions. A non-prismatic channel of length $L = 24000\ m$, constant bed slope $S_0 = 0.0005$ and Manning's roughness coefficient $n = 0.0667\ m^{-1/3}s$ has been modeled. Channel width is determined by expression $B = 8.0 + 12.0(x/L)$, where x represents the corresponding cross section stationary, measured from the upstream boudary. As shown in Fig.20, channel width linearly changes from $8.0m$ at upstream do $20.0m$ at downstream boundary. Using the same approach as in the previous example, two cases are observed to test uniform and non-uniform physical grid for unsteady flow conditions. In case of the equidistant physical grid constant distance between the cross sections of $\Delta x = 1000.0\ m$ is used, forming 25 computational points. In case of non-equidistant grid random, unequal cross-section distances shown in Fig.20 are applied, resulting with, also, 25 computational points. The minimal cross-section distance is $\Delta x_{\min} = 500.0\ m$ and the maximal distance is $\Delta x_{\max} = 1700.0\ m$. Computational lattice size $\Delta\xi = 1.0$ is used for both cases. Hydrograph shown in Fig.21 is set as upstream boundary condition, to ensure the unsteadiness of the flow, while for the downstream boundary condition normal depth obtained from the Chezy-Manning equation is applied. To determine the unknown distribution functions at boundaries, Eq.(228) and the iterative solution of the Eq. (232) are used. Stability is obtained by setting $\tau = 0.501$ and $\Delta t = 2.0\ s$ for the both cases. Total of 12600 computational steps are performed to do a 420.0 min simulation. Validation is obtained again by the HEC-RAS software that uses bidiagonal four-point implicit finite-difference Preissman scheme [21] . Four cross sections equally distributed along the channel are used as comparison check points, where cross sections stationaries for the non-equidistant grid are marked in Fig.20. The historical record of water surface elevation for the equidistant grid is shown in Fig.22, left, and for the non-equidistant grid is in Fig.23, right. The comparison of the LBM and HEC-RAS model for equidistant and non-equidistant grid shown in Fig.24 and Fig.25, respectively. All compared results are in a very good agreement.

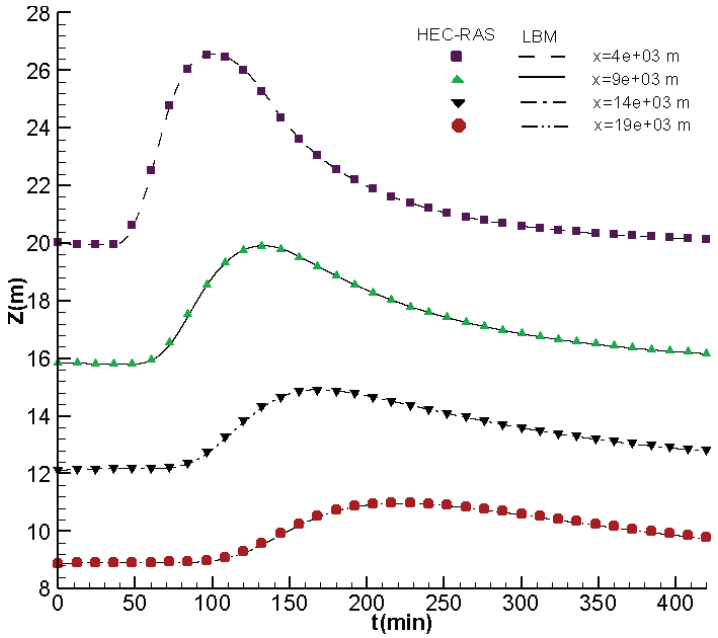


Figure 22: Comparison of historical record of water surface elevation in prismatic channel - equidistant grid

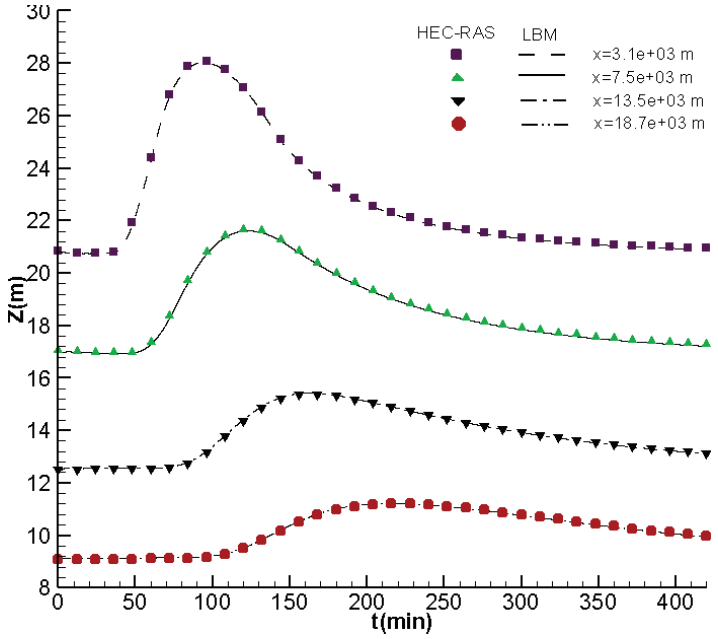


Figure 23: Comparison of historical record of water surface elevation in prismatic channel - non-equidistant grid

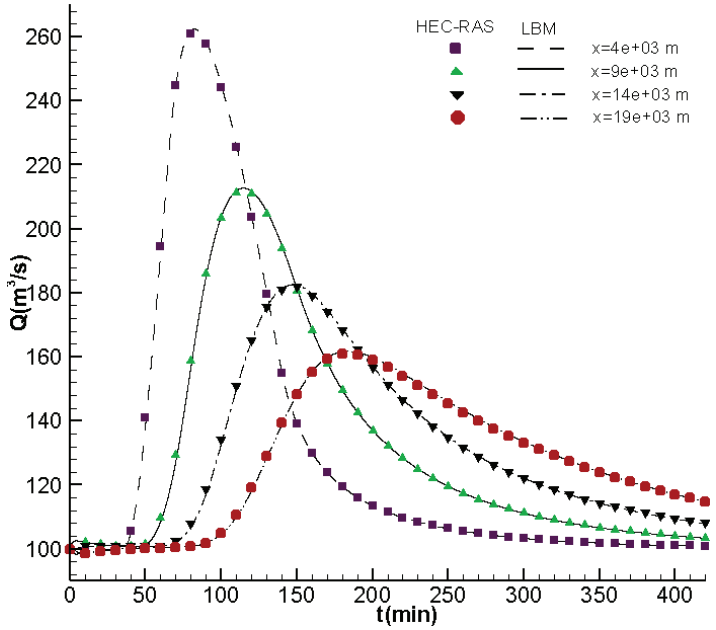


Figure 24: Comparison of historical record of discharge in prismatic channel - equidistant grid

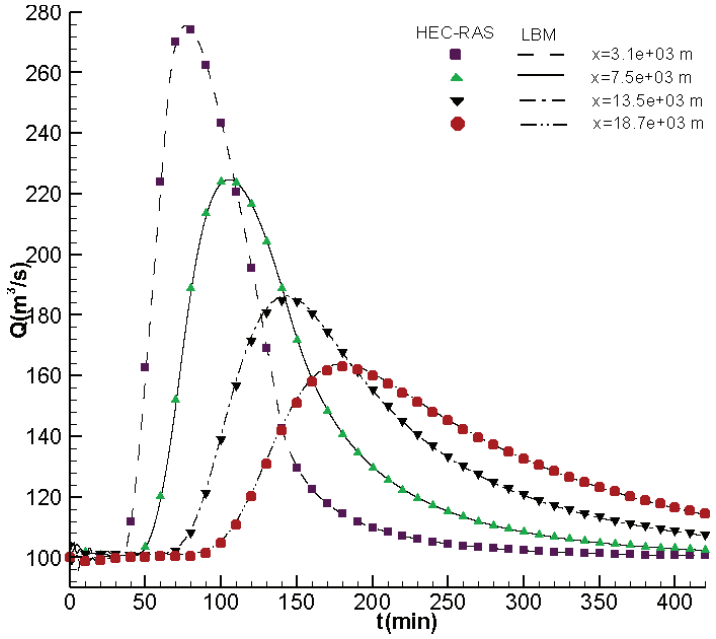


Figure 25: Comparison of historical record of discharge in prismatic channel - non-equidistant grid

6.1.3 Unsteady flow in a natural watercourse - Danube River case study

The final step when testing newly developed non-uniform grid based LBM for the Saint-Venant equations is to apply the model on a watercourse with arbitrary cross-sectional and longitudinal geometry, as it is shown that the model functions very well when simple geometry is modeled. The goal is to perform a long-lasting simulation under natural conditions. One section of the Danube River is chosen to form a model.



Figure 26: The Danube River experimental reach

The Danube River has the total length of 2860 km. It originates in Germany, passes through Austria, Slovakia, Hungary, Croatia, Serbia, Romania, Bulgaria, Moldova and Ukraine and discharges into the Black Sea. Its drainage basin extends into nine more countries. It has 31 tributaries and many closed bifurcation systems (river islands). Approximately 10.2% of the Danube's length crosses through Serbia. To test the proposed model, the Serbian section of the Danube River stretching between the Iron Gate I Hydroelectric Power Station (rkm 970.35) and the Smederevo gauging station in Serbia (rkm 1116.23) is used, as shown in Fig.26. This section has total length of 145.88 km, has four tributaries: Velika Morava, Nera, Pek and Porečka, and two closed bifurcation systems. Measured morphological data is used to form a model. Along the observed section of the river total of 160 cross-sections are available. The distance between them varies between

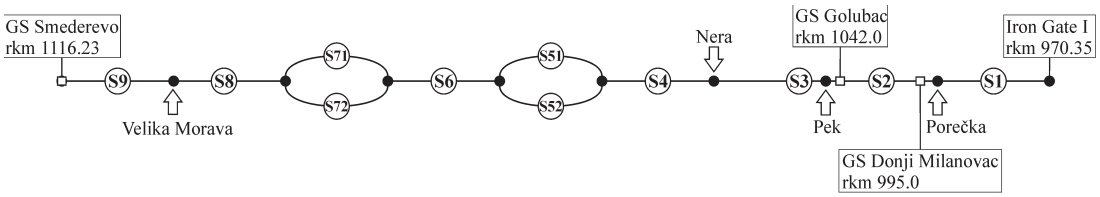


Figure 27: Shematic model.

$800 \div 1300m$. One cross-section is shown in Fig.28. The total length of the experimental reach is divided into nine sections, each of them separated by a tributary or river islands, as shown in Fig.27. The characteristics of the sections are given Table 2. Sections S51, S52, S71 and S72 represent river islands. The measured cross-section geometry of sections S5 and S7 is separated at the highest points of the river island into two separate river branches. If the river island floods, two river branches merge into one and form sections S5 and S7.

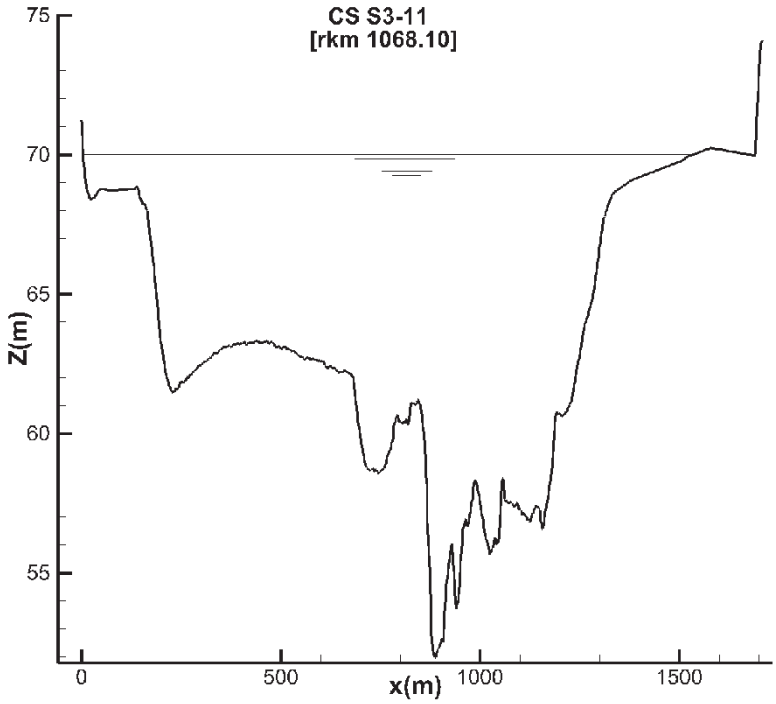


Figure 28: Cross-section of the river bed

Lattice Boltzmann D1Q3 model, defined by Eq.(118) is used. Equilibrium distribution

Section	Station	Length	Number of cross-sections
	rkm	km	
S1	970.35÷993.00	22.65	23
S2	993.00÷1057.40	64.40	62
S3	1057.40÷1075.00	17.60	19
S4	1075.00÷1078.00	3.00	7
S51	1078.00÷1082.00	4.00	6
S52	1078.00÷1082.00	4.00	6
S6	1082.00÷1087.50	5.50	8
S71	1087.50÷1091.00	3.50	5
S72	1087.50÷1091.00	3.50	5
S8	1091.00÷1104.35	13.35	20
S9	1104.35÷1116.23	11.88	10

Table 2: Properties of the computational sections

functions defined by Eq. (122), and force term is calculated from the Eq. (123).Physical variables Q and Z are calculated based on the obtained distribution functions by Eqs.(125),(126) and from the cross-section area - water surface level curves obtained by the program **CURVES**. Boundary conditions for this experimental reach, upstream hydrograph at gauging station Smederevo (Fig.29) and downstream water level at GS Iron Gate I during August 2006 are obtained by the Republic Hydro-meteorological Service of Serbia (Fig.30). Distinct unsteady flow can be observed. At the beginnings and ends of sections S5 and S7, inner boundary conditions defined by Eqs.(256a) and (265). Tributary rivers Nera, Pek and Porečka have insignificantly small flows, but for tributary Velika Morava River $Q_t = 90\, m^3/s$ is applied with boundary conditions defined by Eqs. (238) and (240) between the sections S8 and S9. Manning's roughness coefficient is $n = 0.0318\, m^{-1/3}s$ for the whole experimental reach, lattice size is $\Delta\xi = 1.0$ and the relaxation time is $\tau = 0.57$. The stability is obtained for the time step $\Delta t = 10.0\ s$.

Before the unsteady flow simulation steady flow is achieved by imposing constant flow $Q = 2570.0\ m^3/s$ and constant water level $Z = 69.44\ m$ in duration of four days. The same values discharge and water level are assigned as initial conditions for the whole domain of the model. After stabilization of the model, for the next 31 days boundary conditions shown in Fig.29 and Fig.30 are applied. The unknown distribution functions at the upstream and downstream boundary are determined from Eqs. (228) and (230). The 31 day simulation

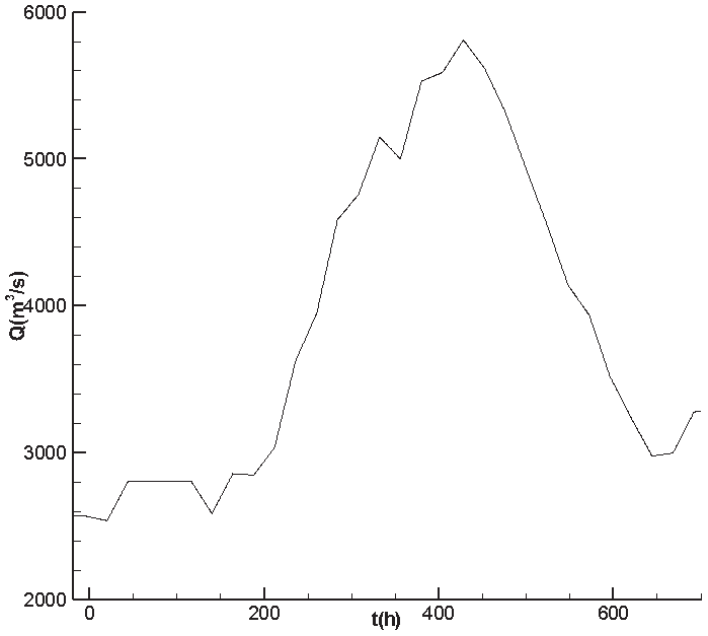


Figure 29: Upstream boundary condition at GS Smederevo.

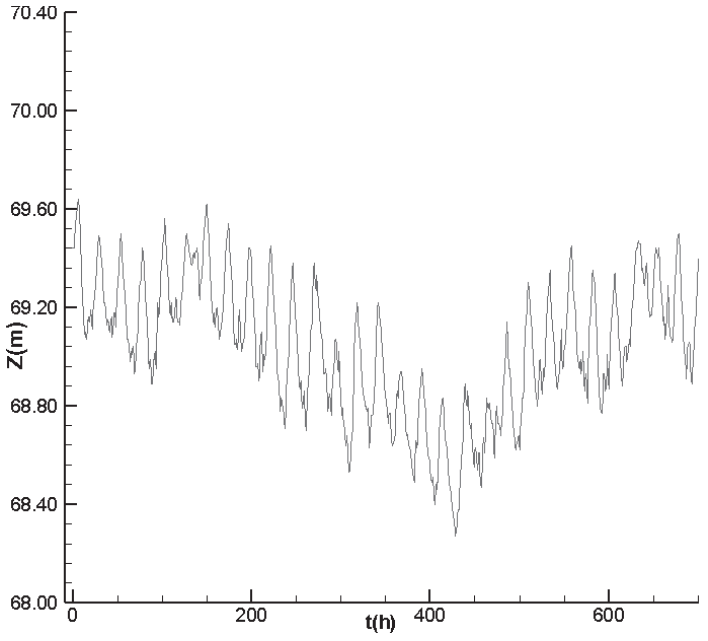


Figure 30: Downstream boundary condition at Iron Gate I.

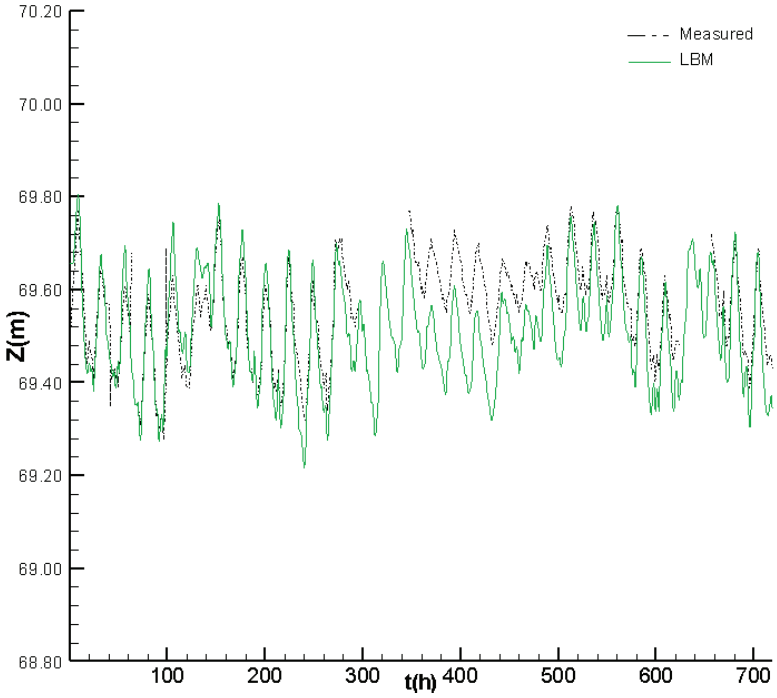


Figure 31: Comparison of the historical record of water surface elevation at GS Golubac.

is obtained with 267840 steps in 12.34 min. For the comparison of the results, measured historical discharge for August 2006 at Iron Gate I, and historical water levels at gauging stations Golubac (rkm 1042.00) and Donji Milanovac (rkm 995.00), based on the RHMZ data, are used. Comparison of the LBM with RHMZ measurements of historical water level for GS Golubac and GS Donji Milanovac are given in Fig.31 and Fig.32, respectively, and the comparison for the historical discharge at Iron Gate I is shown in Fig.33. Obtained results are in a very good agreement for both data sets. Deviations between calculated and measured values of water levels are in range of 10.0 cm, which is very satisfactory for this kind of significantly unsteady flow regime. Significant difference of 18 cm is observed only between August 16^{th} to 21^{st} at GS Golubac. When analyzing the historical discharge, deviations between the compared results are in the range of 200.0 m^3/s, and the most significant difference of 840.0 m^3/s is observed only once, on August 10^{th}.

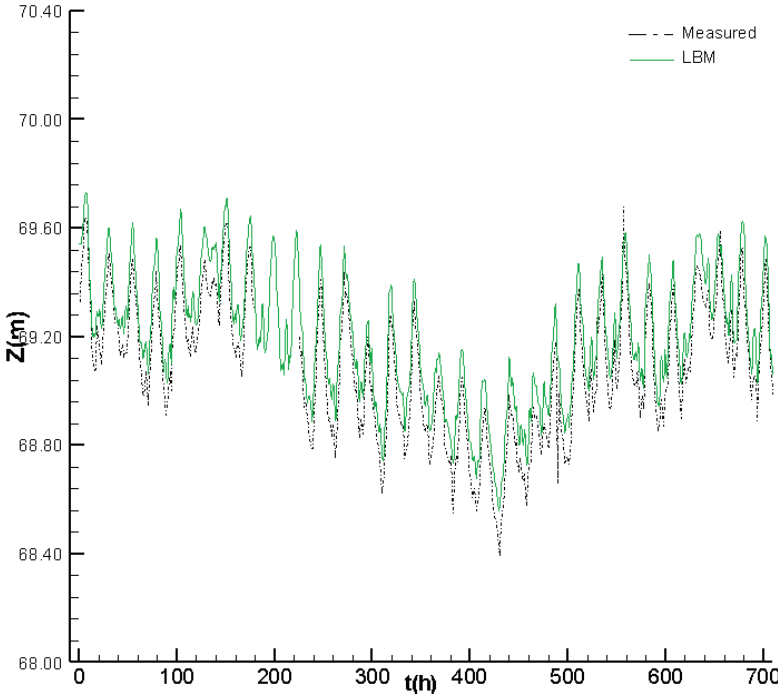


Figure 32: Comparison of the historical record of water surface elevation at GS Donji Milanovac.

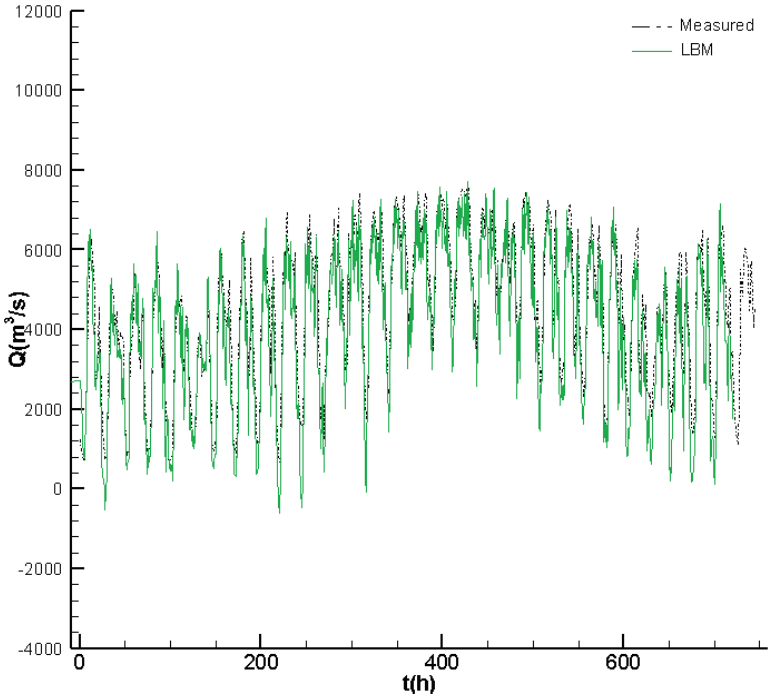


Figure 33: Comparison of the historical record of discharge at GS Iron Gate I.

6.2 One-dimensional open-channel sediment transport

Under the second phase of this research, the unsteady open-channel flow model is upgraded with the suspended-sediment transport model. First, the LBM model for the transformed suspended-sediment mass-conservation equation was tested on a basic advection-diffusion in a prismatic channel, independently of the flow model, and the comparison is made with the analytical solution of the advection-diffusion equation for both equidistant and non-equidistant lattice grid disposition. In the last case study, the combined one-dimensional unsteady flow with suspended-sediment transport LBM model was tested on the chosen section of the Danube River, and the comparison of the LBM results is made with the measured data obtained from the RHMZ. To compensate insufficient suspended-sediment empirical data, statistical data processing have been performed, based on the available measured values. As this part of the research is still in a early stage, only suspended-sediment transport is analyzed. In further research (that is ongoing), the focus is to test and validate the complete sediment transport lattice Boltzmann model developed in Chapter IV.

6.2.1 Advection-diffusion in a prismatic channel

In order to test the derived suspended-sediment LBM defined by Eqs. (158)-(162), prismatic channel of length $L = 5000.0\ m$, with constant cross-section area $A = 1.0\ m^2$ is used. The number of sediment size-classes is $KS = 1$. As the initial condition suspended-sediment concentration distribution along the channel length $C_k^{init}(x)$, characterized with a high peak, shown in Fig.34, which is challenging for the LBM, because of the sudden changes and steep slopes of the curve. The initial suspended-sediment concentration is obtained from the following equation:

$$C_{ks}^{init}(x,0) = \frac{C_0}{\sqrt{\varepsilon_s \pi t_0}} e^{\frac{-(x-x_0)^2}{4\varepsilon_s t_0}}, \tag{270}$$

where $C_0 = 3308.75$, $t_0 = 3484.8\ s$, $x_0 = 1400.00\ m$, $\varepsilon_s = 3.0\ m/s$, and x is spatial coordinate along the channel length. Upstream boundary condition is suspended-sediment

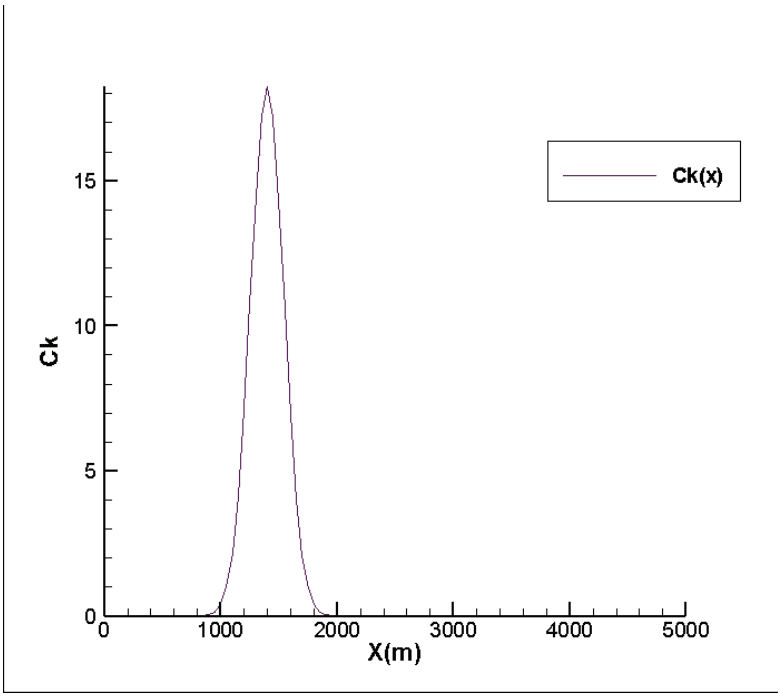


Figure 34: Initial suspended-sediment concentration distribution.

concentration value obtained from the equation:

$$C_{ks}^{up}(0,t) = \frac{C_0}{\sqrt{\varepsilon_s \pi (t_0 + t)}} e^{\frac{-(-u \cdot t - x_0)^2}{4\varepsilon_s (t + t_0)}}, \tag{271}$$

where t is time, and $u = 0.5\ m/s$. Using this concentration values, for every time-step, unknown distribution function at the upstream boundary is calculated from Eq. (267). The last term of the Eq. (158), the force term, is set to zero, because only advection and diffusion terms have been tested in this case. Again, two grid disposition cases have been formed (equidistant and non-equidistant), and tested for the same conditions. For the equidistant grid case, spatial step $\Delta x = 50.0\ m$ is used, with lattice distance of $\Delta\xi = 1.0$, forming 101 computational points. For the non-equidistant spatial grid, arbitrary cross-section distance is scattered along the channel length varying from $40.0 \div 90.0\ m$, so that the number of 101 computational points is preserved. Simulation time is $T = 2520.0\ s$. Lattice size is again set to be $\Delta\xi = 1.0$.For the both cases, stability is achieved for $\tau = 0.76$, and time step $\Delta t = 1.0\ s$, therefore, both simulations are performed with 252 computational steps. Results of the LBM for both cases are compared with analytical solution given by

the following equation:

$$C_k^{up}(x,t) = \frac{C_0}{\sqrt{\varepsilon_s \pi (t_0 + t)}} e^{\frac{-(x-u\cdot t-x_0)^2}{4\varepsilon_s (t+t_0)}}. \tag{272}$$

Comparison between the LBM and the analytical solution (AS) for the equidistant and non-equidistant grid are given in Fig.(36) and (35), respectively. Compared results are in excellent agreement for the both grid cases.

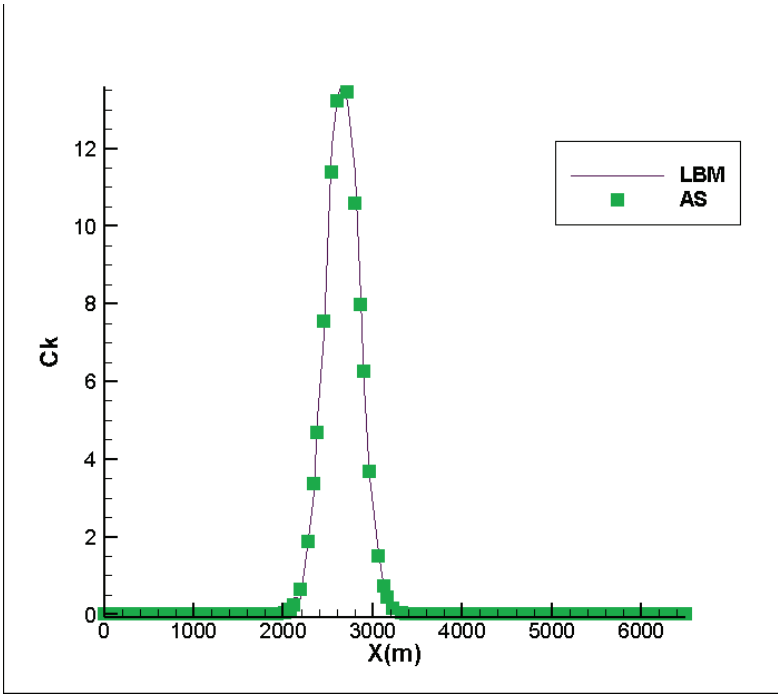


Figure 35: Comparison of suspended-sediment concentation distribution along the prismatic channel for the non-equidistant grid.

6.2.2 Unsteady flow with sediment transport in a natural watercourse - Danube River case study

Finally, the one-dimensional multiphase unsteady water flow with suspended-sediment transport in a natural watercourse has been tested. Section of the Danube River of length 176.29 km, from GS Bezdan (rkm 1430.44) to GS Novi Sad (rkm 1254.15), have been used to form a model (Fig.37). This section of the Danube has no tributaries nor river islands, therefore, one the whole experimental reach can be modeled as one section with 73 computational points (cross-sections). Distance between cross-sections is in the range between

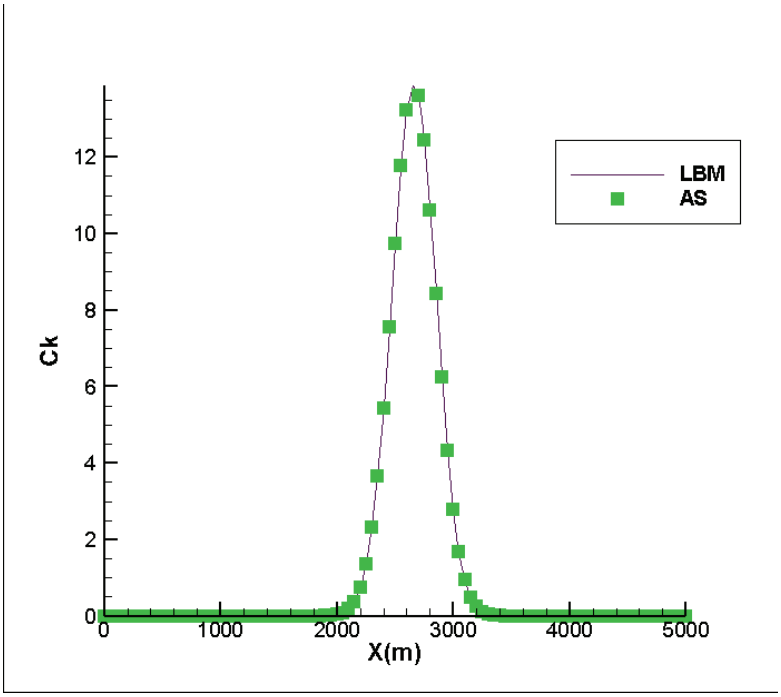


Figure 36: Comparison of suspended-sediment concentation distribution along the prismatic channel for the equidistant grid.



Figure 37: The location of the experimental reach.

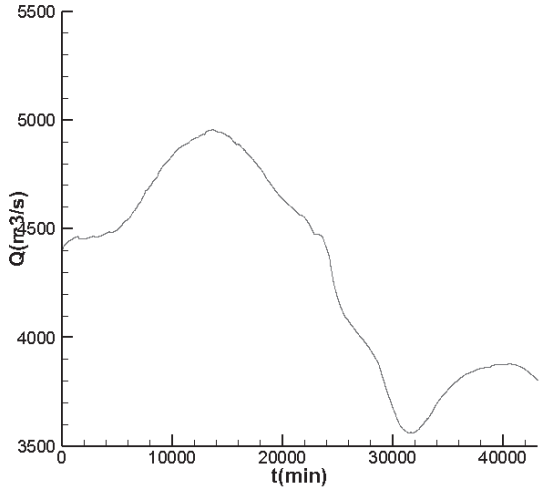


Figure 38: Upstream boundary condition at GS Bezdan - dicharge.

$850.00 \div 5460.00\ m$. Combined LBM has been used: lattice Boltzmann model for the transformed Saint-Venant equations with LBM for transformed suspended-sediment mass-conservation equation. A 31 day simulations has been performed. Discharge (Fig.38) and suspended-sediment concentration measurements (Fig.40) at gauging stations Bezdan during May 2006 have been used as upstream boundary conditions, while water level (Fig.39) measurements and GS Novi Sad have been used as downstream boudary condition. LBE for the transformed SVE (118), with the equilibrium distribution function (122), and force term (123) is modeled with the relaxation time $\tau_f = 0.58$. Physical variables Q and Z are calculated based on the obtained distribution functions by Eqs.(125), (126) and from the cross-section area - water surface level curves obtained by the program **CURVES**. Relaxation time used for the LBM for the transformed suspended-sediment mass-conservation equation (Eqs. (158)-(162)) is $\tau_g = 0.82$, number of sediment size-classes is $KS = 1, .$and sediment mass-diffusivity coefficient is $\varepsilon_s = 20.0\ m/s$. Lattice size is set to be $\Delta\xi = 1.0$. Stability of the model is obtained for time step $\Delta t = 10.0\ s$.

First, steady water flow is achieved by imposing constant water level $Z = 85.77\ m$ and constant flow $Q = 4550.0\ m^3/s$.After stabilization of the model, keeping the obtained

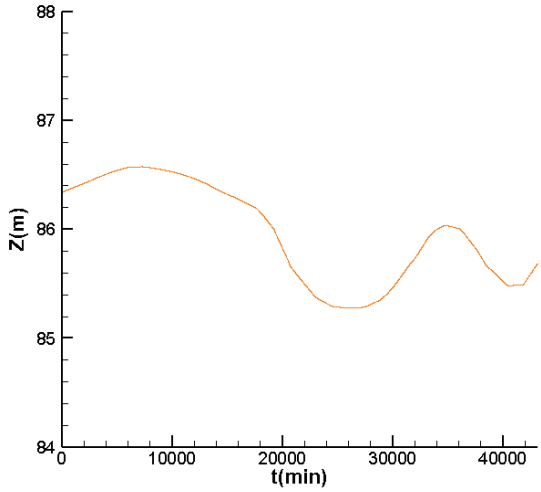


Figure 39: Downstream boundary condition at GS Novi Sad - water surface level.

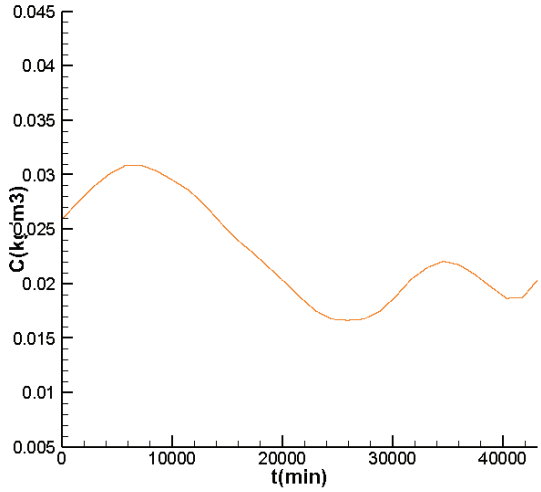


Figure 40: Upstream boundary condition at GS Bezdan - suspended-sediment concentration.

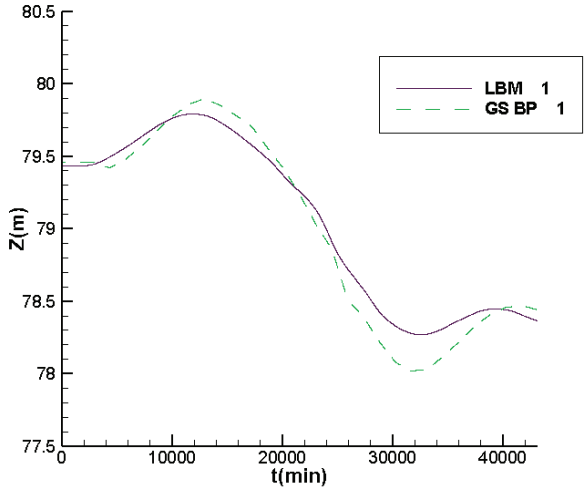


Figure 41: Comparison of historical record of water level - GS Bačka Palanka

steady flow state, steady suspended-sediment transport is accomplished by forcing constant suspended-sediment concentration $C_{ks} = 0.0259\ kg/m^3$. Following the stabilization of the combined model, 31 day long simulation of unsteady flow with suspended-sediment transport has been performed. Discharge and water level measurements shown in Fig. 38 and Fig.39, respectively, are set as upstream and downstream boundary condition for the flow model. Taking this values, the unknown distribution functions at the upstream and downstream boundary are calculated from Eqs. (228) and (230), respectively. The unknown distribution function of the sediment transport LBM at the upstream boundary is determined from Eq. (267), using the values of the concentration obtained from measurements shown in Fig.40. At the downstream boundary, bounce-back condition is imposed, calculating the unknown distribution function from Eq. (268).

To validate the water flow model adequate comparison of obtained results with the corresponding daily based stage hygrograph is made. The comparison of water surface level for the gauging station Bačka Palanka (rkm 1298.66) is shown in Fig.41. Obtained results are in a acceptable agreement. Deviations between calculated and measured values of water levels are in range of 10.0 cm, which is very satisfactory. Maximal observed difference is 25 cm. Measured data for suspended-sediment concentration is available only

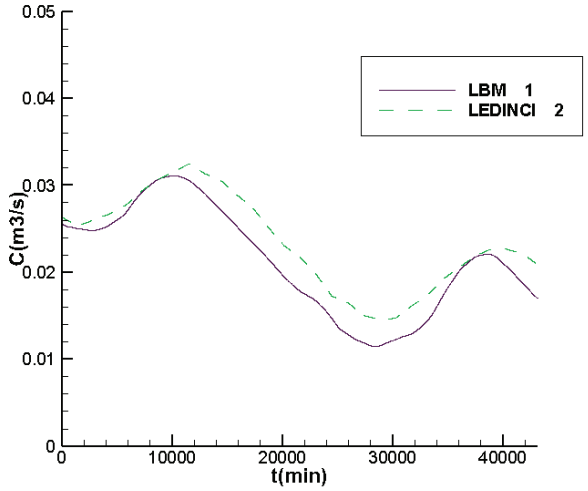


Figure 42: Comparison of suspended-sediment concentartions - GS Ledinci

for GS Bezdan. This data was already used to form the upstream boundary condition. In the absence of additional measurements, which would be used to verify the results, discharge - suspended-sediment concentration dependence ($C(Q)$) curve is formed, based on the available measurements during May 2006 for GS Bezdan. This dependence curve is best fitted with order 2 polynomial trendline in form:

$$C(Q) = 4.0 \cdot 10^{-10} \cdot Q^2 + 5.0 \cdot 10^{-6} Q - 0.0029. \tag{273}$$

This polynomial trendline equation has been applied on the discharge measurements during May 2006, and the obtained concentration values have been used to verify the results. Obtained results are in a acceptable agreement. Average deviations between compared values of concentration are in range of 0.002 kg/m^3, which is acceptable, minding that only suspended-sediment transport is modeled. The maximal observed difference is 0.004 kg/m^3, which is satisfactory, minding the unsteady flow condition and the fact that only suspended sediment is modeled. In the forecoming segment of this research, the complete sediment transport model, derived in the Chapter IV will be modeled.

CHAPTER VII

CONCLUSION

In this thesis, first, the one-dimensional unsteady open-channel flow lattice Boltzmann model is developed, tested and verified. In addition, water flow model is upgraded with the sediment transport model, which, based on the physical problem, can be used independently or simultaneously. The goal was to develop a robust numerical model that solves complex physical processes in natural open-channel watercourses.

The one-dimensional open-channel unsteady water flow lattice Boltzmann model offers two aspects of the contributions. First, lattice Boltzmann method is a relatively new approach in modeling unsteady flow. A review of the literature in Chapter II shows the existing models and commonly accepted directions in modeling the considered processes. The finite-difference Preissman scheme and Holly-Preissmann method are the most widely used methods in free-surface one-dimensional subcritical numerical modelling. LBM, being a mesoscale numerical method, does not fall behind from the existing methods when it comes to accuracy, and has its advantage when long-term simulations of spatially large physical domains are modeled due to its suitability for parallel programming. Using this method partial differential equations are locally discretized on the lattice nodes. Collision and streaming processes are independent, which allows parallel execution of the computational operations. The result is significantly shorter computational time, which allows spatial and temporal expansion of the model. At the other hand a novel form of the lattice Boltzmann method for solving the Saint-Venant equations is presented. In order to establish the LBM as tool for solving practical problems when one dimensional modeling of flow in natural watercourses is considered, two major improvements of the standard LBM have been successfully introduced and validated. First improvement is the formulation of the water surface that eliminates the bed slope term (since for natural geometry the bed slope term is difficult to define). The second is the non-uniformity of the physical computational

grid, which opens opportunity for optional arrangement of computational points along the modeled reach. Instead of disturbing the numerical model itself, governing equations are transformed from the physical to the computational domain, and calculation of terms defined in the non-equidistant physical space in the equidistant computational grid is enabled. Furthermore, the concept of arbitrary cross-section geometry is introduced. With a special attention, all the elements that would unnecessarily burden the model and thus extend the computational time are eliminated, and, as a result, a relatively simple algorithm that solves very complicated physical processes of unsteady flow in natural watercourses is obtained. Besides the cross-sectional geometry, tributary flow and bifurcation boundary conditions are derived and successfully implemented in the model. In order to validate the model three cases are analyzed: a steady non-uniform flow in prismatic channel, an unsteady flow in non-prismatic channel, and unsteady flow in a natural watercourse - Danube River case study. The results for the channels with simple geometry are compared with corresponding HEC-RAS models. For the Danube River case study the chosen 145.88 km long section or the river includes four tributaries and two closed bifurcation systems. Results are verified by comparison with the field measurements. Excellent agreement between the all compared results is obtained confirming the capacity of the proposed model to serve as a fully competitive practical tool comparable to the standard modelling software.

Furthermore, the one-dimensional sediment transport lattice Boltzmann model is developed in addition to the existing unsteady flow model. Sediment is characterized by a different behavior with regard to its location; suspended-sediment is considered to move with the water flow, while bed and near-bed sediment particles do not follow the same patterns. Therefore, the domain of sediment transport is divided into three unities: suspended-sediment, active layer bed sediment and bed sediment (stratum). The governing equations describe the behavior of each sub-domain and the exchange mechanisms between them. Using the same approach as for the unsteady flow model, equations are transformed from non-uniform physical domain to uniform computational grid, maintaining required uniformity of the lattice structure imposed by the symmetry of the predefined lattice velocities. The existing solution algorithm is upgraded in the way that it is now able to solve sediment

transport equations using the resulting physical variables from the unsteady flow model as input data. Prior to creating the model that solves unsteady flow with sediment transport in natural watercourses, a test model for the advection-diffusion equation is made, and the results are in an excellent agreement with the analytical solution of the equation. The multiphase water-sediment unsteady flow is tested on another Danube River case study, on a 176.29 km long section. In the absence of measured data that could be used for the verification, the statistical data processing have been performed and used for the comparison. Considering the early phase of this part of the research, obtained results are in an acceptable agreement. Further course of the research is implied; to develop a fully functional one-dimensional unsteady flow with sediment transport lattice Boltzmann model, where the sediment mixture is represented with more than one sediment size-classes. Forthcoming research will also be directed to computational optimization, especially in terms of computer code parallelization.

CHAPTER VIII

REFERENCES

1. M.B. Abbott. Computational hydraulics.Elements of the theory of free surface flows. Pitman, London, 1979.

2. R. Appadu, M. Z. Dauhoo, and S. D. D. V. Rughooputh. Control of numerical effectsof dispersion and dissipation in numerical schemes for efficient shock-capturing throughan optimal courant number. Computers & Fluids, 37:767–783, 2008.

3. P. L. Bhatnagar, E. P. Gross, and M. Krook. A model for collision processes in gases. i. Small amplitude processes in charged and neutral one-component systems. Physical Review, 94(3):511-525, 1954.

4. S. M. Bhallamudi and M. H. Chaudhry. Numerical modeling of aggradation and degradation in alluvial channels. Journal of Hydraulic Engineering, 117(9):1145–1164, 1991.

5. G. W. Brunner. Hec-ras, river analysis system hydrauclic reference manual. Technical Report CPD-69, US Army Corps of Engineers, Hydrologic Engineering Center, 2010.

6. Lj. Budinski. MRT lattice Boltzmann method for 2D flows in curvilinear coordinates. Computers & fluids,96:288-301, 2014.

7. Lj. Budinski. Application of the LBM with adaptive grid on water hammer simulation. Journal of Hydroinformatics, 18(4):687-701, 2016.

8. Lj. Budinski, J. Fabian, and M. Stipić. Lattice Boltzmann method for groundwater flow in non-orthogonal structured lattices. Computers and Mathematics with Applications, 70:973-991, 2015.

9. J. M. Buick and C. A. Greated. Gravity in a lattice Boltzmann model. Physical Review E, 61(5):5307-5320, 2000

10. B. Servan-Camas, F. Tzai.Non-negativity and stability analyses of lattice Boltzmann method for advection-diffusion equation. Journal of Computational Physics, 228(1): 236-256, 2009

11. S. Chen and G. D. Doolen. Lattice Boltzmann method for fluid flows. Annual Review of Fluid Mechanics, 30:329-364, 1998.

12. S. Chen, H. D. Chen, D. Martinez, and W. Matthaeus. Lattice Boltzmann model for simulation of magnetohydrodynamics. Phys. Rev. Lett., 67:3776-3779, 1991.

13. H. Chen and X. Shan. Lattice Boltzmann model for simulating flows with multiple phases and components.Physical Review E, 47:1815-1819, 1993.

14. J. Clemmens and F. M. Holly. Description and evaluation of program duflow. Journal of Irrigation and Drainage Engineering, 119(4):724–734, 1993.S. D. Conte and C. deBoor. Elementary Numerical Analysis. McGraw-Hill, New York, 1972.

15. D. d'Humieres, I. Ginzburg, M. Krafczyk, P. Lallemand, and L. Shi. Multiple-relaxationtime lattice Boltzmann models in three dimensions. Philosophical Transactions of the Royal Society London A, 360:437-451, 2002.

16. DHI. Mike 11, a modeling system for rivers and channels. user guide. Technical report, DHI, Water, Environment and Health, 2009.

17. R. E. Ewing and H. Wang. A summary of numerical methods for time-dependent advection-dominated partial differential equations. Journal of Computational and Applied Mathematics, 128:423–445, 2001..

18. H. Fang, M. Chen, and Q. Chen. One-dimensional numerical simulation of non-uniform sediment transport under unsteady flows. Journal of Sediment Research, 23(4):315–328, 2008.

19. J. B. Frandsen. A simple LBE wave runup model. Progress in Computational Fluid Dynamics, 8(14):222-232,255 2008.

20. U. Frisch, B. Hasslacher, Y. Pomeau. Lattice-gas automata for the NavierStokes equation. Physical Review Letters, 56:1505-1508, 1986.

21. U. Frisch et al.. Lattice Gas Hydrodynamics in Two and Three Dimensions. Complex Systems 1(4), 1987

22. Ginzburg. Equilibrium-type and link-type lattice Boltzmann models for generic advection and anisotropic-dispersion equation. Advances in Water Resources, 28:1171-1195, 2005.

23. Ginzburg, G. Silva, L. Talon. Analysis and improvement of Brinkman lattice Boltzmann schemes: Bulk, boundary, interface.Similarity and distinctness with finite elements in heterogeneous porous media. Physical Review E : Statistical, Nonlinear, and Soft Matter Physics, American Physical Society„ 91 (2), 32 p., 2015.

24. A.K. Gunstensen and D. Rothman. Lattice Boltzmann model of immiscible fluids. Physical Review A, 43(8):4320-4327, 1991.

25. J. Hardy, 0. de Pazzis, and Y. Pomeau. Molecular dynamics of a classical lattice gas: Transport properties and time correlation functions. Phys. Rev. A,13:1949-1961, 1976.

26. Higuera and J. Jimenez. Boltzmann approach to lattice gas simulations. Europhys lett., 9:663 -668, 1989.

27. F. M. Holly and J. L. Rahuel. New numerical/physical framework for mobile-bed modelling, part 1: Numerical and physical principles. Journal of Hydraulic Research, 28(5):401–416, 1990a.

28. F. M. Holly and J. L. Rahuel. New numerical/physical framework for mobile-bed modelling, part 2: Test applications. Journal of Hydraulic Research, 28(5):545–564, 1990b.

29. M. Jr. Holly and J. B. Parrish. Description and evaluation of program carima. Journal of Irrigation and Drainage Engineering, 119(4):703–713, 1993.

30. F. M. Jr. Holly and A. Preissmann. Accurate calculation of transport in two dimensions. ASCE Journal of the Hydraulic Division, 103(HY11):1259–1277, 1977.

31. Yang J. C. Holly, F. M. Jr. and M. Spasojevic. Numerical simulation of water and sediment movement in multiply-connected networks of mobile bed channels. Technical Report 131, Iowa Institute of Hydraulic Research, The University of Iowa, 1985.

32. J. Huang, A. G. L. Borthwick, and R. L. Soulsby. One-dimensional modelling of fluvial bed morphodynamics. Journal of Hydraulic Research, 46(5):636–647, 2008.

33. M. Isic. Linijski model interackcije vode i nanosa u mreži prirodnih vodotoka. PhD thesis, Građevinski fakultet Subotica, Subotica, 2014.

34. Islam, N. S. Raghuawanshi, and R. Singh. Development and application of hydraulic simulation model for irrigation canal network. Journal of Irrigation and Drainage Engineering, 134(1):49–59, 2008

35. M. F. Karim, F. M. Jr. Holly, and Y. C. Yang. Ialuvial: Numerical simulation of mobilebed rivers; part i, theoretical and numerical principles. Technical Report IIHR Reprt No. 309, Iowa institute of Hydraulic Research, The University of Iowa, Iowa city, Iowa, 1987.

36. J. M. V. A. Koelman. A Simple Lattice Boltzmann Scheme for Navier-Stokes Fluid Flow. EPL 15(6):603, 1991

37. S. D. Kuiry, P. D. Bates. Coupled 1d-quasi-2d flood inundation model with unstructured grids. Journal of Hydraulic Engineering, 136(8):493–506, 2010.

38. A.J. C. Ladd. Numerical simulations of particulate suspensions via a discretized Boltzmann equation. Journal of fluid mechanics 271, 285-309, 1994.

39. M. Lai, E. Krempl, D. Ruben, Introduction to continuum mechanics, Butterworth-Heinemann is an imprint of Elsevier, 1993.

40. P. D. Lax. Weak solutions of Nonlinear Hyperbolic Equations and Their Numerical Computation. Comunications on Pure and Applied Mathematics„ 7:159-193,1954

41. P. D. Lax and B. Wendroff. System of conservation laws. Comunications on Pure and Applied Mathematics, 13:217–237, 1960.

42. B. P. Leonard. A stable and accurate convective modelling procedure based on quadratic upstream interpolation. Computer Methods in Applied Mechanics and Engineering, 19:59–98, 1979.

43. H. Liu, H. Wang, S. Liu, C. Huc, Y. Ding, and J. Zhang. Lattice Boltzmann method for the Saint-Venant equations. Journal of Hydrology, 524:411-416, 2015.

44. M. Markl, C. Korner. Free surface Neumann boundary condition for the advection-diffusion lattice Boltzmann method. Journal of Computational Physics, 301(C): 230-246, 2015.

45. N. S. Martys, X. Shan, and H. Chen. Evaluation of the external force term in the discrete Boltzmann equation. Physical Review E, 58(5):6855-6857, 1998.

46. R. McNamara and G. Zanetti. Use of the Boltzmann equation to simulate lattice-gas automata. Phys. Rev. Lett., 61:2332-2335, 1988.

47. Q. K. Nguyen and H. Kawano. Simultaneous solution for flood routing in channel networks. Journal of Hydraulic Engineering, 121(10):744–750, 1995.

48. G. S. O'Brien, C.J. Bean, F. McDermott.A comparison of published experimental data with a coupled lattice Boltzmann-analytic advection–diffusion method for reactive transport in porous media. Journal of Hydrology 268: 143–157, 2002

49. S. Patel, M. Min, T. Lee.A spectral-element discontinuous Galerkin thermal lattice Boltzmann method for conjugate heat transfer applications. International Journal for Numerical Methods in Fluids,82(12): 932-952

50. Y. Peng, J. G. Zhou, R. Burrows. Modeling Free-Surface Flow in Rectangular Shallow Basins by Using Lattice Boltzmann Method. Journal of Hydraulic Engineering, 137(12), 2011.

51. A. Preissmann. Propagation des Intumescences dans les canaux et Rivieres. pages 433-442, Grenoble, France, 1961.

52. Y. H. Qian. Lattice Gas and lattice kinetic theory applied to the Navier-Stokes equations. PhD thesis, Universite Pierre et Marie Curie, Paris, 1990.

53. Y. H. Qian, D. D'Humières and P. Lallemand. Lattice BGK Models for Navier-Stokes Equation. EPL 17(6), 1991.

54. W. Rodi. Numerical calculations of flow and sediment transport in rivers. In Proceedings of International Symphosium on Stochastic Hydraulics, Beijing, 2000.

55. D.H. Rothman and S. Zaleski. Lattice-gas cellular automata - simple models of complex hydrodynamics. Cambridge University Press, Cambridge, UK, 1997.

56. R. Salmon. The lattice Boltzmann method as a basis for ocean circulation modelling. Journal of Marine Research, 57:503-535, 1999.

57. C. Sart, J. P. Baume, P. O. Malaterre, and V. Guinot. Adaptation of preissmann's scheme for transcritical open channel flows. Journal of Hydraulic Research, 48(4): 428–440, 2010.

58. J.G. Simmonds. Brief on Tensor Analysis. Springer, New York, 1994.

59. M. Spasojevic and F. M. Jr. Holly. 2-d bed evolution in natural watercourses - new simulation approach. Journal of the Waterway, Port, Coastal and Ocean Division, Proceedings of the ASCE, 116(4):425–443, 1990.

60. K. R. Tubbs and F. T. C. Tsai. GPU accelerated lattice Boltzmann model for shallow water flow and mass transport. INTERNATIONAL JOURNAL FOR NUMERICAL METHODS IN ENGINEERING, 86(3):316-334, 2011.

61. US Army Corps of Engineers. HEC-RAS River Analysis System - Hydraulic Reference System(5.0.1), 2016.

62. L. C. van Rijn. Sediment transport, part ii: Suspended load transport. Journal of Hydraulic Research, 110(11):1613–1641, 1984.

63. L. C. van Rijn, H. van Rossum, and P. Termes. Field verification of 2-d and 3-d suspended sediment models. Journal of Hydraulic Engineering, 116(10):1270–1288, 1990.

64. P. van Thang, B. Chopard, L. Lef´evre, D. A. Ondo, and E. Mendes. Study of the 1D lattice Boltzmann shallow water equation and its coupling to build a canal network. Journal of Computational Physics, 229(19):7373-7400, 2010.

65. D. A. Vieira and W. Wu. One-dimensional channel network model cche1d version 3.0 -user's manual. Technical Report NCCHE-TR-2002-02, National Center for Computational Hydroscience and Engineering, 2002a.

66. D. A. Vieira and W. Wu. One-dimensional channel network model cche1d version 3.0 - model capabilities and application. Technical Report NCCHE-TR-2002-05, National Center for Computational Hydroscience and Engineering, 2002b.

67. W. Wu. Depth-averaged two-dimensional numerical modeling of unsteady flow and nonuniform sediment transport in open channels. Journal of Hydraulic Engineering, 130(10):1013–1024, 2004.

68. W. Wu. Computational River Dynamics. Taylor & Francis Group, London, 2008.

69. C.T. Yang, C.C.S. Song. Theory of minimun energy and energy dissipation rate. Encyclopedia of Fluid Mechanics, 1:359-399, 1986.

70. C.T. Yang, F.J.M. Simoes.GSTARS computer models and their applications, part I: Theoretical Development. International Journal of Sediment Research,23(3):197-311, 2008.

71. C.T. Yang, F.J.M. Simoes.GSTARS computer models and their applications, part II: Applications. International Journal of Sediment Research,23(4):197-311, 2008.

72. E. Yeh, R.V. Skibbens, J. W. Cheng, E.D. Salmon, K. Bloom. Spindle dynamics and cell cycle regulation of dynein in the budding yeast. J Cell Biol. 130(3):687-700, 1995.

73. H. Yoshida and M. Nagaoka. Multiple-relaxation-time lattice Boltzmann model for the convection and anisotropic diffusion equation. Journal of Computational Physics, 229:7774-7795, 2010.

74. J. G. Zhou. A LATTICE BOLTZMANN MODEL FOR GROUNDWATER FLOWS. International Journal of Modern Physics C, 18(6):973-991, 2007.

75. J. G. Zhou. Rectangular lattice boltzmann method. Physical Review E, 81:1-10, 2010.

76. J. G. Zhou. Enhancement of the LABSWE for shallow water flows. Journal of Computational Physics, 230:394-401, 2011.

77. J. G. Zhou. Lattice Boltzmann Methods for Shallow Water Flows. Springer-Verlag, Berlin, 2004.

78. J. G. Zhou. A lattice Boltzmann method for solute transport. International Journal of Numerical Methods in Fluids. 61(8): 848-863, 2009.